NASA Electronic Parts and Packaging (NEPP) Program

NEPP Task: Reliability of Advanced Wet and Solid Tantalum Capacitors

Leakage currents and gas generation in advanced wet tantalum capacitors

Alexander Teverovsky

ASRC Federal Space and Defense

Alexander.A.Teverovsky@nasa.gov

Worked performed at NASA Goddard Space Flight Center

2015

Leakage currents and gas generation in advanced wet tantalum capacitors

Abstract

Currently, military grade, established reliability wet tantalum capacitors are among the most reliable parts used for space applications. This has been achieved over the years by extensive testing and improvements in design and materials. However, a rapid insertion of new types of advanced, high volumetric efficiency capacitors in space systems without proper testing and analysis of degradation mechanisms might increase risks of failures. The specifics of leakage currents in wet electrolytic capacitors is that the conduction process is associated with electrolysis of electrolyte and gas generation resulting in building up of internal gas pressure in the parts. The risk associated with excessive leakage currents and increased pressure is greater for high value advanced wet tantalum capacitors, but it has not been properly evaluated yet. In this work, in Part I, leakages currents in various types of tantalum capacitors have been analyzed in a wide range of voltages, temperatures, and time under bias. Gas generation and the level of internal pressure have been calculated in Part II for different case sizes and different hermeticity leak rates to assess maximal allowable leakage currents. Effects related to electrolyte penetration to the glass seal area have been studied and the possibility of failures analyzed in Part III. Recommendations for screening and qualification to reduce risks of failures have been suggested.

Table of Contents

Executive summary

Part I. Leakage currents.

Leakage currents in tantalum capacitors are the most important, quality related characteristics of the part. However, analysis of the existing requirements shows that contrary to other types of capacitors that have DCL specifications based on their Capacitance Voltage product (CV) values, no simple relationship between CV and DCL exists for wet tantalum capacitors. There is also no standard for setting the acceptance criteria for DCL, and the limits are established by manufacturers based on their experience, market values, and internal procedures. This results in a large spread of DCL limits (more than 3 times) for capacitors with similar CV values. Even for the same type of capacitors the DCL limit might remain the same for parts with CV values changing 4 to 5 times. Considering that the actual DCL values are from 2 to 100 times less than the specified limits, this indicates the need to revise requirements for DCL.

Leakage currents measured at room temperature within 5 minutes of electrification are due to charge absorption and are not related to conductions through the tantalum pentoxide dielectric. Absorption currents are reproducible from sample to sample even for lots with a large spread of intrinsic leakage currents caused by conduction and/or the presence of defects. Absorption currents increase linearly with capacitance and voltage, and have a poor dependence on temperature, which is most likely due to the tunneling of electrons into states (traps) located in the forbidden energy gap of the dielectric at the interface with the electrolyte.

Absorption currents decrease with time according to a power law with the exponent close to 1, and their behavior can be accurately enough described using the Dow model. According to this model, leakage currents measured after 300 sec of electrification can be determined as 10^{-4} $C \times VR$, which is close to the experimental data. Actual DCL values in the range of CV from 10^2 to 10^6 $\mu F \times V$ can be fairly well approximated with a linear function, $DCL_{exp} = 5 \times 10^{-5} \times C \times VR$. Allowing for 2 to 5 times margin, the limit for DCL can be set at $2.5 \times 10^{-4} \times C \times VR$.

Analysis of breakdown voltages shows a decreasing margin for capacitors rated to higher voltages. Breakdown voltages normalized to VR decrease from ~3 at VR = 25 V to ~1.5 at VR = 100 V and to ~ 1.2 at VR = 125 V. The results show that high-voltage capacitors operate at electric fields close to breakdown. This limits the capability of accelerated testing by increasing applied voltage and might explain why life test failures happen more often with high-voltage capacitors.

Contrary to absorption currents, intrinsic currents caused by oxide conduction increase exponentially with temperature and voltage. Experimental data are consistent with the Simmons model and suggest that intrinsic leakage currents are controlled by the barrier at the electrolyte/oxide interface. Estimations showed the barrier height is from 0.9 to 1 eV, and activation energies at rated voltages are in the range from 0.65 eV to 0.85 eV. Extrapolations of temperature dependencies of leakage currents to room temperature showed that intrinsic currents are 2 to 3 orders of magnitude below the absorption currents measured after 5 min of electrification.

In good quality capacitors, currents might continue decreasing with time for more than 100 hours following the power law before stabilizing at a rather low level corresponding to the intrinsic conduction. However, in some types of large CV value capacitors a wide spread of currents, spiking and erratic behavior was observed, thus indicating the presence of defects in the dielectric. Due to large values of the specified currents and the masking effect of absorption currents, capacitors having defects in the dielectric can pass screening, but cause failures due to excessive noise in the systems or excessive gas generation. This indicates that leakage currents in capacitors intended for space applications should be monitored during voltage conditioning.

Degradation of leakage currents with time during HALT is similar to what is observed sometimes during 10,000 hour life testing at 125 ºC. The mechanism of degradation is likely the same as for solid tantalum capacitors and is due to migration of oxygen vacancies. This degradation accelerates strongly with voltage and temperature, and the activation energy of the process is relatively large, ~1.1 eV. For this reasons, the probability of observing increasing currents at operating conditions, where voltages are derated to below 0.6VR and temperatures do not exceed ~ 60 ºC, is typically negligibly small.

Part II. Gas generation, hermeticity, and pressure in the case.

Estimations of possible drying of electrolyte due to the hermeticity leak showed that at the specified limit of 10^{-8} atm*cc/s He, the amount of electrolyte in 10 years will decrease by ~1 mg at 22 °C and ~30 mg at 85 °C. These values are much less than the amount of electrolyte that is typically used in large size wet tantalum capacitors. However, it is comparable with the amount of electrolyte in small case size (T1) capacitors. Electrolyte trapped in the anode slug by capillary forces lessens the risk of drying.

Currently, only gross leak testing is required per MIL-PRF-39006 as a screening procedure during manufacturing of capacitors, which means that some parts might have leak rates much greater than 10^{-8} atm*cc/s He, thus increasing substantially the risk of drying during long-term operations. For space applications, the risk of electrolyte escaping is related not only to the possible degradation of capacitors, but also to contamination of sensitive optical equipment. To avoid this risk, fine leak testing should be carried out as a part of the screening process. It should be noted that this is already a standard procedure for some manufacturers.

Degradation and corrosion of the seal weld might result in increasing leak rates even for initially hermetic parts. Due to electrolysis of electrolyte and gas generation, high internal pressure might be developed with time of operation and thus accelerate the leak of electrolyte. To assure integrity of the case for long-term operations and storage, a high-temperature storage (HTS) testing (1000 hours at 150 ℃) that creates internal pressure of ~ 5 atm in the case is recommended.

Variations of the internal gas pressure with time in tantalum capacitors were calculated at different levels of leak rates. At the leak rate of 10^{-8} atm×cc/s He the characteristic time of pressure stabilization for cases with volume 1 cm^3 is 20 days, and the steady-state pressure at a leakage current of 1 μA is 0.2 atm. An increase in leakage currents raises the pressure proportionally. For example, at 100 μA the steady state pressure is ~ 20 atm and it exceeds 1 atm after approximately 10 days. For capacitors with the leak rate of 10^{-9} atm*cc/s He, which is only 10 times less than the specified level, 1 μA current would increase pressure above 2 atm after 1 year of operation. The lower the leak rate, the higher the level of the pressure, and in hermetic cases it can exceed 100 atm after 10 years of operation at currents ~10 μA.

Hydrogen generation increases embrittlement and reduces the strength of the case. Conservative estimations showed that the level of critical pressure that the case can withstand without rupture decreases from 83 atm for T1 cases to 52 atm for T3 and T4 cases. Large capacitors manufactured per DLA DWG#04003, can safely operate at a much lower pressure, ~21 atm. To assure that the critical level of pressure in hermetic cases (leak rate below 10^{-11} atm*cc/s He) is not reached during 10 years of operation, intrinsic leakage currents should be limited to values, that depending of the case size, vary from ~ 2 μA for DLA DWG#93026/T1 cases to ~ 30 μA for DLA DWG#04003 cases. The requirements for the level of intrinsic currents can be verified by measurements of leakage currents at the end of voltage conditioning and should be carried out as a part of the screening process.

The charge associated with faradaic electrochemical reactions that should be transferred in a T4 size case so the gas pressure would reach the critical level sufficient to cause its rupture is ~ 400 C. This charge can be transferred approximately within an hour at leakage currents ~ 100 mA or after 10 years if current is ~ 1 μA. The first situation might occur if a capacitor operates under reverse bias or the dielectric has been damaged during mechanical test, e.g. vibration, but the latter condition appears typical. However,

during long-term operations, a large portion of the generated hydrogen will leak through the seal and be absorbed by the tantalum case, thus reducing the risk of overpressure by hydrogen substantially. Although hydrogen might escape even from hermetic cases relatively easily, generated oxygen will remain in the case and maintain constant pressure that is ~ 50% of the value calculated for hydrogen generation. This means that a tight control over intrinsic leakage currents is necessary to reduce the risk of catastrophic failures.

Increased internal pressure results in case bulging. However, changes in radius at critical levels of the pressure are relatively small (below ~10 μm) for all case sizes. However, deformation of the top or bottom surfaces might be noticeable. Assessments show that for cases T3 and T4 this deformation can reach ~ 0.16 mm, for DLA DWG#04005 capacitors ~ 1 mm, and for DLA DWG#04003 capacitors ~ 3.6 mm. The level of bulging after life testing of advanced wet tantalum capacitors should be verified, and lots with excessive bulging (more than 50% of the critical level) should not be accepted for L1 projects.

Part III. Electrolyte at the glass seal.

Tantalum outlets and the upper section of the anode riser wires are not oxidized before final welding of the case. For this reason, penetration of electrolyte to the glass seal area might result in excessive and unstable leakage currents, corrosion of the outlet weld, and increased internal gas pressure due to electrolysis of the electrolyte.

In the presence of electrolyte, leakage currents along the glass seal might exceed milliamperes initially, but then reduce slowly with time (for hundreds of hours) roughly according to a power law with the exponent ~ 0.6. The reduction of currents is due to the anodic oxidation of the surface of the outlets and wires and charge absorption. However, the quality of the oxide is worse when compared to the one formed on the surface of anode slugs; first, because the formation voltage and temperature are much less than during anodization of slugs, and second, because the purity of tantalum used for wires and outlets is not as great as for slugs.

Oxide formation occurs relatively fast, within minutes of electrification and the pressure created by hydrogen generation in the process of oxide growth is small, below ~ 0.1 atm. However, the pressure caused by electrolysis during long-term operation might pose a reliability risk. Due to a poor quality of oxides, a substantial portion of the voltage applied to a capacitor might drop across the electrolyte resulting in electrolysis and gas generation. The latter effect might increase pressure in the case and raise the risk of its damage.

A gradual seeping of electrolyte to the glass seal area during operation is likely not a serious reliability concern because of fast oxidation that reduces levels of additional leakage currents and relatively high leak rate of hydrogen. However, possible accumulation of electrolyte on the surface of the glass seal after long-term storage might increase substantially currents during first power turn on in the system and result in a fast pressure increase. For this reason, rescreening of the capacitors after 5 years of storage is recommended.

In many cases, space systems, after integration and testing, are stored for many years before launch or operation. High temperature storage (HTS) testing can be used to demonstrate that the risk of failures due to possible penetration of electrolyte in the glass seal area is low.

Quality of oxides formed on the surface of the outlets and wires at high temperatures is better compared to oxides formed at room temperature. For example, conditioning at 50 V and 145 ºC for ~30 hours resulted in oxides that had leakage currents ~ 2 orders of magnitude lower and breakdown voltages ~35% greater than oxides formed at room temperature for 250 hours. To improve quality of oxides and reduce risks of failures a special conditioning at high temperatures is recommended for button style capacitors that do not have internal sealing.

The risk of failures caused by the presence of electrolyte in the glass seal area might be greater for small, T1 size capacitors because: (i) small size capacitors have lower capacitance, hence lower requirements for DCL, so additional leakage currents that are similar for different case sizes are more likely to cause failures; (ii) it is more difficult to crimp small cases properly; (iii) accurate positioning of Teflon spacers is also more difficult. Small case size capacitors might have also a greater risk of electrolyte drying and their use in space systems require additional quality assurance.

Introduction

The first tantalum non solid electrolyte capacitors that were used in military applications in 1970's had multiple reliability issues related to hermeticity, dendrite growth, poor performance under mechanical stress testing (vibration), and under reverse bias [1]. The parts were sealed with polymers, and due to electrolyte leakage had a limited operational life, ~ 3 years [2, 3]. Over the years, significant efforts has been made to optimize design and materials used for the case, cathode, and electrolyte, and improve reliability to the level required for space applications [1, 4]. Currently, capacitors manufactured per MIL-PRF-39006 are among the most robust electronic components and have an extensive history of successful space applications.

The need to further increase capacitance and reduce volume of the parts resulted in development of variety of commercial, "non-solid" electrolyte capacitors described in multiple DLA and LM drawings (e.g. #93026, #10004, and #0400X). Specifics and performance of these parts are described in publications made by specialists from AVX [5], Vishay [6], and Evans Capacitors [7]. These parts are very attractive for electronic designers, but need additional analysis of their performance and reliability to establish adequate requirements for screening and qualification testing. The thickness of the dielectric in advanced wet tantalum capacitors might be much less than in mil-spec capacitors. For example, in commercial hybrid capacitors, the formation voltage might be as low as 1.3 times the rated voltage [8]. This means that electric fields in the dielectric are close to the breakdown voltage, and it is possible that although slowly, the oxide will grow further, and gas generation associated with the oxide growth process will continue during long-term operations. Thinner dielectrics used in hybrid capacitors were likely the reason for leakage currents in these parts being up to two orders of magnitude greater than in regular tantalum electrolytic capacitors [7].

Direct current leakage (DCL) is the most important indicator of quality of the dielectric that determines reliability of capacitors and for this reason, a special attention should be given to analysis of leakage currents and their variations with time under stress. However, there are only scarce data related to the time, temperature and voltage dependencies of leakage currents in advanced wet tantalum capacitors, and the mechanism of conduction has not been properly analyzed yet. There is also a lack of information

related to statistical analysis of distributions of leakage currents, which does not allow selection and verification of adequate requirements.

Wet tantalum capacitors are typically used in power supply circuits either for filtering or energy storage and fast delivery purposes. Unless the part is used in a system with low-capacity batteries, e.g. medical implantable devices, the level of leakage current is not critical for designers, and the users are typically satisfied with DCL limits set by manufacturers. This limit is set by some internal procedures by manufacturers, and is often driven by marketing considerations. However, criteria for maximum leakage currents are essential for quality assurance purposes and require a thorough analysis.

Reliability of wet tantalum capacitors is due mainly to "self-healing" processes that can repair localized damage to the tantalum pentoxide (Ta_2O_5) dielectric by growing oxide at the defective areas such as cracks, thin oxide areas, or microfissures. The electrochemical oxidation that results in the growth of the Ta_2O_5 dielectric (repairing the damage) is similar to the process that forms the dielectric initially during anodic oxidation of the tantalum pellet by manufacturers. While this self-healing process repairs the damaged dielectric, it also results in electrolysis of the electrolyte, which generates gas, mostly hydrogen (~69% per [2]) that increases internal pressure in the case. The risk related to gas generation caused by excessive currents during random vibration testing have been discussed before [9] and criteria limiting the transfer charge have been suggested.

Processes of gas generation due to excessive DCL occur also in aluminum electrolytic capacitors with electrolytes containing inorganic acids, bases and salts [10]. However, aluminum capacitors are not hermetic and generated gas can be released through the seals and/or safety vents. A stolen recipe of a water based electrolyte resulted in multiple explosions of capacitors in computers and power supplies during 2000 to 2005 period [11].

Failures due to evaporation of electrolyte and related loss of capacitance and increased ESR are considered the major wear out failure mechanisms in these parts. Generally, ~ 90% of failures of aluminum capacitors are caused by increased gas pressure and leaks [12]. Problems similar to aluminum electrolytic capacitors occur also in electrolytic double-layer capacitors. These parts also have liquid electrolyte inside an aluminum can, which is sealed with a rubber bung and the faradaic reactions associated with the electrolyte decomposition might potentially limit the lifetime of the device [13].

Tantalum capacitors are manufactured in hermetic cases and their hermeticity is supposed to be verified by qualification testing at the level of 1E-8 atm_cc/s, He. Analysis of the significance of this criterion for a long-term operation of capacitors in vacuum is one of the objectives of this work.

A special safety venting element is used in the case of aluminum capacitors to prevent explosion if gas generation exceeds the rate of evaporation. No such elements are used for hermetic tantalum capacitors and back in 70's the risk of possible over-pressurizing of the parts during long-term operations was considered as a potentially limiting factor of their reliability. Hayward [3] considered that if excessive pressurization does occur within the unit as a result of misapplication, eventual release of the seal may be more dramatic than the gradual easing of the seal in the non-hermetic cases.

Experience with military grade capacitors shows that the risk of rupture and explosion for hermetically sealed tantalum capacitors during long-term operations is minimal, but with advance of new technology capacitors that might have greater leakage currents this risk should be reevaluated. Evans [14] considered

that the rate of wear-out failures of wet tantalum capacitors is directly related to leakage currents and excessive pressure in the case. This requires analysis of mechanical strength of tantalum cases to set requirements for the acceptable level of gas generation and leakage currents. For tantalum capacitors, this analysis is complicated by diffusion of hydrogen through the tantalum. Absorption of hydrogen in the tantalum case can result in its embrittlement, reduce the strength, and increase the risk of rupture.

High internal gas pressure can increase substantially the rate of electrolyte leak through the internal elastomer and Teflon seals intended to prevent the electrolyte from seeping into the cavity with the glass seal. If electrolyte escapes past this internal seal, leakage current along the glass might increase substantially due to the presence of non-oxidized portion of the anode riser wire and the non-oxidized internal surface of the outlet tube. High leakage currents and relevant oxidation processes would generate additional amounts of hydrogen and further increase the risk of failures. Also, at high pressure the risk of deterioration of the outlet weld might increase substantially. However, the effects associated with the presence of electrolyte at the glass seal area has not been studied yet.

Effects of reverse bias, ripple currents, and random vibration testing on reliability of advanced wet tantalum capacitors have been described in previous NEPP reports [9, 15-17]. A comparative analysis of materials and designs used in military grade and new technology, high volumetric efficiency capacitors is given in [18]. This document provides suggestions for selection, screening and qualification of new technology wet tantalum capacitors. However, issues related to the requirements for leakage currents have not been addressed. The purpose of Part I of this report is to analyze the existing requirements for DCL, determine time, temperature, and voltage dependencies of leakage currents and better understand mechanisms of their formation. Processes of gas generation caused by electrolysis of electrolyte, assessments of internal pressure, stresses in the case, and analysis of internal pressure in cases with hermeticity leaks are discussed in Part II. Issues related to a current leakage along the glass seal in the presence of electrolyte are considered in Part III. Recommendations for leakage current testing during screening and qualification of wet tantalum capacitors to reduce risks of failures are suggested.

Part I. Leakage currents in wet tantalum capacitors.

I.1.   Existing requirements for DCL

MIL-PRF-39006 requires that DCL measurements for conformance inspection are made within 5 minutes of electrification. Considering that leakage currents are decreasing with time, this allows manufacturers to terminate measurements as soon as the required limit is reached, thus accelerating substantially the testing process. The limit for DCL is set at a rated voltage for temperatures 85 ºC and below, and at 2/3VR at 125 ºC in the relevant slash sheet specifications. DCL measurements at 125 ºC are not used for screening, but are carried out during the "stability at low and high temperatures" testing as a part of group V qualification inspection only.

Voltage conditioning is carried out at 85 ºC and rated voltage for 48 hours with capacitors connected to a power source through 1.1 kohm resistors. Measurements of leakage currents during the testing are not required. After the testing, capacitors are visually examined for mechanical damage and leakage of electrolyte. This test is often considered as burning-in; however, the purpose of conditioning is improvement of performance of the parts rather than selection and rejection of defective capacitors that can potentially cause infant mortality failures. It is not clear what improvement is achieved by this procedure, but the need for monitored burning-in will be discussed in the following sections of the report.

Leakage currents in capacitors increase with applied voltage, surface area, S, and decrease with the thickness of the dielectric, d, so DCL $\sim S/d \times V$. The same parameters affect also the value of capacitance, $C \sim S/d$. As a result, leakage currents depend on the product of capacitance and rated voltage, and requirements for maximum leakage current can be expressed as DCL $= \alpha \times C \times VR$, where α is a constant. For solid tantalum capacitors this constant is equal to 0.01 for MnO2 cathode capacitors and 0.1 for polymer cathode capacitors. A similar relationship is used for aluminum electrolytic capacitors:

$$\text{DCL} = \alpha \times C \times VR + B, \tag{I.1.1.a}$$

where B is typically 2 or 3 µA.

According to the European standard, EN 130300 [19], minimal leakage current for aluminum electrolytic capacitors is determined by equation:

$$\text{DCL(5 min)} < (0.3 \times C \times VR)^{0.7} + 4, \tag{I.1.1.b}$$

where current is in µA, voltage is in volts, and capacitance is in microfarads.

Different vendors of aluminum electrolytic capacitors are using different values of α in Eq (I.1.1.a), that depends also on the rated voltage, e.g., $\alpha = 0.002$ for VR $\leq$ 100V, and 0.01 for VR $>$ 100V [20]. However, analysis below shows that there is no simple relationship with CV for wet tantalum capacitors.

For a given rated voltage, leakage current, hence the DCL limit, are expected to increase linearly with capacitance. However, a linear dependence of the specified DCL$_{max}$ is observed at 125 ºC for CRL79 capacitors only (see Fig. I.1.1). For other parts, there is a substantial deviation from linearity.
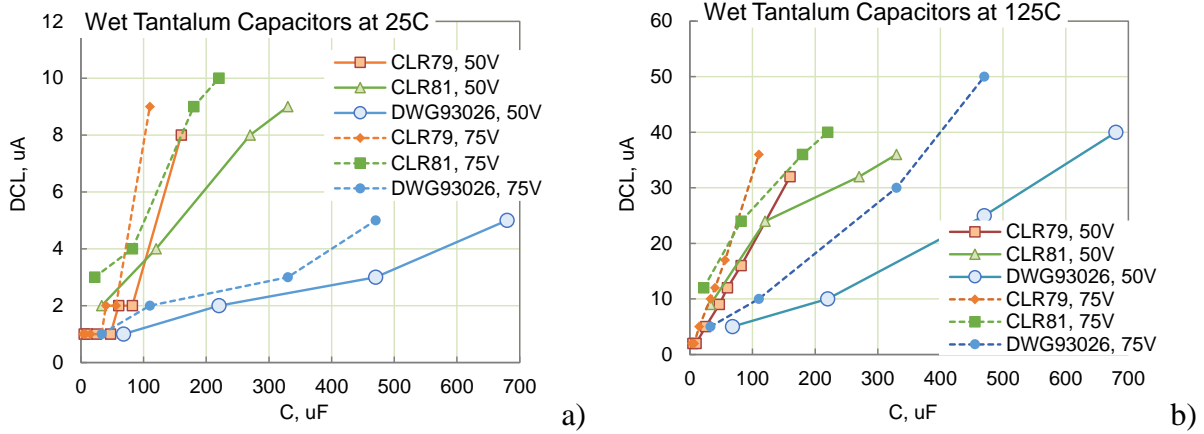
Figure I.1.1. Variation of maximum specified leakage currents with capacitance at 25 ℃ (a) and 125 ℃ (b) for capacitors rated to 50 V and 75 V.

Figure I.1.2 shows correlations between the specified DCL and CV values for two types of military grade capacitors. Although DCL_{max} has a trend of increasing with CV, deviations from the expected correlation are substantial. For CLR79 capacitors the limit for cases size T1, T2, and T3 does not depend on CV at all, and for T4 cases, DCL_{max} varies more than 3 times for similar CV value capacitors. If a current of 1 µA is assumed to flow through the glass seal in T1 and T2 capacitors, which is far greater than actual leakage currents, than it is still not clear why currents through the same seals in T3 and T4 capacitors are set to 2 µA.
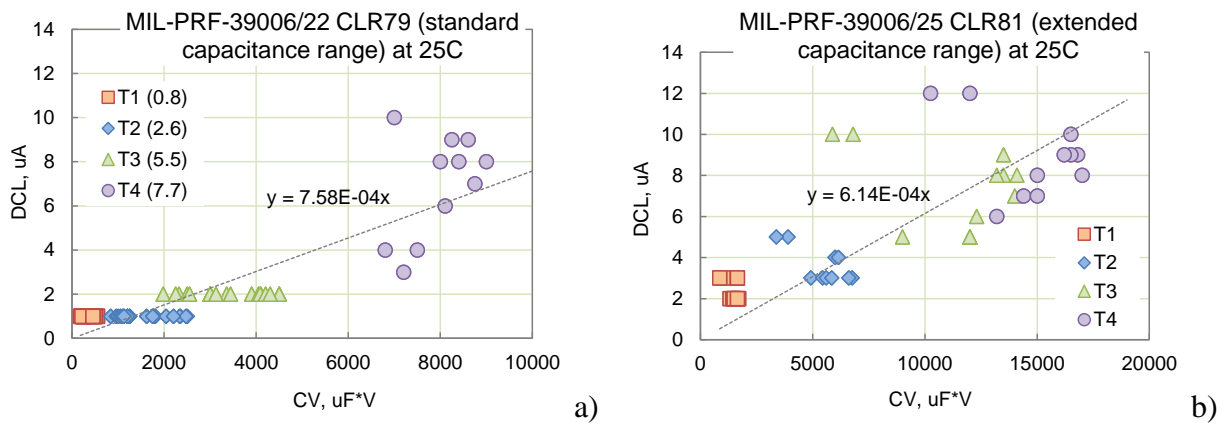
Figure I.1.2. Correlation between the specified levels of DCL and CV values for CLR79 (a) and CLR81 (b) capacitors. Different marks correspond to different case sizes, from T1 to T4.

A comparison of the specified leakage currents for military and DLA drawing capacitors is shown in Fig.I.1.3. Capacitors with similar design and similar CV values might have substantially different requirements for leakage currents. Even for the same type capacitors changes in CV values by 4 to 5 times did not changed the limit (Fig. I.1.3.c, I.1.3.d).
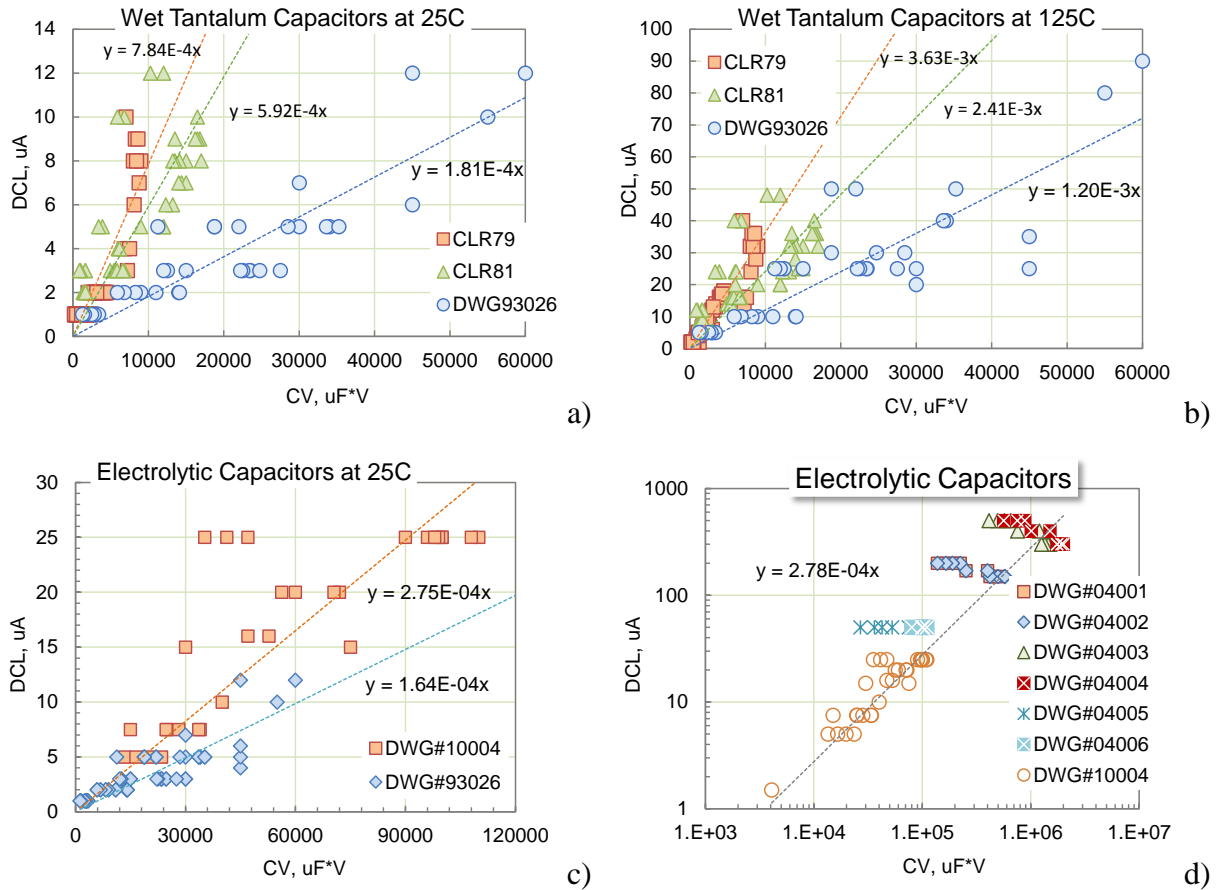
Figure I.1.3. Specified leakage currents for different types of wet tantalum capacitors. (a, b) CLR79, CLR81, and DLA DWG93026 at 25 ºC (a) and 125 ºC (b). c) Comparison between DLA DWG10004 and DLA DWG93026. (d) Large CV values capacitors per DLA DWG0400X and DLA DWG 10004.

Results of analysis show that, contrary to solid chip tantalum capacitors that have DCL requirements based on CV values, the origin of the maximum specified currents for wet capacitors is not clear. There is no requirements for a procedure to establish DCL_{max}, and in most cases, the limits are established by manufacturers based on unspecified internal procedures.

High volumetric efficiency advanced capacitors manufactured per DLA DWG93026 have maximum leakage current ~ 4 times lower compared to military grade capacitors. This indicates problems with DCL requirements even for military-grade capacitors. The spread of requirements for I_{max} for both, military-grade and DLA drawing parts is large, and, most important, the margin between the specified and actual currents is not known.

I.2.   Breakdown voltages in wet tantalum capacitors.

Breakdown voltage, VBR, in different part types were measured to assess the margin between the rated and breakdown voltages and determine possible range of applied voltages for measurements of I-V characteristics and accelerated testing. The measurements were carried out using a constant current stress (CCS) testing [21]. A typical result of measurements is shown in Fig. I.2.1 and indicates a good

reproducibility of VBR measurements. A relatively small drop in voltage when the breakdown level is reached indicate a fast and efficient self-healing process.
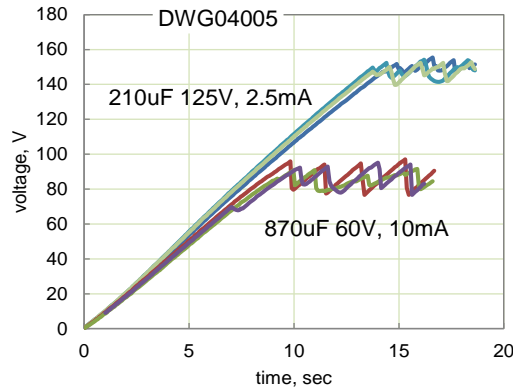

Figure I.2.1. Variations of voltage across three samples of 210 μF 125 V and 870 μF 60V DLA DWG04005 capacitors.

Test results for different part types are shown in Fig.I.2.2 and indicate a decreasing margin for capacitors rated at higher voltages. Normalized breakdown voltage decreases with the rated voltage from ~3 at 25 V to ~1.5 at 100 V and ~ 1.2 at 125 V. High-voltage capacitors operate at electric fields close to breakdown. This limits the capability of accelerated testing by increased voltages especially for high-voltage capacitors and might explain why life test failures for this group happen more often.

High volumetric efficiency capacitors have somewhat lower VBR compared to capacitors manufactured to MIL-PRF-39006. On average, VBR decreases with the rated voltage as:

$$VBR = 21 \times VR^{0.58}$$

Considering that for solid chip tantalum capacitors VBR/VR is in the range from 2.5 to 5 [22], wet tantalum capacitors are manufactured using somewhat lower formation voltages, and as a result have thinner dielectrics and lower VBR. Note that the self-healing capability of wet tantalum capacitors is greater than for solid capacitors, which explains their reliable operation at higher electric fields.

At a given rated voltage, VBR decreases with capacitance indicating that somewhat thinner dielectrics are used for capacitors with higher ratings (see Fig. I.2.2b). It is also possible that capacitors that have larger surface area of electrodes have also a greater probability of having defects that reduce VBR.
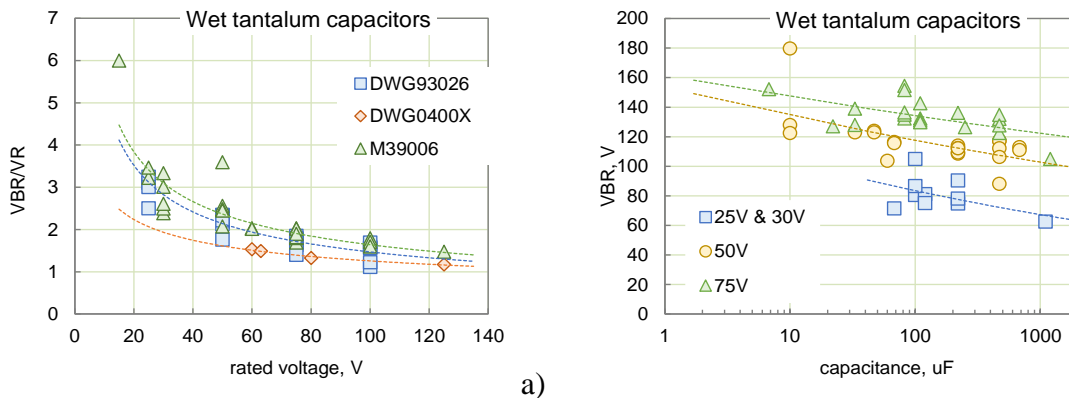

Figure 1.2.2. Variations of the normalized breakdown voltages with the nominal rated voltage (a) and dependence of VBR on capacitance for capacitors rated to different voltages (b).

I.3.   Absorption currents.

Leakage currents in tantalum capacitors are decreasing with time after application of a step voltage. If after some time under polarization, a capacitor is short circuited through an ampere-meter, depolarization currents would flow in the opposite direction. The absolute values of depolarization currents are also decreasing with time, and when plotted against time together with polarization currents, both *I-t* curves look similar (see Fig. I.3.1). Note, that Fig. I.3.1c shows a case when polarizations currents are greater than depolarization currents, which in this case is due to a ~ 1 min delay before measuring depolarization currents. Polarization currents in Fig I.3.1d are stabilizing after ~1000 sec and became more than an order of magnitude greater than depolarization currents. Stable currents are due to conduction of the dielectric and signify intrinsic leakage currents in the capacitors.
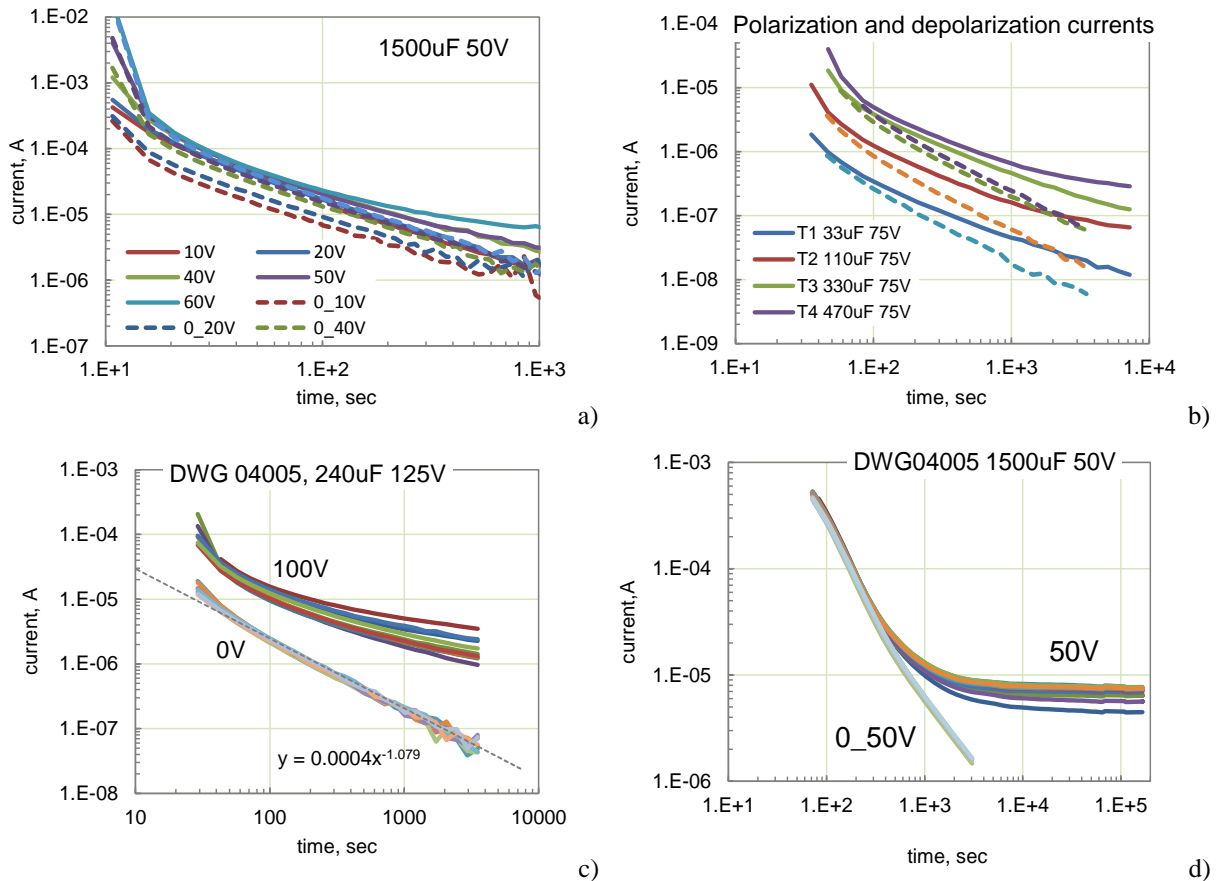

Figure I.3.1. Relaxations of polarization (solid lines) and depolarization (dashed lines) currents in different part types: a) 1500 μF 50 V capacitors at different voltages; b) different types of capacitors rated to 75 V; c) 10 samples of 240 μF 125 V capacitors tested at 100 V; d) 12 samples of 1500 μF 50 V capacitors. Here and below, absolute values of depolarization currents are shown as dashed lines.

A close correlation between polarization and depolarization currrents measured after 5 min is typically observed in normal quality capacitors up to 125 ºC (see Fig. I.3.2). Intrinsic currents start prevailing at higher temperatures. Typically, currents measured within first 1000 sec of electrification are due to absorption processes in the dielectric. A substantial difference between polarization and depolarization currents indicates capacitors with poor quality dielectrics.
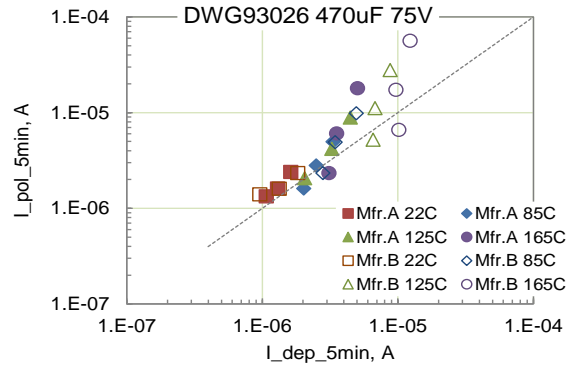
Figure I.3.2. Correlation between polarization and depolarization currents measured after 300 sec at different temperatures for 470 µF 75 V capacitors from two vendors.

Absorption currents are reproducible from sample to sample even for lots with a large spread of intrinsic leakage currents caused by the presence of defects (see Fig. I.3.1c, I.3.1d, I.3.3a, and I.3.3b). As voltage increases, the slope of *I-t* curves for depolarization currents practically does not change, but amplitudes increase linearly (see Fig. I.3.3c). Absorption currents also increase linearly with capacitance (Fig. I.3.3d).
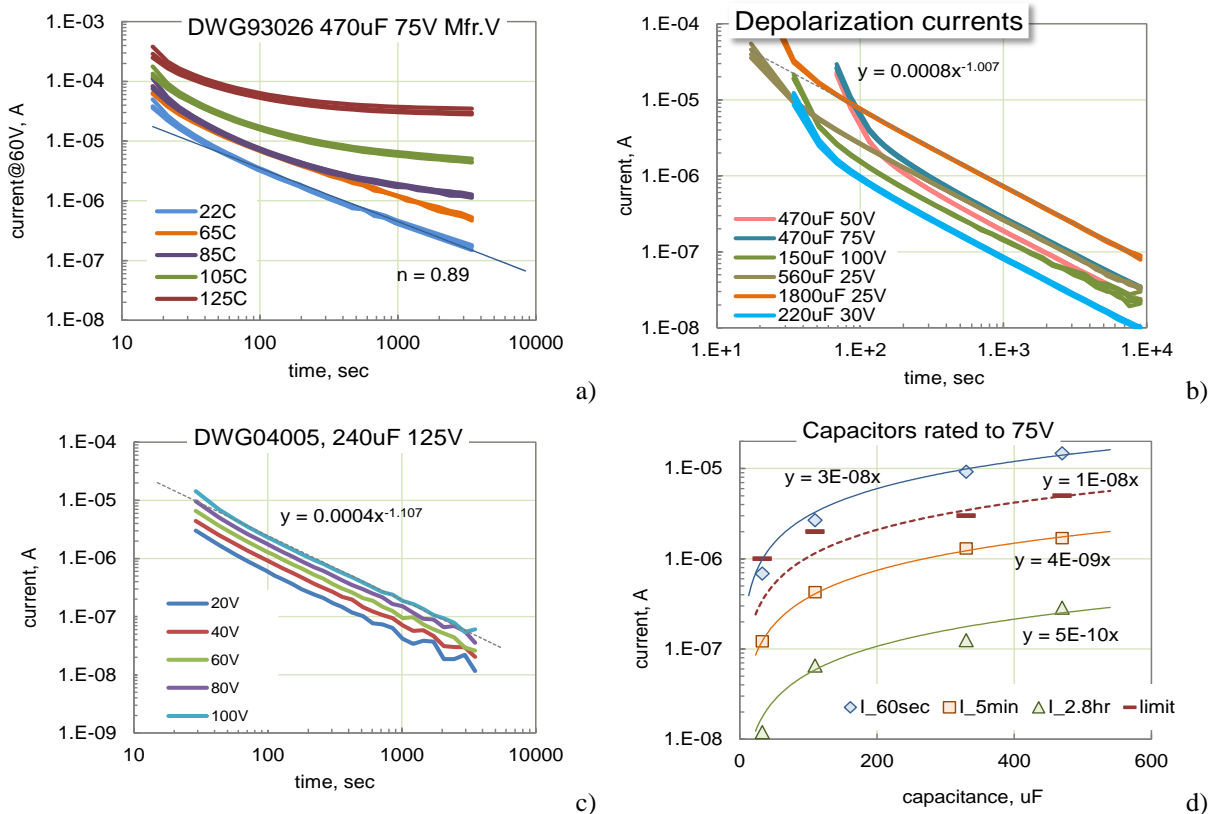

Figure I.3.3. Relaxation of absorption currents during 1 hour for different types of capacitors.
a) polarization currents at different temperatures; b) depolarization currents for different part types at room temperature; c) depolarization currents at room temperature after polarization at different voltages; d) polarization currents measured after 60 sec, 300 sec (5 min), and 10000 sec (2.8 hr) for 33 µF, 110 µF, 330 µF, and 470 µF capacitors rated to 75 V.

Polarization and depolarization currents measured at different temperatures are shown in Fig.1.3.4. Intrinsic leakage currents at high temperatures can be observed after a few minutes of electrification and increase several orders of magnitude as temperature rises from room to 125 ℃. However, absorption currents vary less than 50%.
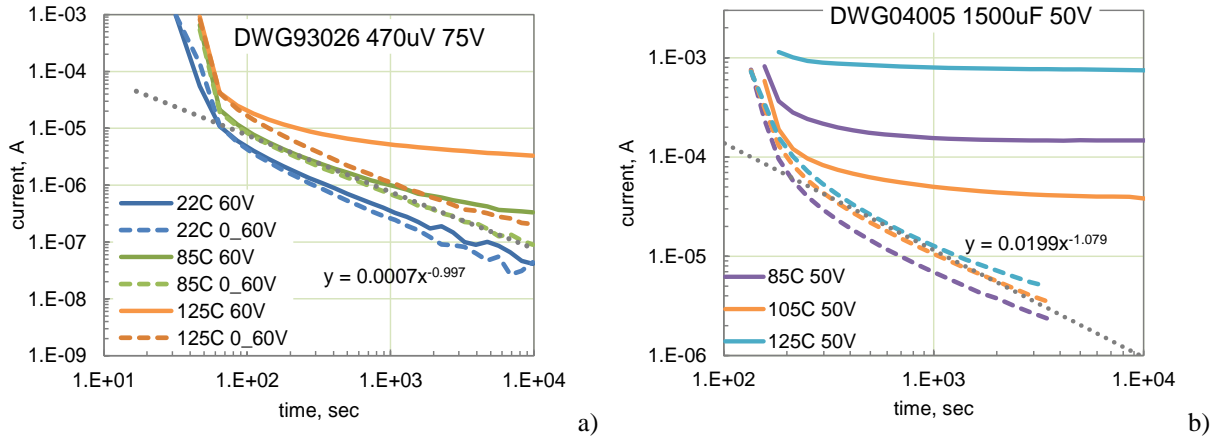

Figure I.3.4. Relaxation of polarization and depolarization currents at different temperatures fro 470 µF 75 V (a) and 1500 µF 50 V (b) capacitors.

To compare currents in high volumetric efficiency capacitors with military grade, M39006 capacitors, relaxation of leakage currents was measured in groups of 8 to 10 capacitors. Results of the testing are shown in Fig. I.3.5 and indicate that in high-quality capacitors, currents measured within 10 hours of electrification are due to absorption processes. Relaxation of the currents, similar to the new technology capacitors, follows a power law and has a very small spread of data. DCL measured after 5 min of polarization increases linearly with capacitance with a slope close to what was observed for high volumetric efficiency parts (Fig.I.3.3d). A deviation for 100 µF capacitors (see Fig. I.3.5b) is due to the test voltage (100 V) being greater than the rated voltage (75 V). In this case, the measured currents are partially due to the intrinsic conduction as can be observed by deviation of the *I-t* characteristics from the power law (see Fig. I.3.5a). Also, one of ten samples in this group had a minor scintillation event (a spike after ~ 200 sec of polarization). This can be explained by a relatively small margin between the rated and breakdown voltages in wet tantalum capacitors. Although due to the effective self-healing processes, no catastrophic failures have occurred, application of voltages greater than the rated might cause excessive leakage currents and, as it will be shown later, increase risks of failures related to gas generation.
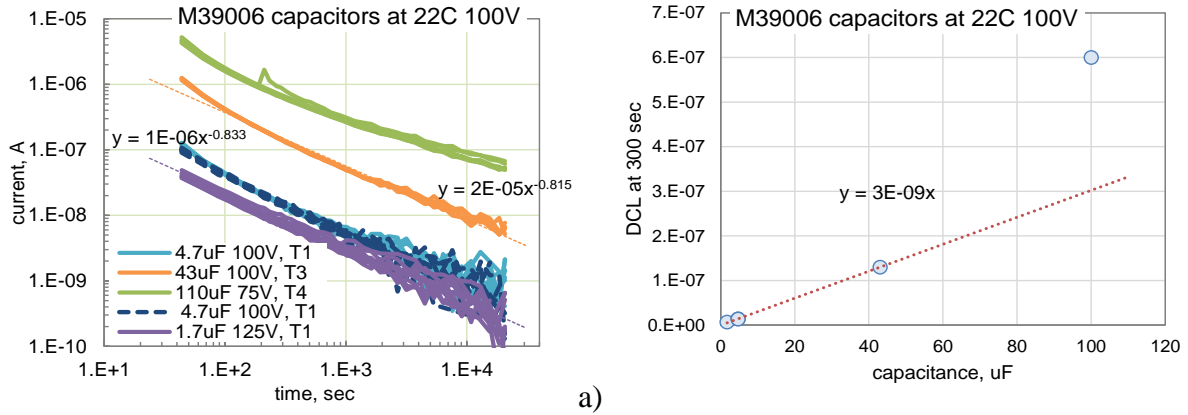
Figure I.3.5. Relaxation of polarization currents in different types of M39006 capacitors (8 to 10 samples in a group) (a) and a variation of DCL measured after 5 min of electrification with the value of capacitoance (b).

Transient polarization and depolarization currents are due to the charge absorption processes and can be defined as absorption currents. Absorption processes are well known in a variety of dielectric materials employed in different types of capacitors, including ceramic capacitors [23, 24]. Relaxation of absorption currents usually follow Curie-von-Schweidler law:

$$I(t) = I_0 \times t^{-n}$$

(I.3.1)

where I_0 and n are constants, and n is close to 1.

Analysis showed that currents that are typically measured in normal quality capacitors at room temperature within 5 min of electrification are due to absorption processes and are reproducible. A wide spread of DCL values within a lot indicates poor quality of dielectrics likely due to presence of defects in oxides. Note that depolarization currents in these capacitors are identical, which indicates that absorption currents do not depend on the presence of the defects.

I.4. Absorption capacitance.

Considering that amplitudes of absorption currents increase with voltage linearly and the slopes of *I-t* curves remain practically the same, the transferred charge, Q_t, or integral of currents with time, is also a linear function of voltage. This allows to define absorption capacitance, C_t, as $C_t = Q_t/V$.

The value of Q_t was calculated by approximating the absorption currents with a power law, Eq.(I.3.1) and integrating with time over a period from 1 sec. to 10^4 sec.

$$Q_t = \int_1^{1000} I_0 \times t^{-n} \times dt = \frac{I_0}{1-n} \times t^{1-n} \Big|_1^{10000}$$

(I.4.1)

Variations of Q_t with voltage for 4 types of similar capacitors rated to 50 V, but from different vendors, are shown in Fig. I.4.1a. Figure I.4.1b shows Q_t-V characteristics for six more types of capacitors. As expected, in all cases the characteristics are linear with the slopes indicating values of C_t.

There is a good correlation between the measured values of C_t and nominal capacitance of the parts C_0 (see Fig. I.4.1a). On average, $C_t = 0.12 \times C_0$. A similar relationship exists for ceramic capacitors [24]. However, for MLCCs C_t is almost two times greater, $C_t = 0.25 \times C_0$. Large value capacitors with $C_0 > 1$ mF, tend to have somewhat greater values of C_t, $C_t = 0.19 \times C_0$ (see Fig. I.4.2b)
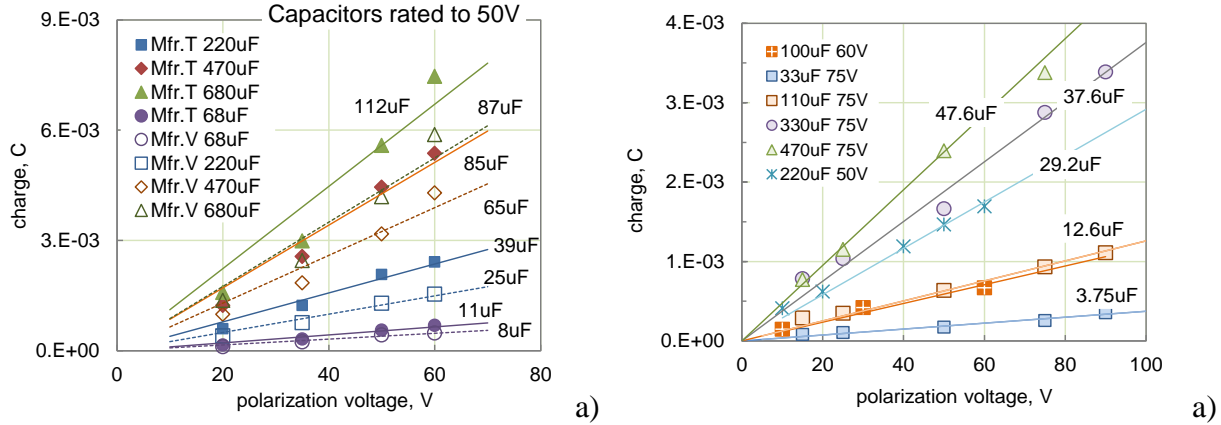

Figure I.4.1. Correlation between the absorbed charge and polarization voltage for capacitors from different manufacturers rated to 50 V (a) and for different part types (b).
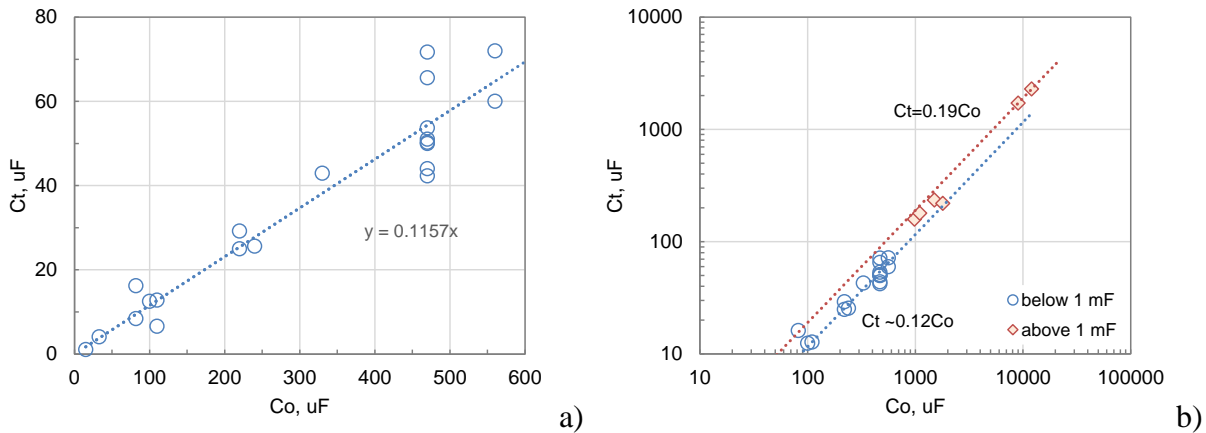

Figure I.4.2. Correlation between absorption and nominal capacitance for capacitors below 560 µF (a) and for all types of tested capacitors (b).

A poor temperature dependence of absorption currents, similar to what was observed for ceramic capacitors, is likely due to the tunneling of electrons into states (traps) located in the forbidden energy gap of the dielectric at the interface with the electrolyte.

I.5.   Comparison of requirements and experimental leakage currents

Results of DCL measurements based on 5 min electrification for various types of wet tantalum capacitors and relevant requirements are plotted against $C_0 \times VR$ values in Fig. I.5.1. Experimental data can be fairly well approximated with a linear function, $DCL_{exp} = 5 \times 10^{-5} \times C_0 \times VR$, where DCL is in µA, C_0 in µF, and VR in volts. The spread of the limiting DCL values (up to 10 times) for capacitors with similar CV values is much larger than for experimental data (~ 2 to 3 times). The margin for DCL is minimal for high CV

value parts (~ 2 times), and it is much greater for low CV (below 1000 µF×V) capacitors where the difference is ~ 2 orders of magnitude. Strangely enough, the margin is much greater for military capacitors than for new technology parts manufactured to DLA drawings. The drawings are typically written based on commercial specifications, and it is possible, that competition with other vendors forced manufacturers to squeeze the margins. In any case, the situation with the specifications for DCL needs to be clarified, and there is a need for establishing a procedure for determining DCL limits.

Considering a relatively small spread of absorption currents, a 5 times margin should be sufficient for normal quality capacitors, so the limit for DCL can be established at $2.5 \times 10^{-4} \times C_0 \times VR$.
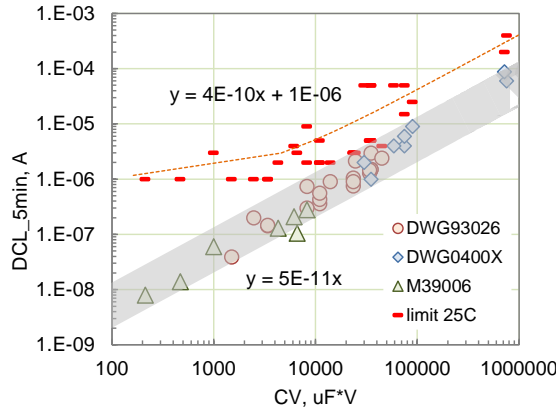

Figure I.5.1. Variations of experimental and specified values of DCL measured after 5 min of electrification with CV for wet tantalum capacitors. Red marks show the specified limits for the parts.

I.6.   A model for absorption currents

As was shown above, DCL measured per the existing procedure are mostly attributed to the absorption processes in the dielectric. This allows for simulation of DCL based on the Dow model similar to what has been done for MLCCs [24].

An equivalent circuit of a capacitor with absorption was suggested first for polystyrene capacitors by Dow in 1958 [25] and with some modifications is presented in Fig. I.6.2. The capacitor has a nominal value, C_0; resistor R_{il} is due to the intrinsic conduction of oxide, and R_d is related to the presence of defects in the dielectric. A series of $r_i - C_{ti}$ elements is connected in parallel to C_0. Here C_{ti} is an element of absorption capacitance and r_i is a resistance that controls charging/discharging of the element C_{ti} with a characteristic time $\tau_i = r_i \times C_{ti}$.

If a step voltage, V_0, is applied at $t = 0$, variations of the current with time can be given by a simple equation:

$$I(t) = \frac{V_0}{R_d} + \frac{V_0}{R_{i\,l}} + \sum_i \frac{V_0}{r_i} \exp\left(-t/\tau_i\right) \qquad (I.6.1)$$

Analysis shows that the exponent n in the Curie - von Schweidler law, Eq. (I.3.1), is equal to 1 if C_{ti} is constant and r_i increases exponentially for each consecutive $r_i - C_{ti}$ element. Experimental data for capacitors with a relatively slow decay, $n < 1$, can be simulated by increasing C_{ti} for larger r_i, and for parts with $n > 1$, by decreasing C_{ti} for larger r_i.

An example of calculations of absorption currents for a 470 μF 50 V capacitor using four $r_i - C_{ti}$ element ($C_{ti} = 1/4C_t$) is shown in Fig. I.6.1b. A comparison with experimental results (see Fig. I.3.3a) shows a reasonably good agreement with simulations. Obviously, by adding more $r_i - C_{ti}$ elements with characteristic times below 10^2 sec. or above 10^5 sec. the applicability of the Curie - von Schweidler law can be extended to a more considerable range of times.
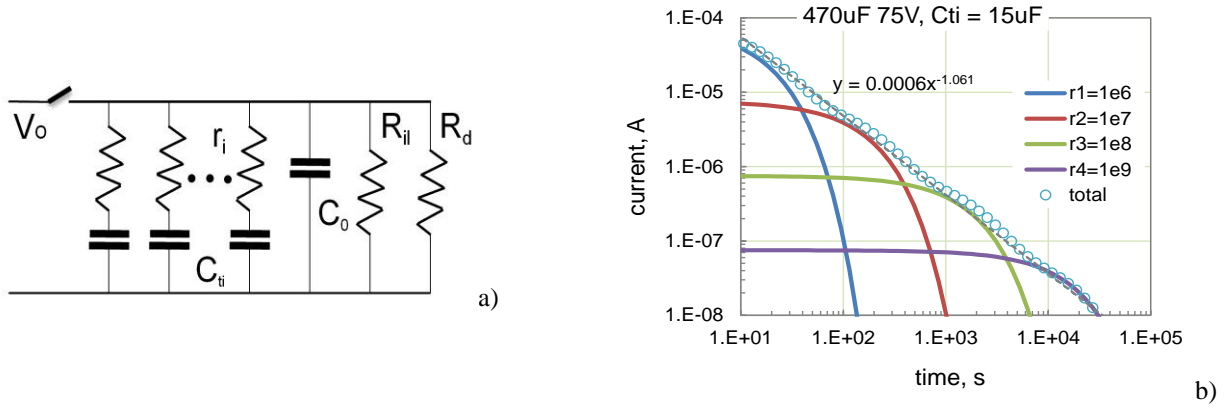

a)

b)

Figure I.6.2. An equivalent circuit for modeling leakage currents in wet tantalum capacitors (a) and simulation of absorption currents in a 470 μF 75 V capacitor for a case when $i = 4$, $C_{ti} = 15$ μF, $r_1 = 1E6$ ohm, and $r_{i+1} = 10\ r_i$

Relatively large values of C_t (~ 12% of C_0) result in large characteristic times, $\tau_i = 0.25 \times r_i \times C_t$, even for relatively small resistances r_i. This allows absorption currents to remain large for a sufficiently long period of time required for DCL measurements ($\Delta t = 300$ sec). Assuming that after the required electrification time, Δt, current in the capacitor is determined by the $r_i - C_{ti}$ element that has $\tau_i = \Delta t$, we can calculate DCL as:

$$DCL \approx \frac{VR}{r_{300}} = \frac{0.25 \times \alpha}{300} \times C_0 \times VR \qquad (I.6.2)$$

At $\alpha = 0.12$, $DCL \approx 10^{-4} \times C_o \times VR$, which is close to the experimental data.

I.7.   Intrinsic leakage currents.

Contrry to absorption currents that decrease with time according to a power law, intrinsic leakage currents are stable, but might change during long-term operation of the capacitors especially at high temperatures and voltages due to degradation processes, e.g. migration of oxygen vacancies (see section I.8).

Absorption and intrinsic leakage currents have also different temperature and voltage dependencies. Absorption currents do not change substantially with temperature and increase linearly with voltage. Intrinsic currents in anodic Ta2O5 dielectrics increase expponentially with temperature and voltage. It is commonly accepted that the conduction of anodic Ta2O5 dielectrics is due to electron transport. However, the mechanism of conduction in different papers was was attributed to the electrode-limited Schottky emission [26, 27], bulk-limited Poole-Frenkel transport [28, 29], or space charge limited conduction, SCLC [30]. In some works, different mechanisms were used to explain behavior of leakage currents at different ranges of temperature and voltage [30-34]. Most research related to the mechanism of conductivity of Ta2O5 dielectrics was obtained using test Metal-Insulator-Metal (MIM) structures or solid

tantalum capacitors; whereas only limited data on temperature and voltage dependence of currents exists for wet tantalum capacitors. This is likely due to a relatively narrow operational temperature and voltage ranges for these capacitors and to the prevalence of absorption currents during relatively short periods of electrification (typically, a few minutes).

In this study, measurements of intrinsic leakage currents were carried out for different types of wet tantalum capacitors in a wide range of temperatures (up to 165 ºC) and voltages typically from 0.2VR to 1.1VR. At each test condition, the currents were monitored with time to assure that transients due to absorption processes do not affect measurements and currents are stable with time.

Fig. I.7.1 shows that *I-V* characteristics of different types of capacitors plotted in *ln(I/V)* - $V^{0.5}$ coordinates can be approximated with straight lines. This is consistent with the Simmons models and suggests that the currents are limited by the energy barrier at the electrolyte/oxide interface.

Simmons [35] have modified Schottky model for solid dielectrics having small electronic mean free paths, so the current density can be written as a function of electric field *E*:

$$J_S = AT^{3/2} \mu E \exp\left(-\frac{\Phi_B}{kT}\right) \exp\left(\frac{\beta_s E^{0.5}}{kT}\right),$$
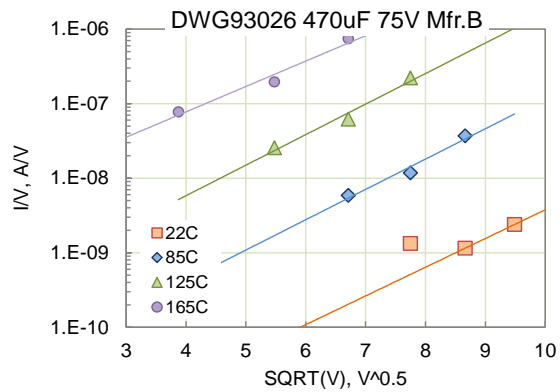
(I.7.1.a)

where, A = 3.08×10^{-4} A/cm^2_K$^{1.5}$, μ is the electron mobility in the insulator, and β_s is the Schottky constant:

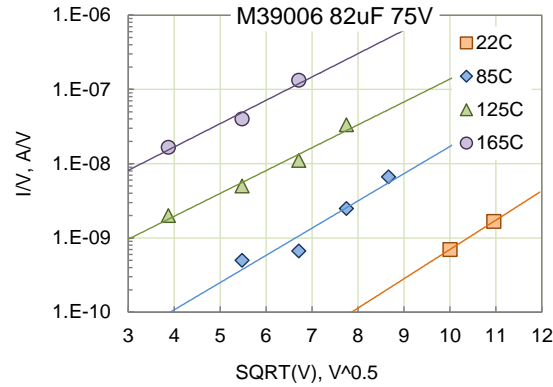$$\beta_s = \left(\frac{q^3}{4\pi\varepsilon\varepsilon_0}\right),$$

(I.7.1.b)

where, *q* is the charge of the electron, *k* is the Boltzmann constant, *T* is the absolute temperature, ε_0 is the permittivity of the free space, and $\varepsilon \sim 5$ is the high-frequency dielectric constant for Ta2O5 dielectrics.

a)

b)
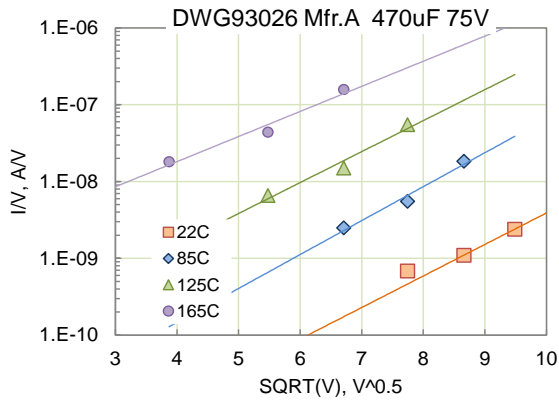
Figure I.7.1. Variations of leakage currents with square root of voltage for different types of wet tantalum capacitors.

According to Eq.(I.7.1), the slope of the *I-V* curves plotted in *ln(I/V)* - $V^{0.5}$ coordinates is inversely proportional to the absolute temperature, $\alpha = \beta_s/(kT \times d^{0.5})$. The thickness of the dielectric was calculated as $d = 1.7 \times a_F \times VR$, nm. The form factor, $a_F = V_F/VR$ was assumed 2.5 for the DLA drawing parts and 3.5 for the mil-spec capacitors. For capacitors rated to 75 V this gives dielectric thickness of 320 nm for DLA drawing and 450 nm for military grade capacitors respectively. Fig. I.7.2 shows that the slopes of I-V characteristics, α, are in a reasonable agreement with the Simmons model at temperatures in the range from 85 ºC to 165 ºC.
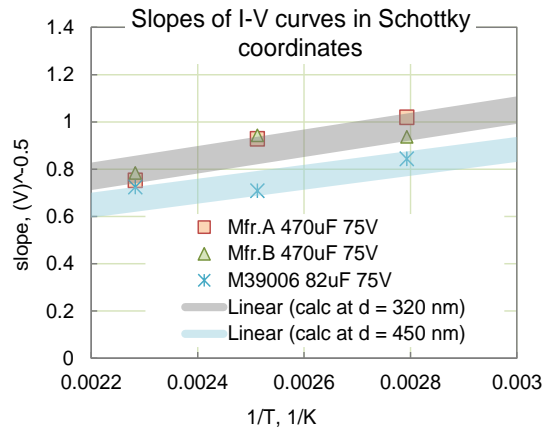

Figure I.7.2. Variation of slopes of the *I-V* curves in Schottky coordinates with temperature. Wide stripes are calculated slopes per the Simmons model, Eq.(I.7.1)

Temperature dependencies of currents at different voltages in Arrhenius coordinates are presented in Fig. I.7.3 and Fig. I.7.4. Activation energies, E_a, calculated as slopes of *I-T* characteristics in Arrhenius coordinates for are in the range from 0.65 eV to 0.85 eV. This range is close to the data reported in [27] for the Ta2O5/electrolyte systems, from 0.6 eV to 0.7 eV, and for solid tantalum capacitors [36], from 0.5 eV to 0.75 eV. The values of E_a obtained in this work depend on the part type and applied voltage. The effect of electrolyte type on leakage currents has been reported before [27], so the value of activation energy might slightly vary for different manufacturers.
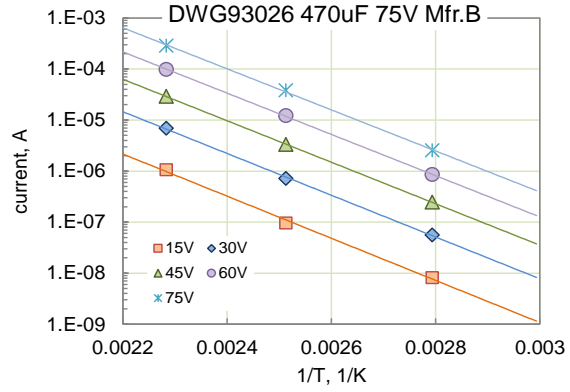
A decrease of E_a with voltage can be explained within the Simmons model:
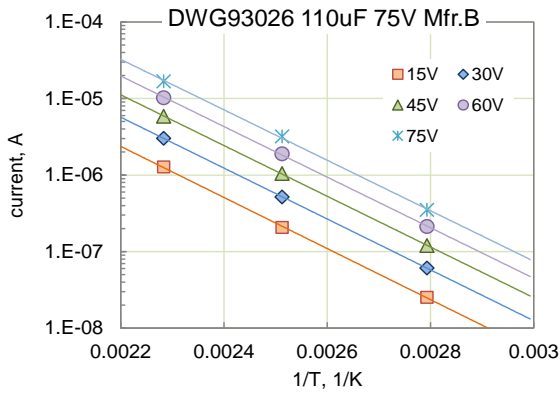
$$E_a = \Phi_B - \beta'_s E^{1/2},$$ (I.7.2)

where $\beta'_s = 0.034$ eV*(mm/V)$^{0.5}$
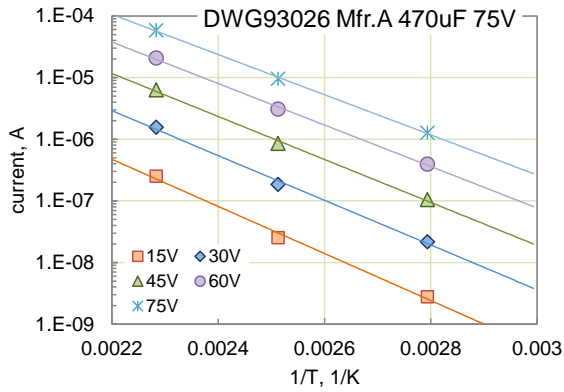
a)

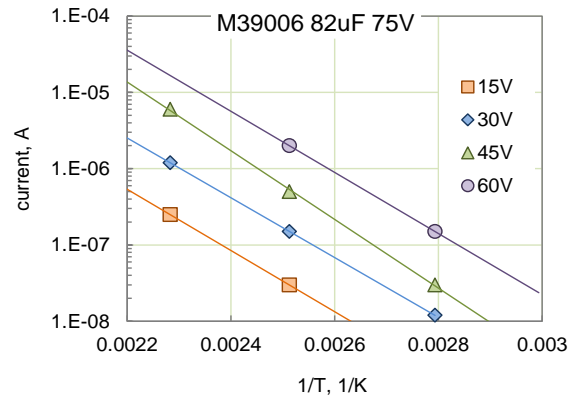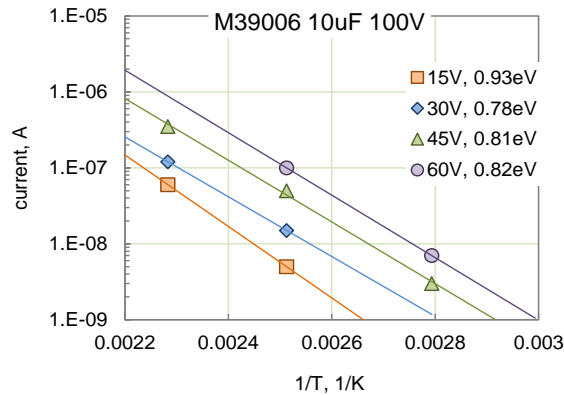b)

c)

d)

e)

Figure I.7.3. Temperature dependence of leakage currents for different types of capacitors.

Fig. I.7.5 shows that variation of activation energies with square root of voltage can be approximated with linear functions, and the slopes of $E_a - V^{0.5}$ lines is close to the calculated values. Based on results in Fig. I.7.5, the barrier height is in the range from 0.9 eV to 1 eV.
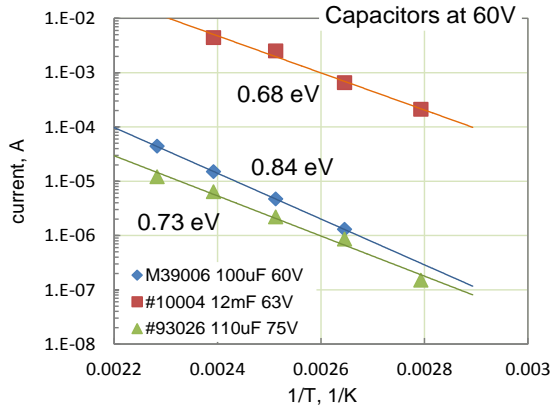
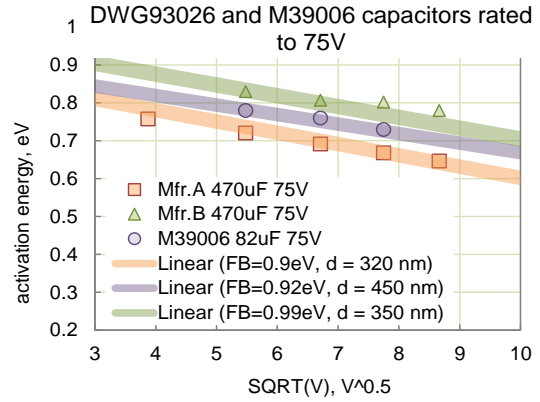Figure I.7.4. Temperature dependence of leakage currents in different types of wet tantalum capacitors.

Figure I.7.5. Voltage dependence of activation energy. Wide stripes are results of calculation per Eq.(I.7.2).

Extrapolations of high-temperature data to room conditions show that the intrinsic leakage currents of wet tantalum capacitors should be several orders of magnitude below the specified limits. For example, per DLA DWG93026 the specified value for 470 µF 75 V capacitors is 5 µA. The actual values measured at room temperature after 5 min electrification are ~ 1.6 µA, while the extrapolated values for the intrinsic currents are two to three orders of magnitude less, from 20 nA to 6 nA. This is consistent with results of long-term measurements of leakage currents in wet tantalum capacitors (see next section).

I.8. Long-term variations of leakage currents.

Results of long-term monitoring of leakage currents in different types of capacitors at room temperature and rated voltages are shown in Fig. I.8.1 and Fig. I.8.2. In normal quality capacitors, currents continue decreasing for more than 100 hours following the power law with the exponent close to 1 (Fig. I.8.1a and I.8.2a). Some deviations from the power law at low currents are likely due to the accuracy of the measurement system used that was ~ 1 nA.

Several samples of 470 µF 75 V capacitors shown in Fig. I.8.1b had anomalies manifested as increasing and unstable currents after ~one hour of operation. This behavior might be due to the presence of contamination in the tantalum pellet. It might cause excessive noise in the system and increase the risk of failures related to gas generation.

Similar instabilities in DCL were also observed in 12 mF 63 V capacitors (Fig. I.8.1c). These capacitors also featured a relatively large DCL values and wide spread of currents that were decreasing slowly with time. Long-term (up to 1000 hours) variations of currents with time that can be approximated with a power law, but the exponent, $n = 0.11$, is relatively small compared to what is observed for absorption currents. The reason for such behavior is not clear. It is possible that the oxide in these capacitors continue growing resulting in decreasing electric field in the dielectric, hence decreasing the currents.

A wide spread of leakage currents and instabilities caused by momentarily breakdowns followed by self-healing (scintillation events) were also observed during 100-hour testing at rated voltages and room temperatures for capacitors manufactured per DLA DWG#04005 and 10004 (see Fig. I.8.2c, e, and g). Note, that depolarization currents in all cases were highly reproducible and closely follow the power law

with the exponent close to 1. Obviously, absorption currents might obscure the presence of defects in dielectrics, and the effectiveness of DCL measurements for quality assurance purposes is low.

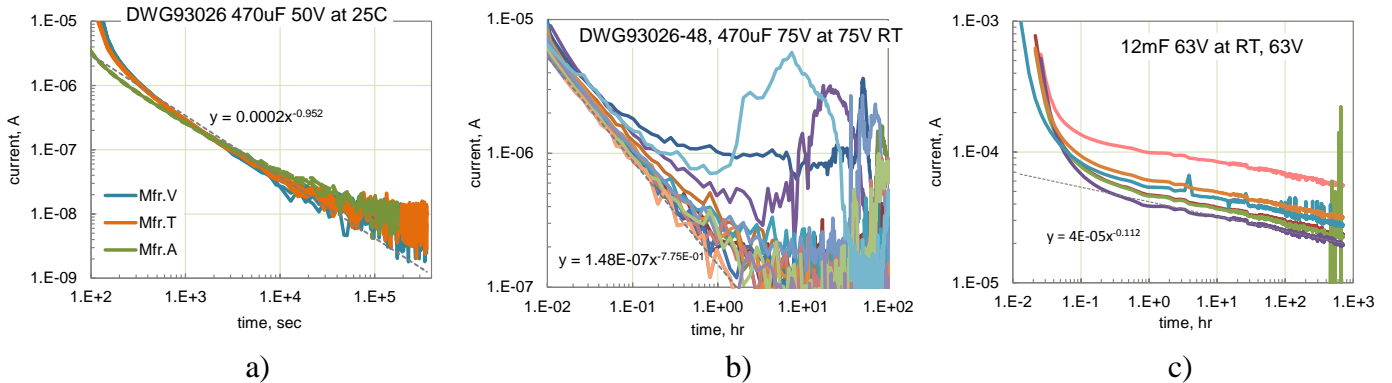a)   b)   c)

Figure I.8.1. Variations of leakage currents with time in different types of wet tantalum capacitors.
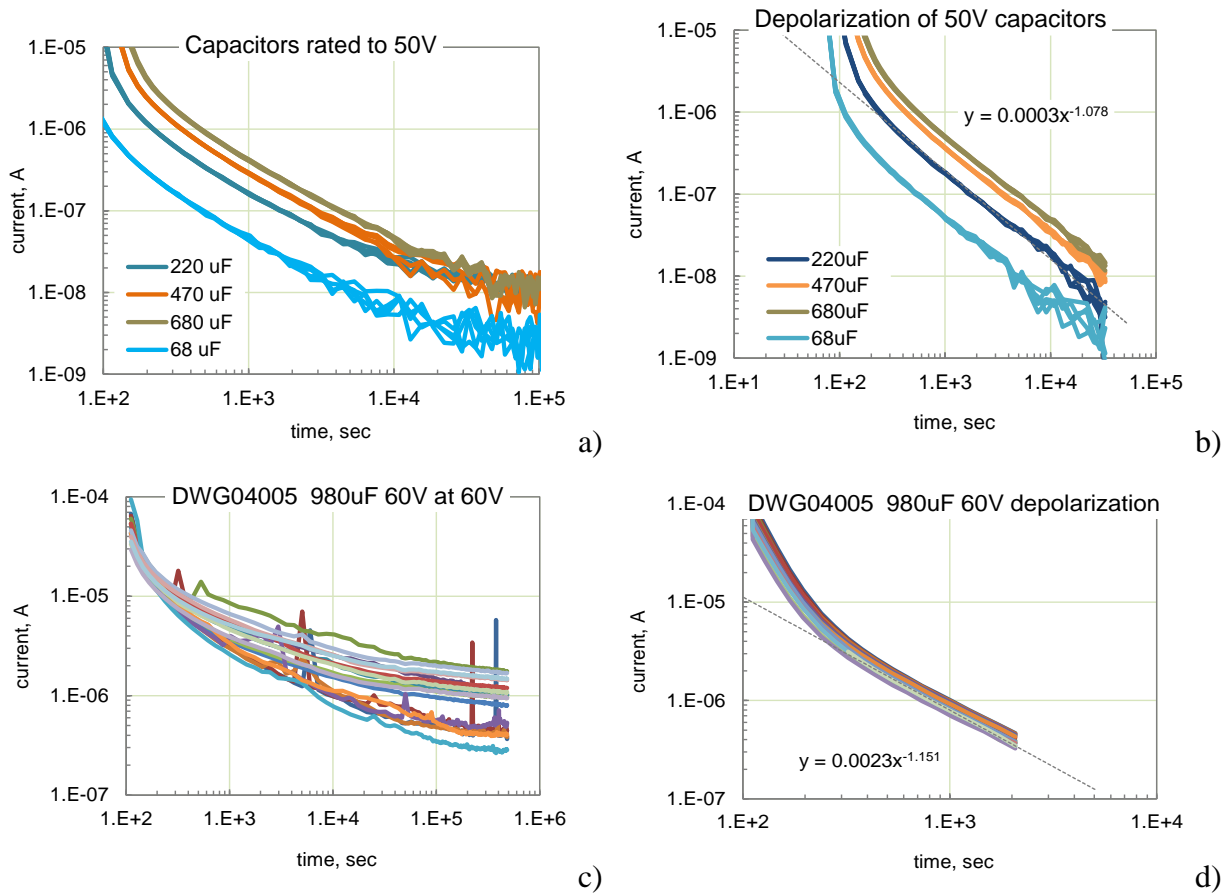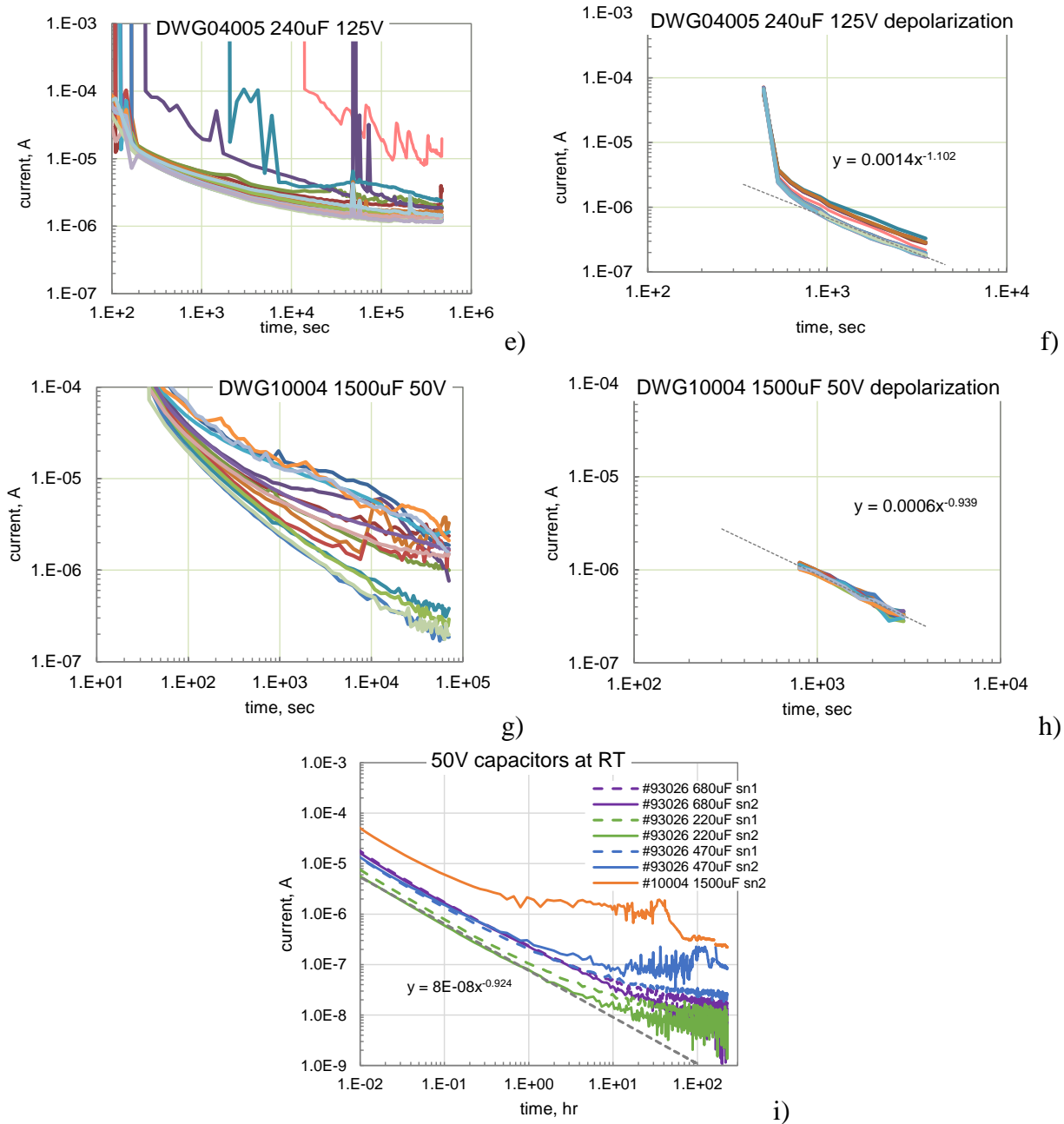
Figure I.8.2. Long-term variations of leakage currents at room temperature under rated voltages (a, c, e, g, i) and depolarization currents (b, d, f, h) in different types of wet tantalum capacitors.

Variations of currents in 330 μF 75 V capacitors and two lots of 470 μF 75 V capacitors during 100-hour testing at high temperatures (125 ℃ and 105 ℃) are shown in Fig. I.8.3. In both cases, currents are increasing with time after ~ 20 hours during 125 ℃ testing and ~50 hours during 105 ℃ testing. This degradation is similar to what was observed for solid tantalum capacitors and is likely due to migration of oxygen vacancies [37]. The trend of increasing with time leakage currents is often observed during long-term (up to 10,000 hours) life testing of wet tantalum capacitors [6]. Degradation caused by migration of oxygen vacancies has relatively large activation energy, ~1.1 eV, and strongly depends on the applied

voltage. For this reasons, the probability of observing this degradation at operating conditions, where voltages are typically derated to below 0.6VR and temperatures do not exceed ~ 60 ℃, is small.

Two lots with different date codes that were used for testing at 105 ℃ had different behavior of leakage currents. Lot LDC2 had a much wider spread of leakage currents. One sample in this lot had a sharp increase of DCL by more than 20 times after ~ 3 hours of testing, behaved erratically for dozens of hours, but eventually, after ~ 30 hours the current started gradually decreasing to the initial value. Samples in LDC2, contrary to LDC1 virgin samples, passed various qualification tests that might have caused damage to the dielectric. This damage was not detected during the qualification testing likely because no monitoring of leakage currents is currently required.

The results indicate that that leakage currents in wet tantalum capacitors are decreasing with time for a good quality parts only. Poor quality parts, even if they passed DCL measurements during screening might have unstable currents. This not only creates excessive noise in the system, but also increases risks of failures related to electrolysis of electrolyte, gas generation, and rupture of the case.
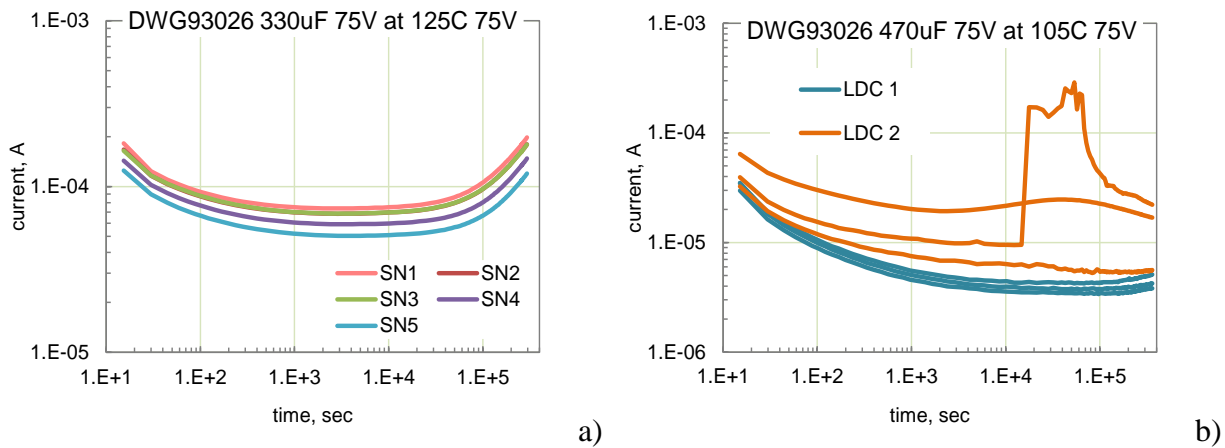

Figure I.8.3. Variations of leakage currents with time at high temperatures. a) DLA DWG93026, 330 µF 75 V capacitors during 100-hour HALT at 125 ℃ and 75 V. b) Two lots of DLA DWG93026, 470 µF 75 V capacitors during 100-hour HALT at 105 ℃ and 75 V. Note that samples with LDC1 are virgin and with LDC2 are after qualification testing.

Part II. Gas generation and internal pressure in wet tantalum capacitors.

II.1. Assessments of the electrolyte leak in wet tantalum capacitors.

Due to the case seal leak, a certain amount of the electrolyte might be lost with time of operation or storage of wet tantalum capacitors. Contrary to aluminum electrolytic capacitors that are not hermetic and evaporation of electrolyte is one of the major reliability concerns, tantalum capacitors are manufactured in hermetic cases and their hermeticity is supposed to be assured by qualification testing at the level of 1E-8 atm_cc/s, He. However, only 12 samples are tested, and one is allowed to fail. All samples are required to be screened for gross leak test only, so the parts are guaranteed to have leaks less than ~ 1E-5 atm_cc/s, He. Although the electrolyte drying is likely an extremely rare event in wet tantalum capacitors, it is important to understand what level of assurance, that such events would not happen, is provided by the existing seal leak requirements.

Assuming that the partial pressure of electrolyte outside the case is negligible, the amount of electrolyte, Δm, escaped after time t can be estimated if the vapor pressure inside the package, P_{el}, and the value of the electrolyte leak rate, L_{el}, that is determined at a pressure difference of 1 atm, are known:

$$\Delta m = L_{el} \times P_{el} \times t \ , \tag{II.1.1}$$

The pressure of vapor above the electrolyte (~40% solution of the sulfuric acid in water) in the package of wet tantalum capacitor is exponentially increasing with temperature [38]:

$$\log(P_{el}) = A_{el} - \frac{B_{el}}{T} \ , \tag{II.1.2}$$

where P_{el} is in tor, $A_{el} = 8.87$ and $B_{el} = 2286$ are constants; T is the temperature in K.

The pressure of saturated water can be calculated using a similar equation:

$$\log(P_w) = A_w - \frac{B_w}{C_w + T} \ , \tag{II.1.3}$$

where $A_w = 8.07$, $B_w = 1730.6$, and $C_w = -39.6$ for 0 °C $< T <$ 99 °C, and $A_w = 8.14$, $B_w = 1810.9$, and $C_w = -28.5$ for 100 °C $< T <$ 200 °C.

Figure II.1.1 shows variations of the pressure for the sulfuric acid when temperature varies from room to 200 °C. For comparison, the same chart shows variations of the saturated water pressure. At 22 °C, the pressure of electrolyte in a tantalum capacitor would be 13.2 tor or 0.017 atm, which is slightly below the pressure of saturated vapor for pure water: 19.7 tor, or 0.026 atm. As temperature increases, the difference in pressures decreases, and at 200 °C it is 14.4 atm for the electrolyte and 15.4 atm for pure water.

Leaks smaller than 10^{-6} atm*cc/s are considered to be due to a molecular flow, so the leak rate for a gas with a molecular mass M can be calculated using the Knudsen's formula:

$$L = \frac{\sqrt{2\pi}}{6} \sqrt{\frac{RT}{M}} \frac{d^3}{l} (P_1 - P_2) \ , \tag{II.1.4}$$

where P_1 is the pressure inside the case; P_2 is the pressure outside the case; d is the diameter of the leak; l the length of the leak.

Maximum measured leak rate specified for tantalum capacitors per MIL-PRF-39006 at room temperature, T_0, is $R_1 = 10^{-8}$ atm*cc/s He, which, as it will be shown in section II.2, corresponds to the standard air leak rate of $L_{air} = 1.55{\times}10^{-7}$ atm×cc/s air (M = 29 g/mol). The molecular weight of the electrolyte can be estimated proportionally for the mixture of sulfuric acid (M = 98 g/mol) and water (M = 18 g/mol), which yields 58 g/mol. Because the leak rate is inversely proportional to the square root of molecular weight, the leak rate for sulfuric acid is $1.1{\times}10^{-7}$ atm×cc/s ($1.1{\times}10^{-8}$ Pa×m^3/s).

Taking into account that the pressure of electrolyte follows Eq. (II.1.2) and the amount of leaked gas can be calculated as $n = PV/RT$, the rate of leak was calculated at different temperatures (see Fig. II.1.2). At room temperature the electrolyte is leaking at a rate of $4.1{\times}10^{-12}$ g/s and the rate increases to $8.9{\times}10^{-11}$ g/s at 85 °C and to $2.2{\times}10^{-9}$ g/s at 200 °C.
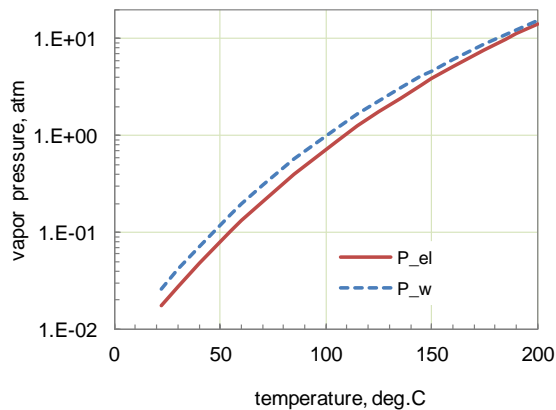

Figure II.1.1. Variations of saturated vapor pressure above 35% solution of H_2SO_4 in water and above pure water.
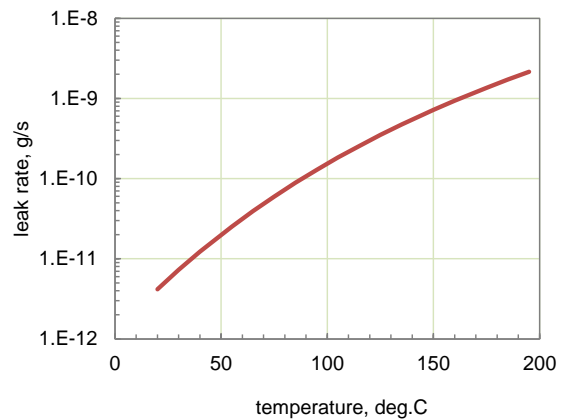
Figure II.1.2. Variation of the electrolyte leak rate with temperature for a case with the measured leak rate 10^{-8} atm*cc/s He.

The amount of electrolyte that escapes with time from a case of a tantalum capacitor was calculated per Eq.(II.1.1) at different temperatures from room to 200 °C (see Figure II.1.3). These calculations were made for a capacitor with a measured leak rate equal to the specified limit of 10^{-8} atm*cc/s He. The results show that in 10 years after sealing, the amount of electrolyte will decrease by 1.3 mg at 22 °C and by 28 mg at 85 °C. These values are less than the amount of electrolyte typically used in wet tantalum capacitors, from ~50 mg in T1 cases to several hundred milligrams in T4 and larger, 04005 cases. Exposure of the part to 200 °C for one month would cause loss of the electrolyte by 5.6 mg only, which is negligible for large size cases. Note, that the calculated values of Δm after 10 years of storage are comparable with the amount of electrolyte in small case size (T1) capacitors. For these parts it would be reasonable to tighten the requirements for the hermeticity leak testing.

The fine leak testing for military grade capacitors is required during qualification testing only, whereas only gross leak test is carried out during screening. This means that some parts might have measured leak rate up to 10^{-5} atm*cc/s He and pass the screening. At this leak rate the risk of electrolyte drying during long-term operation is substantial. For space applications, the risk of electrolyte escaping is related not

only to a possible degradation of capacitors, but also to contamination of sensitive optical equipment. To avoid these risks, fine leak testing should be done as a part of the screening process. Also, a high-temperature storage testing, 1000 hours at 150 C, as it was suggested in [39] would provide assurance that the leak of electrolyte is contained and does not pose a reliability risk.
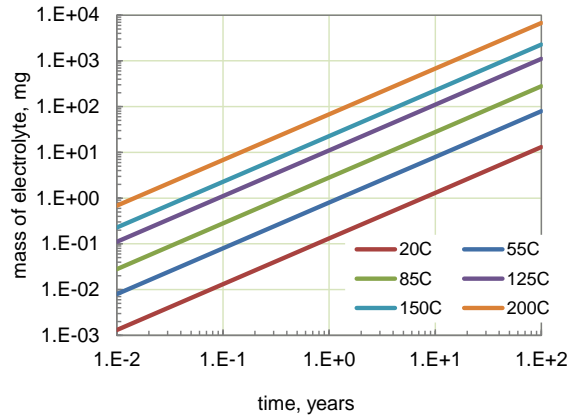

Figure II.1.3. Amount of electrolyte escaped at different temperatures from a capacitor having a measured helium leak rate of 10^{-8} atm*cc/s.

II.2.   Hydrogen generation and distribution.

A voltage applied to a normal quality wet tantalum capacitor drops mostly across a thin tantalum pentoxide dielectric, and the voltage across the electrolyte is negligibly small. However, in the presence of a defect in the dielectric, in local areas corresponding to these defects the voltage across the electrolyte might raise above the threshold voltage (~1.2 V for water). In these areas the electrolyte decomposes resulting in hydrogen generation at the cathode according to the half-reaction:

$$2e^- + 2H_2O(L) => H_2(g) + 2OH^- (aq) .$$ (II.2.1.a)

Anodic reaction results in generation of oxygen:

$$4OH^- => O_2(g) + 2H_2O + 4e^-.$$ (II.2.1.b)

Part of the oxygen might be used to continue oxidation of tantalum in cases the defects are cracks in the dielectric, but in case of contaminations in the oxide, e.g. carbon, oxygen will be released in a gaseous form and increase pressure in the case. A schematic of the process of gas generation is shown in Fig. II.2.1. It is assumed that in capacitors with a good quality of the tantalum pentoxide dielectric the applied voltage is dropped mostly across the dielectric and leakage currents are due to absorption, I_{abs}, and intrinsic conduction, I_{ic}, of the dielectric. In the presence of defects, such as cracks, thinning of the dielectric and foreign particles, the local current density is high and a large proportion of the applied voltage can be dropped across the electrolyte. Although the total current associated with defects might be small compared to I_{abs} and I_{ic}, during a long period of time it might generate enough gas pressure to cause failures of the part.

During electrolysis of water, for each mole of generated oxygen, two moles of hydrogen are generated, so if a portion of oxygen consumed by oxidation is negligible, 2/3 of the built pressure is due to hydrogen and 1/3 to oxygen. In the following analysis, the excessive gas pressure is assumed to be generated by hydrogen. At normal conditions, reverse reaction of H2 and O2 resulting in formation of water does not occur. This process is possible at high temperatures (above 570 ºC) only and results in combustion.
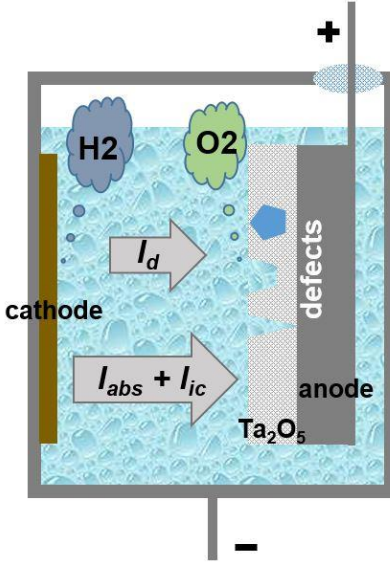
Figure II.2.1. A simplified schematic of a gas generation process in a case of wet tantalum capacitor.

According to reaction at the cathode, II.2.1a, 2 moles of electrons are required to produce a mole of hydrogen. According to the Faraday's law, the mass of hydrogen, m, is proportional to the transferred charge, Q:

$$m = \frac{M}{z \times F} \times Q ,$$ (II.2.2)

where, $M = 2$ g/mol is the molar mass of hydrogen, $z = 2$ is the number of moles of electrons needed to form one mole of H2, and $F = 96,485$ C/mol is the Faraday constant. In this case,

$$n_m = \frac{m}{M} = 5 \times 10^{-5} \times Q ,$$ (II.2.3)

where Q is in Coulombs and $n_m = m/M$ is the amount of moles of H2.

Assuming that leakage current in a capacitor, I, is constant, $Q = I \times t$. Variations of the amount of hydrogen with time of electrolysis at different levels of the current are shown in Fig. II.2.2a. For a capacitor having leakage current of 1 µA approximately 3 mg of hydrogen can be generated after 10 years of operation.

Assuming that all generated hydrogen remains in the case of a volume V, the gas pressure, P, can be calculated using the gas law:

$$P = n_m \times \frac{RT}{V} ,$$ (II.2.4)

where $R=8.13$ J/K is the universal gas constant; T is the absolute temperature.

Variations of pressure with time in a case with volume 1 cm^3 at different currents in a capacitor are shown in Fig. II.2.2b. Even at a relatively small leakage current of 1 µA, the gas pressure after 10 years of operation can reach ~ 40 atm. As it will be shown in section II.4, this pressure is close to the critical level that can cause rupture of the case.
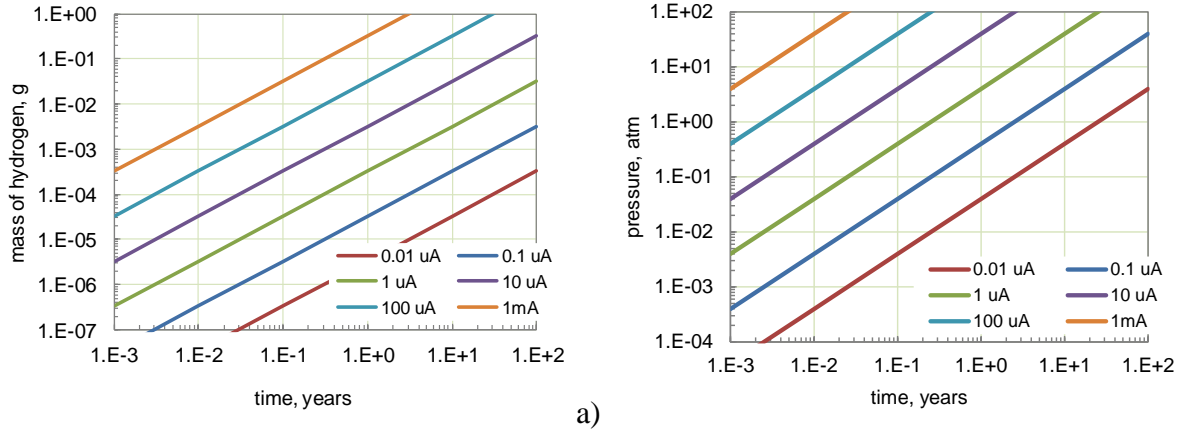
Figure II.2.2. Mass of hydrogen released by the electrochemical decomposition of electrolyte (a) and increase in pressure in a 1 cm^3 case (b) calculated at different levels of leakage current.

These calculations were made in an assumption that all generated gas builds up pressure in the can. To get more accurate estimations, we need to take into account the possibility of hydrogen leak, absorption in the electrolyte, cathode layers, and in tantalum.

Absorption in electrolyte.

At room temperature, the solubility of hydrogen in water is 1.6 mg of H2 in 1 kg of H2O and the diffusion coefficient of H2 in water is $D \approx$ 5E-5 cm^2/sec [40]. It is reasonable to assume that the electrolyte would have a similar diffusion coefficient and solubility. The time of diffusion of H2 into a layer of electrolyte is l^2/D, where l is the thickness of the electrolyte layer. Assuming $l \sim 1$ mm, the time of diffusion is ~ 200 sec, so the process of hydrogen diffusion occurs relatively quickly.

The amount of hydrogen dissolved in the electrolyte can be estimated using the Henry's law, according to which the solubility of a gas in a solvent is directly proportional to the partial pressure of that gas above the solvent:

$$n_{el} = k_H \times V_{el} \times \Delta P \quad , \tag{II.2.5}$$

where k_H is a constant that for H$_2$/water system is 7.8×10^{-7} mol/cc_atm.

Assuming that a similar value of k_H is valid for electrolyte, for a volume of electrolyte $V_{el} = 1$ cm^3 and pressure of 1 atm, Eq.(II.2.5) yields $n_{el} = 7.8×10^{-7}$ mol. This corresponds to the absorbed mass of hydrogen of 1.6×10^{-6} g. At a pressure of 40 atm the absorbed mass would be $\sim 6.4×10^{-5}$ g, which is still much less than the estimated amount of hydrogen generated at 1 μA over a period of 10 years, 3×10^{-3} g.

Absorption in tantalum.

It is known that tantalum may absorb large quantities of hydrogen that results in its embrittlement and increase in electrical resistance. The tensile strength of tantalum reduces from 450 MPa at 1 ppm H to 170 MPa at 312 ppm H. It is generally accepted that 100 ppm is the hydrogen threshold level for maintaining acceptable ductility levels in tantalum [41]. Annealing tantalum in a high vacuum at high temperatures (~ 800 °C) eliminates the effect. Absorption of atomic hydrogen that happens typically at cathodes in electrolytic cells can occur at room temperatures. The absorption increases in cold work areas of tantalum because of generation of high concentration of dislocations and vacancies. This makes crimped areas especially vulnerable to embrittlement and fracture. Failures due to the case rupture at the

crimped areas have been observed before [16]. Experience with DPA of capacitors after life testing also shows that the brittleness of tantalum cases for the tubular style and cathode plates for the button style capacitors increase substantially. Obviously, the greater the rate of hydrogen generation during operation, the more brittle tantalum cathode became.

Diffusion coefficient of hydrogen in tantalum at room temperature is relatively large $\sim (1\text{-}2) \times 10^{-6}\,cm^2/sec$, and the activation energy is relatively low, 0.14 eV to 0.18 eV [42-44]. Considering that the thickness of the tantalum case is $\sim$ 0.2 to 03 mm, the diffusion time is in the range from 200 sec to 900 sec, which is negligible compared to operation times of capacitors.

At room temperature and pressure of hydrogen of 1 atm, concentration of H in tantalum (H/Ta) is 0.71 [45]. Atomic weights of H and Ta are 1 and 181 respectively. At a density of 16.4 g/ cm^3 one cm^3 of tantalum will have 16.4/181 =0.091 mol of Ta and 0.71×0.091 = 0.064 mol of H. The latter corresponds to 0.064 g of hydrogen in cm^3. Considering that the volume of tantalum in a cylindrical case having thickness 0.2 to 0.3 mm and volume of 1 cm^3 is ~0.1 to 0.2 cm^3, the amount of hydrogen absorbed at P_{H2} = 1 atm is from 6 mg to 13 mg, which is comparable with the estimated amount of hydrogen generated after 10 years of operation at leakage currents of a few microamperes.

Absorption in cathode layer (RuO2)

Hybrid tantalum capacitors manufactured by Evans Capacitors employs ruthenium oxide as a cathode material [7, 8]. The hydrous form of ruthenium oxide (RuO2.xH(2)O) is considered one of the best materials for electrochemical pseudocapacitors. The charge storage mechanism is believed to be faradaic and involves bulk electrochemical protonation of the oxide [46, 47]:

$RuO_x(OH)_y + zH^+ + ze^- \longleftrightarrow RuO_{x-d}(OH)_{y-d}$
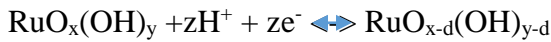
For rough estimations we can assume that each molecule of RuO2 is capable to react and store a charge of one proton. Considering a molecular mass of RuO2 133 g/mol, density 6.97 g/cm^3, for a cathode disk having diameter 1.2 cm and the thickness of RuO2 layer 100 μm, total amount of ruthenium oxide is 5.9×10^{-4} mol. This corresponds to the absorbed charge of 57.2 C. At a current of 10 μA, this charge can be transferred in ~2.2 months. After that, hydrogen gas will be generated according to reaction II.2.1.a. These estimations show that although a substantial amount of hydrogen can be absorbed in the cathode layer, a tight control over the leakage currents is necessary to assure long-term reliable operation of wet tantalum capacitors.

Effect of the seal leak

To assess the leak rate of hydrogen, we need first to assess the standard air leak rate based on the measured leak, R_1, which is determined using a helium leak detector according to MIL-STD-202, TM112, procedure IIIc. For a part with volume V and the standard air leak rate L the measured helium leak rate R_1 can be calculated as follows:

$$R_1 = \frac{L \times P_E}{P_o} \times \left(\frac{M_A}{M}\right)^{1/2} \times \left\{1 - \exp\left[-\frac{L \times t_1}{V \times P_o} \times \left(\frac{M_A}{M}\right)^{1/2}\right]\right\} \times \exp\left[-\frac{L \times t_2}{V \times P_o} \times \left(\frac{M_A}{M}\right)^{1/2}\right] \tag{II.2.6}$$

where P_E is the pressure of He exposure (usually 4 atm); P_0 is the atmospheric pressure (usually 1 atm); M_A is the molecular weight of air (28.7 grams); M is the molecular weight of helium (4 grams); t_1 is the

time of exposure to P_E (4 hours); t_2 is the dwell time between release of pressure and leak detection (1 hour).

Variations of the measured leak rate with the standard air leak rate are shown in Figure.2. The maximum acceptable leak rate for tantalum capacitors is $R_1 = 10^{-8}$ atm×cc/s He. According to Eq.(II.2.6) and Figure II.2.3, this level of the measured leak rate corresponds to the standard air leak rate of $L_{air} = 1.55 \times 10^{-7}$ atm×cc/s air.
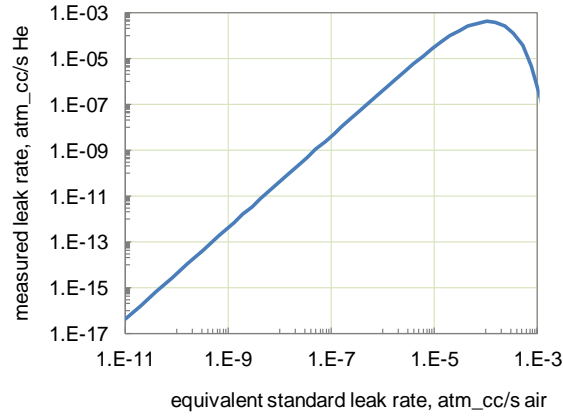

Figure.II.2.3. Measured leak rate, R_1 vs. the standard leak rate, L, calculated per Eq.(8).

Considering that the leak rate is inversely proportional to the square root of the molecular weight, the leak rate for hydrogen would be $L_{H2} = 1.55 \times 10^{-7} \times (M_{air}/M_{H2})^{0.5} = 5.9 \times 10^{-7}$ atm×cc/s $= 5.9 \times 10^{-8}$ Pa×m^3/s. Dividing by RT, at room temperature equal to 2439 J, the leak rate is $L_{H2} = 2.4 \times 10^{-11}$ mol/s $= 4.8 \times 10^{-11}$ g/s. At this rate, ~15 mg of H2 would be released during 10 years if the pressure of H2 inside the can is maintained at 1 atm. A comparison with data in Fig. II.2.2 shows that this value is similar to the amount of H2 generated for 10 years at $I \sim 1$ µA, so the seal leak should be considered for calculations of the pressure inside the can.

The leak rate through the seal should be compared with the flow of hydrogen across the surface of the case caused by permeability of tantalum to hydrogen. For diatomic molecule the solubility of a gas is described by the Sieverts' law that states that the solubility is proportional to the square root of the partial pressure of the gas, $c = K_s \times P^{0.5}$, where c is in wt% of hydrogen in Ta. For this case, the flow across the surface S can be expressed as:

$$Q = S \times D \times K_s \times \rho_{Ta} \times \frac{\sqrt{P}}{d} \quad , \tag{II.2.7}$$

where S and d are the surface and wall thickness of the case, and K_s is the Silvert's constant, $\rho_{Ta} = 16.4$ g/cm^3 is the density of tantalum.

Approximations using data presented in [48] to room temperature result in $K_s \approx 50$ atm$^{-0.5}$. Assuming that a tantalum case of volume 1 cm^3 with $d = 0.2$ mm and $S = 6$ cm^2 has internal hydrogen pressure of 1 atm, at $D \approx 10^{-6}$ cm^2/s, the flow is: $Q = 6 \times 10^{-6} \times 50 \times 16.4 \times 1^{0.5}/0.02 \approx 10^{-4}$ g/s.

This flow exceeds substantially the flow of H2 estimated based on the seal leak rate. Note that diffusion coefficients of oxygen in tantalum (~10^{-20} cm^2/s, [49]) are many orders of magnitude less than for

hydrogen. This means that while hydrogen might escape even from hermetic cases relatively easily, generated oxygen will remain in the case and maintain constant pressure unless seal leak is large enough to allow for oxygen escape.

II.3. Internal gas pressure

Excessive pressure in the case of a tantalum capacitor is formed by the balance between generation and release of gas molecules. The rate of gas generation in moles per second is determined by leakage current as a result of electrolysis and can be presented as:

$$G = \frac{I}{z \times F} \quad, \tag{II.3.1}$$

A part of the generated gas molecules will escape from the package through seal leaks. The rate of release of gas molecules, R, in moles per second, is determined by the leak rate L in assumption that the partial pressure of the electrolyte outside the package is negligible:

$$R = \frac{L}{RT} \times \frac{P}{P_0} \quad, \tag{II.3.2}$$

where, as it was shown above $L = 6 \times 10^{-8}$ Pa$\times$m^3/s, P is the internal pressure in the case, P_0 is the atmospheric pressure, at which the leak rate was determined, and RT at room temperature is 2439 J. Considering that the pressure is determined by the amount of gas in the case (Eq. (II.2.4)), the above equation can be presented in a form:

$$R = \frac{L}{P_0 \times V} \times n \quad, \tag{II.3.3}$$

Using these definitions, variation of concentration of gas molecules in the case can be expresses as follows:

$$\frac{dn}{dt} = G - R \ , \quad \text{or} \quad \frac{dn}{dt} = \frac{I}{zF} - \frac{n}{\tau} \ , \tag{II.3.4}$$

where the characteristic time of the pressure build-up is $\tau = \dfrac{P_0 \times V}{L}$.

A solution to this equation can be presented as follows:

$$n(t) = \tau \frac{I}{zF} \times \left(1 - e^{-t/\tau}\right), \tag{II.3.5}$$

Respectively, variation of the case pressure with time is:

$$P(t) = \frac{P_0 \times RT}{L} \times \frac{I}{zF} \times \left(1 - e^{-t/\tau}\right), \tag{II.3.6}$$

For the case having the measured leak rates 10^{-9} atm$\times$cc/s He and 10^{-8} atm$\times$cc/s He calculations for a capacitor having volume 1 cm^3 at leakage currents in the range from 0.01 µA to 100 µA are shown in Fig. II.3.1. At the leak rate 10^{-8} atm$\times$cc/s He the characteristic time is 19.5 days, and the steady-state pressure at leakage current of 1 µA is ~0.2 atm. An increase in leakage currents increases the pressure

proportionally. For example, at 100 µA the steady state pressure is ~ 20 atm and exceeds 1 atm after approximately 10 days.

The lower the leak rate, the higher the level of pressure that can be achieved. For capacitors with the leak rate of 10^{-9} atm*cc/s He, which is only 10 times less than the specified level, 1 µA current would increase pressure above 2 atm after 1 year of operation. For a case with volume of 1 cm^3 variations of the steady-state pressure with leakage current at different levels of the measured helium leak rate are shown in Fig. II.3.2. Even at leakage currents as low as 0.01 µA, the pressure increases to ~2 atm when the leak rate is ~ 10^{-11} atm*cc/s He. However, due to a large characteristic time (2.2 years), it will take more than 5 years to achieve this level of pressure.
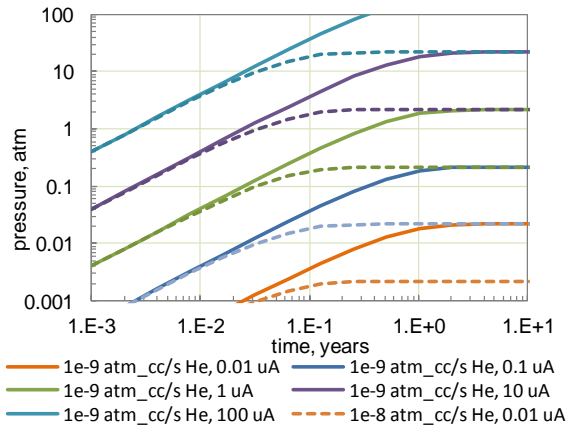

Figure II.3.1. Variations of pressure in a wet tantalum capacitor with volume 1 cm^3 at different levels of leakage currents and the measured leak rate of 10^{-8} atm*cc/s He (dashed lines) and 10^{-9} atm*cc/s He (solid lines).
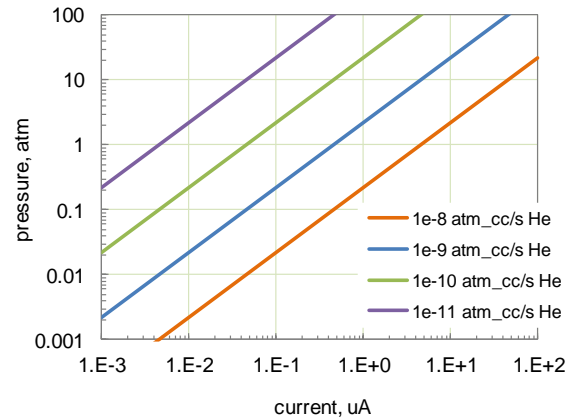
Figure II.3.2. Steady-state pressure at V = 1 cc and variation of characteristic time with the leak rate for different types of package.

Case sizes (the length of the cylinder, L and its radius, R) as well as the calculated volume, V_0, for different types of wet tantalum capacitors are shown in Table II.3.1. Because a part of the case volume is occupied by the anode slug, Teflon isolators, and gaskets, the volume available for gas accumulation was calculated as 0.5×V_0 for 93026-style capacitors and 0.35×V_0 for 0400X-style capacitors.

Table II.3.1. Size of wet tantalum capacitors.

	#93026 T1	#93026 T2	#93026 T3	#93026 T4	#93026 L2	#04005	#04003
L, mm	11.5	16.3	19.5	27	25.6	7	15
R, mm	2.4	3.6	4.8	4.8	3.6	7.5	18
V, cm^3	0.21	0.66	1.41	1.95	1.04	1.24	15.27
available volume, cm^3	0.10	0.33	0.71	0.98	0.52	0.43	5.34

Characteristic times of the pressure variations for different types of capacitors were calculated based on the value of the available volume shown in Table 1. Results of these calculations are shown in Fig. II.3.3 In the expected range of leaks, from 10^{-9} to 10^{-11} atm*cc/s He, τ varies from 20 days to half a year for the smallest size, case T1 capacitors, to many years for large-size, DLA DWG04003, capacitors.
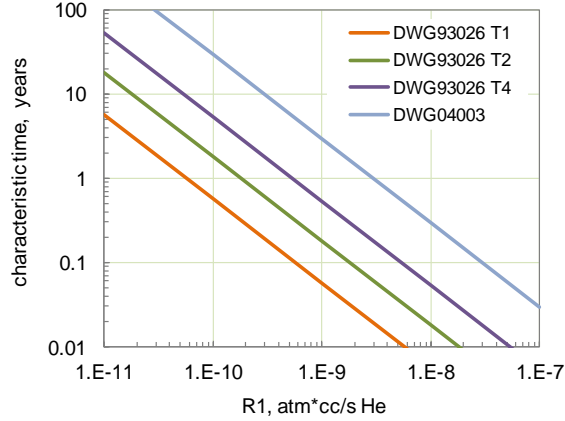

Figure II.3.3. Characteristic times for pressure build-up for different types of capacitors.

II.4.   Effect of internal gas pressure: deformation and rupture of the case.

Let us consider a cylindrical tantalum case of radius R, length L, and a thickness of the wall h. Additional pressure, P, caused by gas generation would increase the stress in the case, σ, cause deformation, and might eventually result in its rupture when the stress exceeds the strength of the material, σ_{cr}.

The level of stress at the cylindrical surface of the case and increase in the radius, ΔR, can be estimated as:

$$\sigma = \frac{P \times R}{h} \quad , \tag{II.4.1}$$

$$\Delta R = \frac{\sigma}{E} \times R ,. \tag{II.4.2}$$

where $E = 185$ GPA is the Young's modulus of tantalum.

The stress at the bottom of the case can be calculated as a stress in a membrane of radius R that is clamped at the periphery:

$$\sigma = \frac{3}{8} \times (1 + \mu) \times \frac{P \times R^2}{h^2} \quad , \tag{II.4.3}$$

where $\mu = 0.34$ is the Poisson's ratio.

The maximum deformation of the case at the center of the membrane (deflection) can be calculated as:

$$\varpi_{max} = \frac{P \times R^4}{64 D} , \tag{II.4.4}$$

where D is the toughness of the membrane:

$$D = \frac{E \times h^3}{12 \times (1 - \mu^2)},$$
(II.4.5)

Case sizes and calculated deformations for the excessive pressure $P = 1$ atm are shown in Table II.4.1.

Table II.4.1. Deformation of tantalum capacitors at excessive pressure of 1 atm

	#93026 T1	#93026 T2	#93026 T3	#93026 T4	#93026 L2	#04005	#04003
L, mm	11.5	16.3	19.5	27	25.6	7	15
R, mm	2.4	3.6	4.8	4.8	3.6	7.5	18
h, mm	0.2	0.25	0.25	0.25	0.25	0.25	0.38
D, N*m	0.14	0.27	0.27	0.27	0.27	0.27	0.97
stress_cyl, Pa	1.2E+06	1.4E+06	1.9E+06	1.9E+06	1.4E+06	3.0E+06	4.7E+06
strain, cyl, %	6.5E-04	7.7E-04	1.0E-03	1.0E-03	7.7E-04	1.6E-03	2.5E-03
ΔR, mm	1.5E-05	2.8E-05	5.0E-05	5.0E-05	2.8E-05	1.2E-04	4.6E-04
Stress_membr., Pa	7.2E+06	1.0E+07	1.9E+07	1.9E+07	1.0E+07	4.5E+07	1.1E+08
Strain_membr, %	3.9E-03	5.6E-03	1.0E-02	1.0E-02	5.6E-03	2.4E-02	6.0E-02
ω_m (bulging), mm	3.7E-04	9.6E-04	3.0E-03	3.0E-03	9.6E-04	1.8E-02	1.7E-01

The ultimate strength for tantalum is ~280 MPa. Due to hydrogen absorption and crimping, the strength of the case might be weakened substantially. For conservative estimations we can assume that the critical stress in a case of a tantalum capacitor that might cause its rupture is $\sigma_{cr} = 100$ MPa. In this case, the critical pressure can be estimated as:

$$P_{cr}^c = \frac{\sigma_{cr} \times h}{R}$$
(II.4.6)

Results of calculations of P_{cr} and deformations at the critical pressures for different case sizes are shown in Table II.4.2. The level of critical pressure that the case can withstand decreases from 83 atm for T1 cases to 52 atm for T3 and T4 cases. Large capacitors, DLA DWG04003, have the minimal pressure that can be safely developed in the case (21 atm). The increase of radius in all cases is relatively small, below 10 μm; however, the bulging is noticeable for relatively large cases: 0.16mm for cases T3 and T4, ~ 1 mm for DLA DWG#04005 capacitors, and ~ 3.6 mm for DLA DWG#04003 capacitors.

Experiments with DLA DWG#04005 capacitors showed that bulging in parts after high-temperature storage at 150 ℃ was ~ 0.1 mm. Considering that the vapor pressure at 150 ℃ is ~ 5 atm (see Fig. II.1.1), the calculated value of the membrane deformation in the center is 0.09 mm. The agreement between experimental and calculated data is quite reasonable.

Table II.4.2 shows also the amount of gas that is necessary to reach the critical pressure, the relevant transfer charge, and the level of leakage currents necessary to transfer this charge during 10 years of operation. The calculations were made in an assumption that the case is hermetic, and the leak rate is below 10^{-11} atm*cc/s He, which correspond to characteristic times of the pressure rise of more than ~10 years for all types of cases (see Fig. II.3.3). Although the presence of some fine leak would allow to relax

these requirements, considering that the exact level of the leak rate is not known, it is reasonable to require that long-term leakage currents remain below the critical values shown in the Table II.4.2.

Note that standard DCL measurements made within 5 min of electrification reflect absorption processes and cannot be used for comparison with the critical current. For the purpose of verification, the currents should be measured by the end of voltage conditioning as described above.

Even if leakage currents are above the critical levels, failure might not happen if the dielectric is uniform and have low enough conductivity, so the voltage drop across the electrolyte is below the level necessary to initiate electrolysis. However, discrimination between capacitors with uniform dielectric and dielectric having defects is extremely difficult if not impossible. For this reason, tightening the requirements for acceptable levels of leakage currents is necessary to increase confidence in reliable operation of the parts.

Experience with military grade wet tantalum capacitors shows that the probability of rupture or explosion of the cases during long-term operations are very low. Advanced, high volumetric efficiency capacitors have greater leakage currents compared to the CLR-style capacitors and have greater probability to have defects in the dielectric, hence higher risk of failure.

Table II.4.2. Critical pressure and critical current for 10 year operation.

	#93026 T1	#93026 T2	#93026 T3	#93026 T4	#93026 L2	#04005	#04003
P_{cr}, atm	83.3	69.4	52.1	52.1	69.4	50.8	21.2
ΔR_{cr}, mm	1.3E-03	1.9E-03	2.6E-03	2.6E-03	1.9E-03	6.1E-03	9.7E-03
ω_{m_cr} (bulging), mm	3.1E-02	6.7E-02	1.6E-01	1.6E-01	6.7E-02	9.2E-01	3.6E+00
free volume, cm3	0.1	0.33	0.71	0.98	0.52	0.43	5.34
n_{cr}, mol	3.5E-04	9.6E-04	1.5E-03	2.1E-03	1.5E-03	9.1E-04	4.7E-03
Q_{cr}, C	67.2	184.8	298.5	412.1	291.2	176.3	913.6
$I_{cr\_}10$ years, μA	2.1	5.9	9.5	13.1	9.2	5.6	29.0

Part III. Leakage Currents along the Glass Seal

III.1. Background.

Most high-reliability wet tantalum capacitors used for space applications have tubular (or cylinder) cases with axial leads (e.g. MIL-PRF-39006, DLA#93026, #10004). Hermeticity of these parts is assured by a two-level system. The primary, or internal seal is provided by the case crimping and Teflon gasket with a small rubber o-ring. The glass seal and welding of the tantalum tubular outlet are used for a final seal of the case. The internal seal is necessary to prevent electrolyte from seeping into the glass seal area. The surface of the outlet and the upper section of the anode riser tantalum wire are not oxidized, so in case of electrolyte penetration to the glass seal area, excessive leakage currents, electrolysis, and electrochemical reactions associated with oxide formation might occur.

Difott [4] based on extensive studies of wet tantalum capacitors suggested that due to the cold flow of the compressed Teflon gaskets and loss of elasticity of the silicone rubber O-ring gaskets, the risk of internal dehermetization that might result in permeation of electrolyte into the glass seal area is increasing during long-term operations or storage of the capacitors. Although no direct evidence for this type of failures has been reported in literature, it is possible considering that even at a relatively low level of permeation, a substantial amount of electrolyte can be accumulated with time during long-term storage of capacitors. Gas generated in the process of electrolysis might increase pressure in the case and cause its rupture during operation. However, no data on the conductivity along the glass seal in the presence of electrolyte and assessments of the risks associated with gas generation were found in the literature.

The optimal level of crimping that would provide the necessary hermeticity of the internal seal without excessive and damaging cold work of the case is difficult to determine. In practice, this optimization is achieved empirically and, although it is not required per the existing specifications, some manufacturers are using direct testing of the internal seal.

There is no standard process in establishing DCL requirements, and in most cases, they are set based on proprietary manufacturer procedures. In this situation, the margin between the required and actual leakage currents is not known, and excessive currents caused by additional conduction of the seal having a layer of electrolyte on the surface might be overlooked. Also, there is no data on the level of leakage currents along the glass seal. Analysis of leakage currents in tantalum capacitors, and in particular, processes associated with the presence of electrolyte on the surface of the glass would allow a better understanding of possible reliability risks and help in determining risk mitigation measures.

Tantalum capacitors in button-style, or single-seal cases (e.g., DLA#04003, 04005, 10011) have higher volumetric efficiency, but do not have internal sealing, so the non-oxidized areas of tantalum are in contact with electrolyte. This might be one of the reasons for excessive leakage currents in these parts compared to the tubular-style designs (e.g., DLA#93026, 10004). Also, for the same reason, corrosion at the outlet weld areas and hermeticity failures happen more often in these types of capacitors (see for example, Fig. III.3.4b). Some improvements have been achieved by using washers between the anode slugs and outlets, but this measure is still much less effective compared to the crimpling in the tubular-style capacitors.

In this work, leakage currents along the glass seal in the presence of condensed electrolyte have been measured with time at different temperatures and voltages using specially manufactured test samples. Gas

generation and the level of internal gas pressure caused by the electrolysis have been estimated, and risks of failures for different case sizes assessed. Recommendations for additional qualification procedures are suggested.

III.2. Experiment.

Model structures of wet tantalum capacitors were prepared by sealing a certain amount of electrolyte (~40% H2SO4) in five samples of case size T1 and T3 test structures. Fig.III.2.1 shows X-ray views of the test samples and approximate amount of the electrolyte added. The large dark area on the cases corresponds to location of the tantalum cathode sleeve that was anodically oxidized at 3V. SN5 and SN2 had tantalum wires simulating anode riser wires in capacitors, while other parts were sealed with wires shorter than the outlets.

Initial measurements of leakage currents at 1.5 V showed ~ 2.5 mA (maximum available current) at first moments of electrification that within seconds reduced microampere levels. External examinations did not reveal any anomalies or evidence of corrosion at the seal.
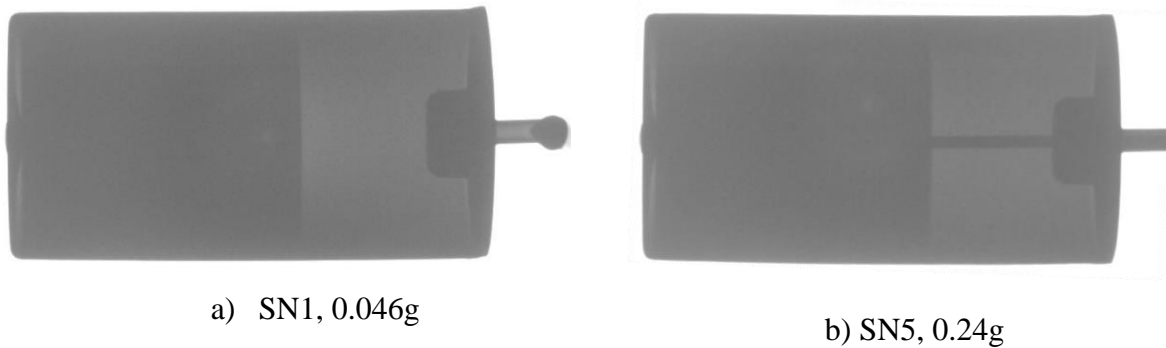

a) SN1, 0.046g

b) SN5, 0.24g

Figure III.2.1. X-ray views and amount of electrolyte in case T3 SN1 and SN5 model structures of wet tantalum capacitors. The amount of electrolyte in other samples was ~ 0.1 g.

Leakage currents were measured with time at different voltages and were calculated based on the voltage drops across 22 kohm resistors connected in series to the test structures.

III.3. Results and discussion.

First electrical tests were carried in a vertical position of the test structures with anodes directed upward at 1.5 V for 1000 sec, at 5 V for 1 hour, and at 10 V for 100 hours. After these initial tests and depolarization at 0 V for 4000 sec, measurements at 1.5 V and 5 V were repeated, and the next testing was carried out at 20 V for 100 hour. Results of these measurements are shown in Fig.III.3.1. At 1.5 V initial currents were below 10 µA and decreased to below 1 µA after a few minutes. The currents continue decreasing with time, and *I-t* variations can be approximated with a power law $I \sim t^{-m}$. Similar dependencies are also applicable to measurements at 5 V and 10 V with the values of *m* in the range from 0.6 to 0.8. This power relationship is similar to what is observed for wet tantalum capacitors during initial stages of electrification that is due to the charge absorption processes. However, current relaxation in wet tantalum capacitors related to absorption has values of *m* close to 1. Kinetic studies of oxide growth at constant voltage by Vermilyea [50] showed that variations of currents with time after several minutes of anodization also follow a power law with the exponent close to -1.

Anomalies in *I-t* curves were observed during 100 hour testing at 10 V in SN4 and SN5. Stabilization of the current at ~ 10 μA for SN4 in the 0.3 hour to 20 hour interval is likely related to the presence of contaminations in the Ta tube or wire that prevented proper oxide growth. Increase of currents after a few hours of electrification in SN5 might be due to a breakdown at the defective areas. Decrease of currents and observed instability might be attributed to a formation of gas bubbles in areas of electrolyte condensation that reduced DCL by diminishing the effective surface area for the current flow.
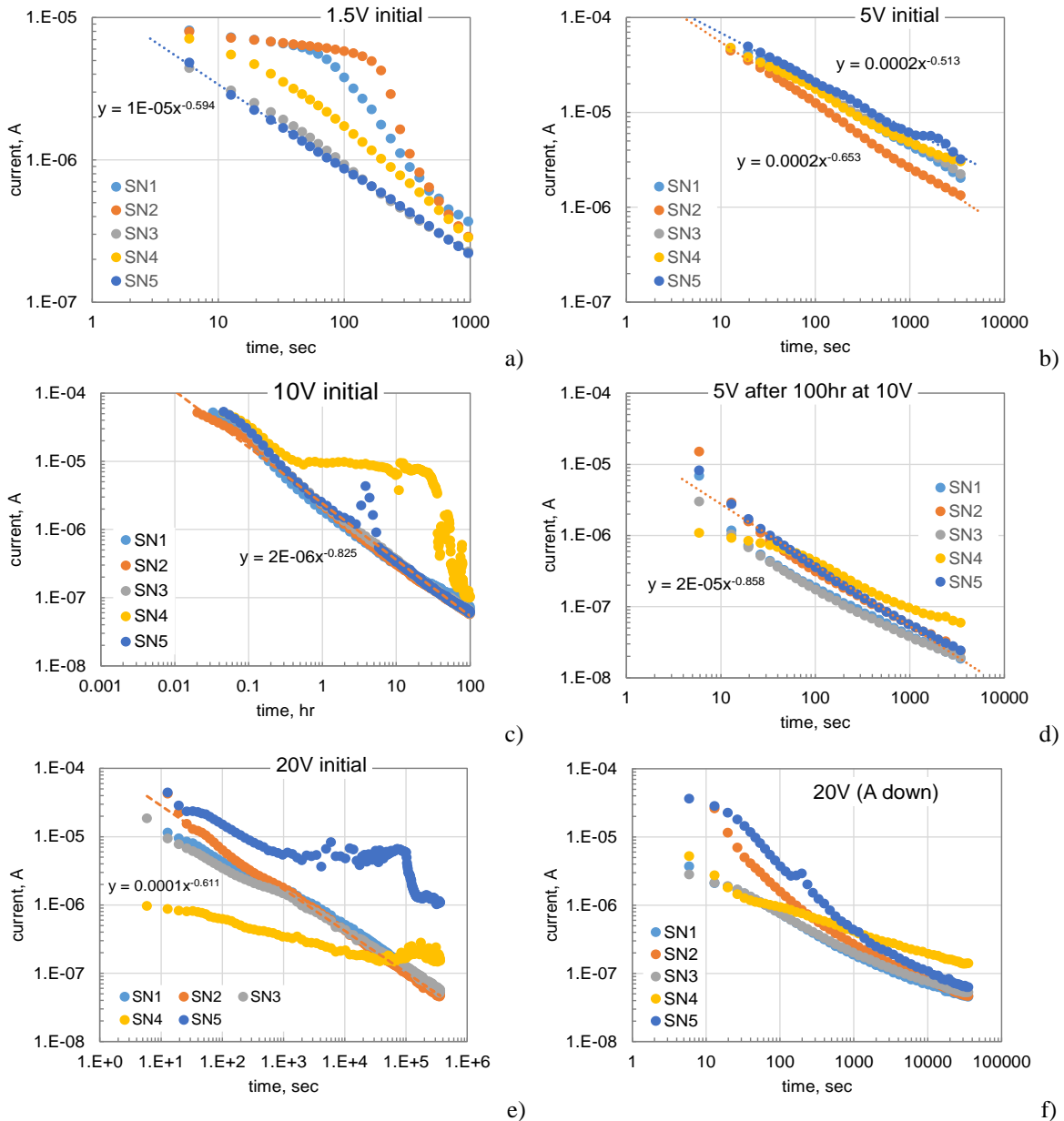

Figure III.3.1. Leakage currents along the glass seal in model structures with anodes in the upward position at room temperature and different voltages.

It should be noted that tantalum wires in real capacitors, contrary to the samples used in this study, are purified during anode sintering and parts of the wires close to slugs are anodized during oxide formation on the surface of the slug. However, most of the samples in this study had wires of a minimal length (see

Fig. III.2.1a), so the observed effects are due mostly to currents through the outlets that have quality identical to the one used for tantalum capacitors.

Depolarization currents after 100 hour testing at 10 V were below 1E-9 A thus indicating that contrary to normal capacitors, where relaxation is due to absorption currents that have similar amplitudes for polarization and depolarization processes, the observed currents are likely related to a slow oxide growth. This was also confirmed by a substantial decrease of currents at 1.5 V, from ~0.2 to 0.4 µA after 1000 sec initially, to a few nanoamperes after 10 V testing. Currents at 5 V measured after 1000 sec decreased from 2 to 5 µA initially to 0.03 to 0.1 µA after the testing.

Measurements at 20 V (see Fig. III.3.1e) again showed anomalies in SN4 and SN5. This time, currents in SN5 remained at ~ 8 µA for a few hours, and then decreased. Initial currents in SN4 were more than an order of magnitude less than for other samples, and reduced slowly with time. These anomalies can be explained by the same reasons as for 10 V testing. Depolarization currents after 20 V testing were ~ 2 orders of magnitude less than during polarization, and currents in all parts at 20 V were less than during 10 V testing. Both facts indicate continuation of the oxide growth at 20 V.

Contrary to what was expected, measurements at 20 V with the anodes in the downward position (Fig. III.3.1d) showed that the currents were several times less than in the upward positions. In the downward position, the thickness of the layer of electrolyte on the glass, hence the conductivity, should be greater than during the upward tests. The data can be explained considering that the currents are limited not by the electrolyte, but by the oxide formed at the surface of tubes and wires, and oxide growth results in decreasing currents in the consequent tests.

To evaluate the effect of temperature on leakage currents, next experiments were carried out at 20 V for 10,000 sec consequently at 85 ℃, 105 ℃, 125 ℃, and 145 ℃. In all cases anodes were in the downward positions. At each temperature, the polarization cycle was followed by depolarization at 0 V for 10,000 sec. Results of these tests are shown in Fig. III.3.2.

At all temperatures, the currents remained stable or increased slightly for ~ 20 sec, and then decreased with time allowing approximation by a power law with the exponents decreasing with temperature from 0.4 at 85 ℃ to 0.24 at 145 ℃. The level of initial currents slightly decreased as temperature raised from 85 ℃ to 105 ℃, and then remained stable. The results can be explained by the oxide growth that continues at high temperatures even after ~3-hour anodic oxidation at the same voltages but lower temperatures.

Depolarization currents, in most cases, exhibited anomalous extremal I-t dependencies. After initial decreasing for 20 to 200 seconds, currents increased reaching maximum, and then decreased again. Experiments did not show any effect of temperature on the time to maximum. For example, for SN3 the times to maximum were 280 sec at 85 ℃, 120 sec at 105 ℃, 320 sec at 125 ℃, and 1200 sec at 145 ℃. The currents decreased to a few nanoamperes after 10,000 sec at 85 ℃ and 105 ℃; however, they appear to stabilize at ~3 nA at 125 ℃ and at ~10 nA at 145 ℃.

The extremal behavior of depolarization currents is not clear. One of the possible reasons is that the gas bubbles formed during polarization are gradually collapsing during depolarization thus increasing the area available for collecting the charge. Processes of depletion of the absorbed charge prevail when currents
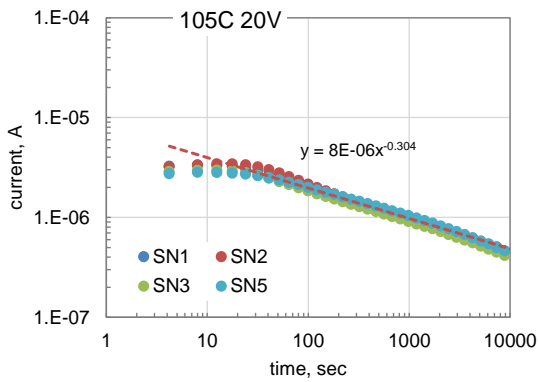
start decreasing again. Stabilization of depolarization currents at high temperatures might be due to the galvanic effect caused by differences in electrochemical characteristics between welded tubes and cases.
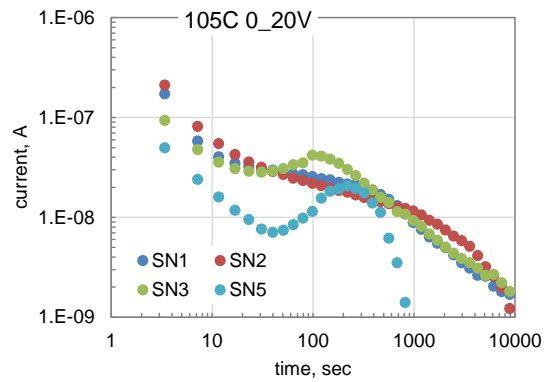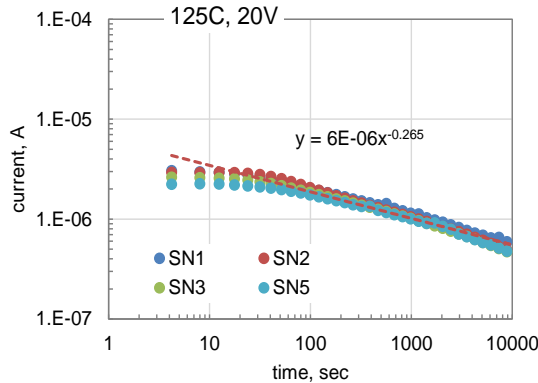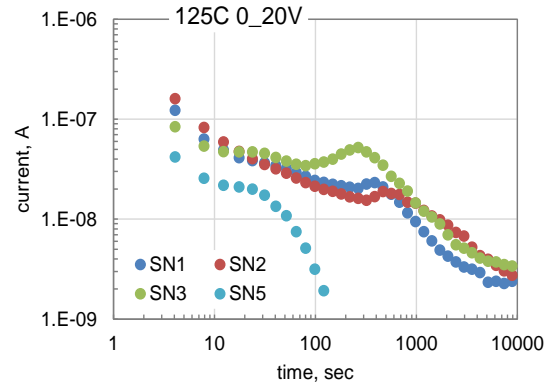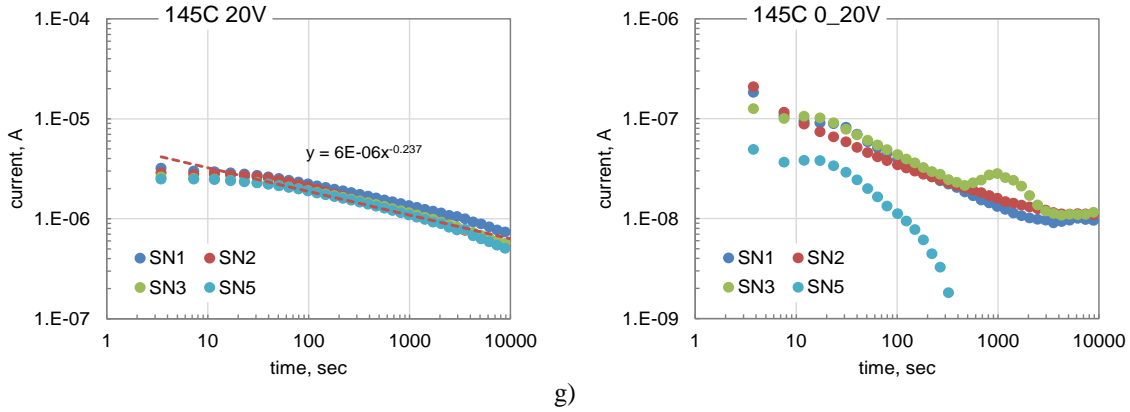

a)

b)

c)

d)

e)

f)

g)

h)
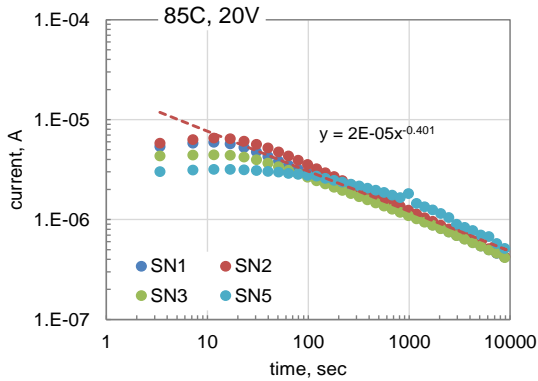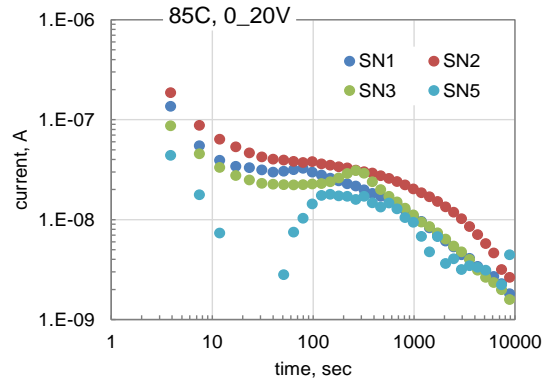
Figure III.3.2. Variations of currents with time during polarization (20 V) and depolarization (0_20 V) cycles at different temperatures.

Results of post high temperature measurements carried out at room temperature with anodes in downward and upward positions are shown in Fig.III.3.3. Changing directions to the upward position resulted in decrease of the initial currents; however, after 10,000 sec of electrification the currents were similar. A comparison with the initial, pre-high-temperature measurements indicates that currents decreased almost an order of magnitude. Apparently the oxide continued growing during high-temperature testing at 20 V.
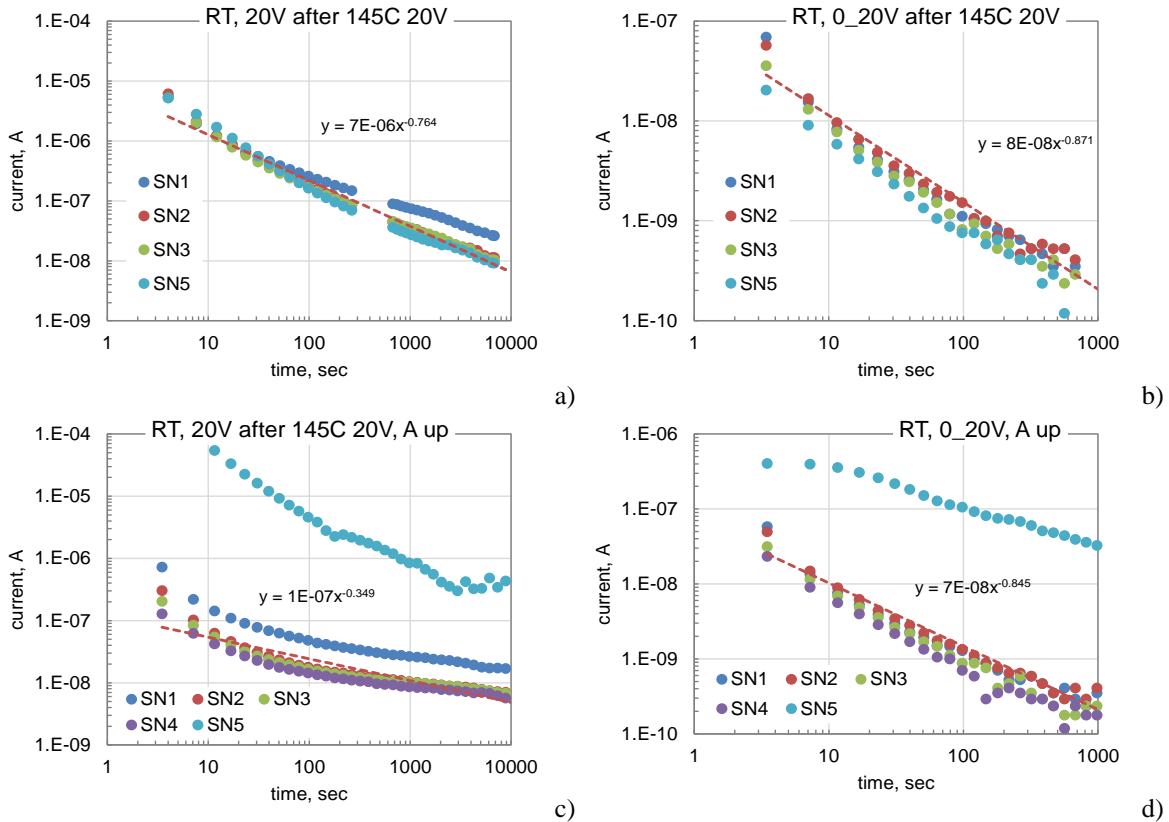

a)

b)

c)

d)

Figure III.3.3. Post 145 ºC testing measurements at room temperature and 20V first at downward (a, b) and then at upward (c, d) anodes positions.

Samples SN5 and SN4 had evidences of the weld corrosion and electrolyte leak after 145 ºC testing (see Fig. III.3.4a). However, measurements of the weight and case diameters did not reveal any substantial changes through the testing. In all five samples variations of the mass and diameter were within the accuracy of the measurements, ~0.5 mg and ~ 20 μm. Similar corrosion is more often observed on the button-style compared to cylinder-style capacitors (see an example in Fig. III.3.4b). This suggests that high quality welding is more difficult to achieve in the presence of electrolyte absorbed on the surface of outlets.
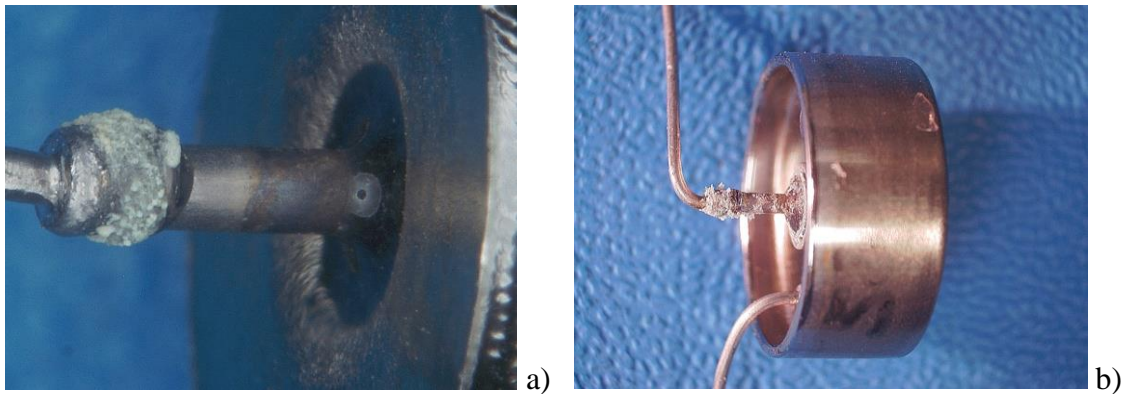

a)   b)

Figure III.3.4. Weld corrosion and electrolyte leak in SN4 after 145 ºC testing (a) and an example of a leak failure in a button-style capacitor (b).

Measurements of leakage currents at room temperature in the upward positions at 35 V and 50 V are shown in Fig. III.3.5. At both voltages, polarization currents had a trend of gradual decreasing with time (m ~0.4 to 0.6). However, I-t characteristics at 35 V had humps after ~ 1 hour, and at 50 V extremums were observed after ~ 20 sec of polarization. Depolarization curves also had anomalies similar to those reported before (see Fig. III.3.2).

a)   b)
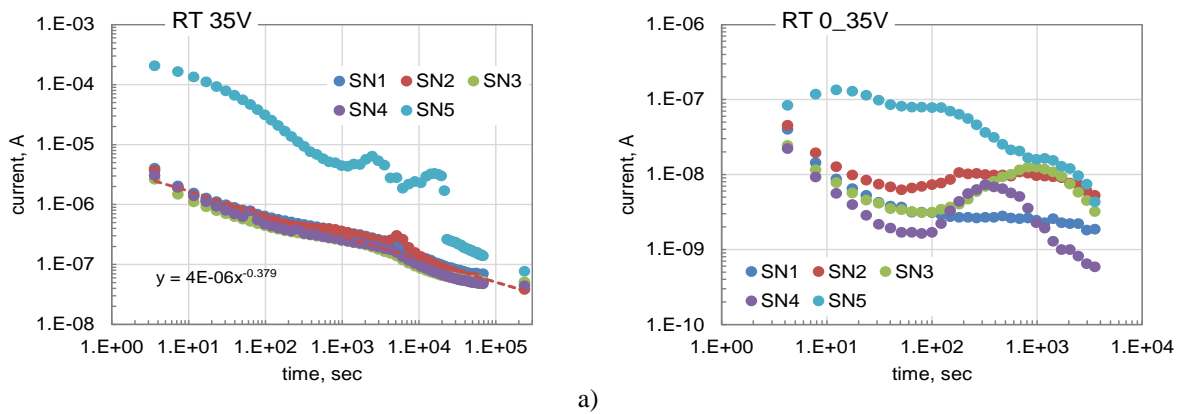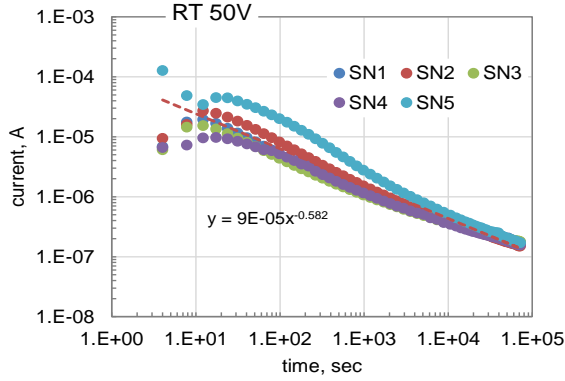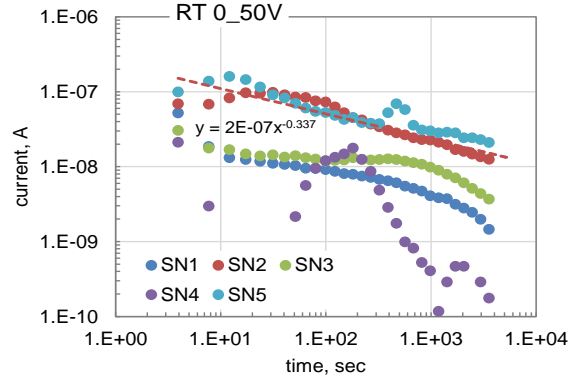
Figure III.3.5. Variations of leakage currents at room temperature and 35 V (a, b) and 50 V (c, d) for the upward position of anodes.

Finally, the samples were tested at different temperatures (consequently at 85 ℃, 105 ℃, 125 ℃, and 145 ℃) and voltages in the range from 1.5 V to 50 V. The currents were monitored for 10,000 sec at voltages below 50 V and for 100,000 sec at 50 V. Results of measurements at 20 V and 50 V are shown in Fig. III.3.6. Currents slightly increased during first 15 to 30 seconds of 20 V testing at all temperatures. After reaching maximum, currents decreased with time according to a power law with the exponent in the range from 0.3 to 0.5. At 50 V a hump on the *I-t* curves after ~300 sec was observed at 85 ℃ only. Currents at 50 V decreased with time relatively slowly, and the exponent *m* varied in the range from 0.28 to 0.25.
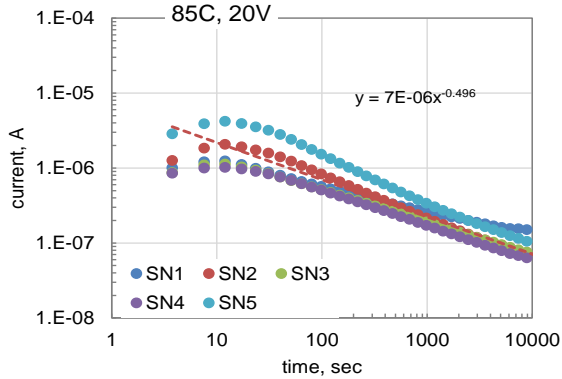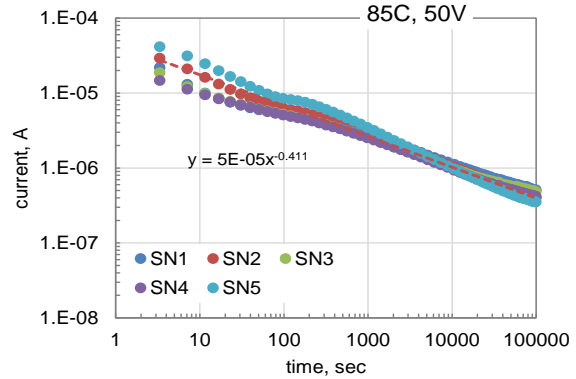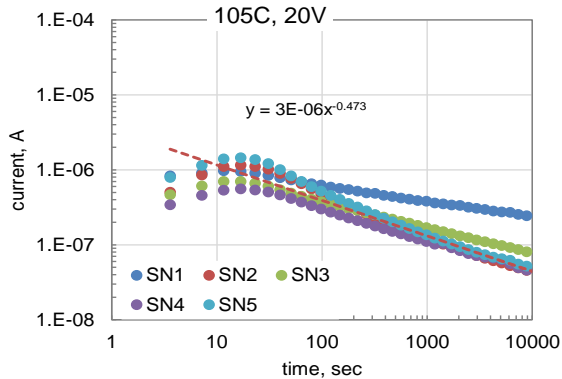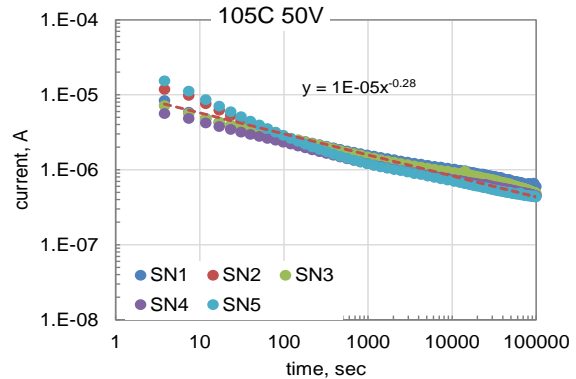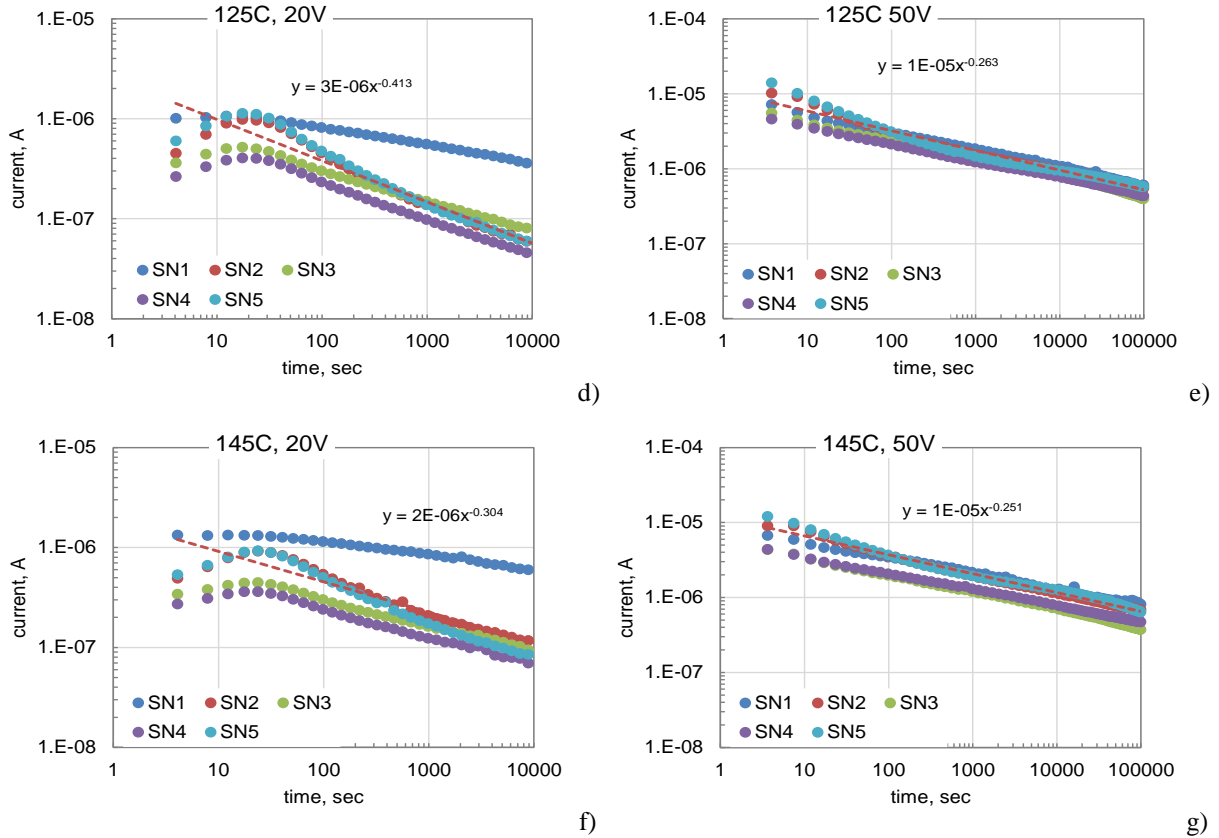
Figure III.3.6. I-t characteristics at 20 V and 50 V consequently at 85 ℃, 105 ℃, 125 ℃, and 145 ℃.

Variations of currents measured after 1000 sec of electrification through the testing at 20 V and 50 V are shown in Fig. III.3.7. Leakage currents at 50 V decreased ~ 3 times as the temperature increased from 85 ℃ to 105 ℃, and slightly increased as the temperature raised to 145 ℃. At room temperature the currents decreased compared to the initial measurements by approximately 2 orders of magnitude. Both effects can be explained by the oxide growth in the process of high-temperature measurements.
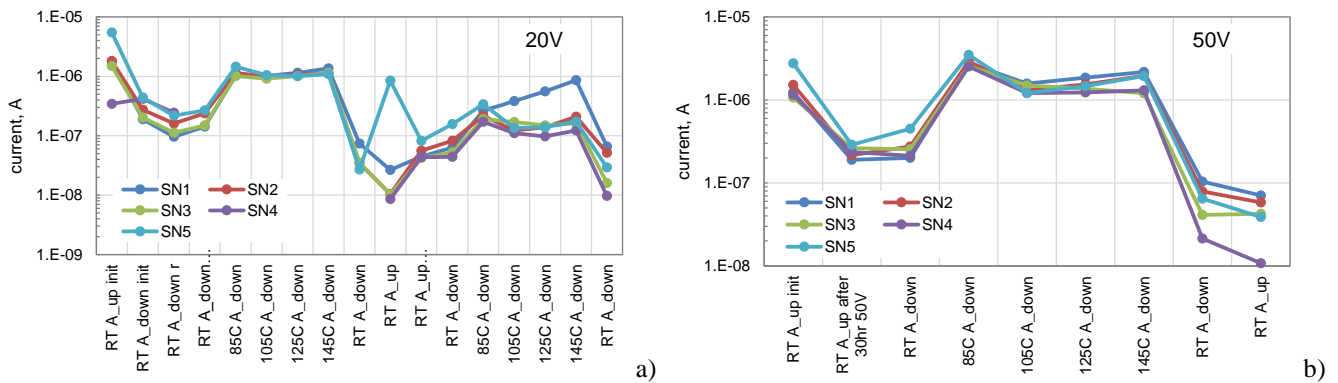
Figure III.3.7. Variation of currents at 20 V (a) and 50 V (b) through the testing.

After testing at 145 ℃ and 50 V for ~30 hours, the parts were measured at room temperature. Currents were monitored for 1 hour consequently at 5 V, 10 V, 20 V, 35 V, and 50 V. Results of these final measurements are shown in Fig. III.3.8. Relaxation of leakage currents at 5 V followed closely the power law with the exponents in the range from 0.8 to 0.85, which indicates absorption currents. Intrinsic leakage

currents ~20 nA appear after ~ 1000 sec in SN1 and SN5, while intrinsic currents in other samples were below the nanoampere range. Absorption currents in SN2 and SN5 are greater than in SN3 and SN4 likely due to the presence of wires. In sample SN4, intrinsic currents were small enough, so absorption currents prevailed over the intrinsic leakage currents during 1 hour of testing. In other samples intrinsic leakage currents could be observed after ~ 1000 sec of polarization and were below ~ 0.1 µA at 50 V. Erratic behavior of leakage currents was observed in SN5. Results show that even when oxides are formed at high temperatures, the quality of dielectric layers is poor and might result in high and unstable leakage currents even at voltages below the forming one.

a)

b)

c)

d)

e)

Figure III.3.8. Post high-temperature testing of leakage currents at room temperature and different voltages. For all samples anodes were in the downward positions.

Leakage currents after 300 sec of polarization (standard electrification time) are below 0.2 µA even at 50 V, and intrinsic currents are below 0.08 µA. Considering that DCL requirements for wet tantalum capacitors are typically above a few microampere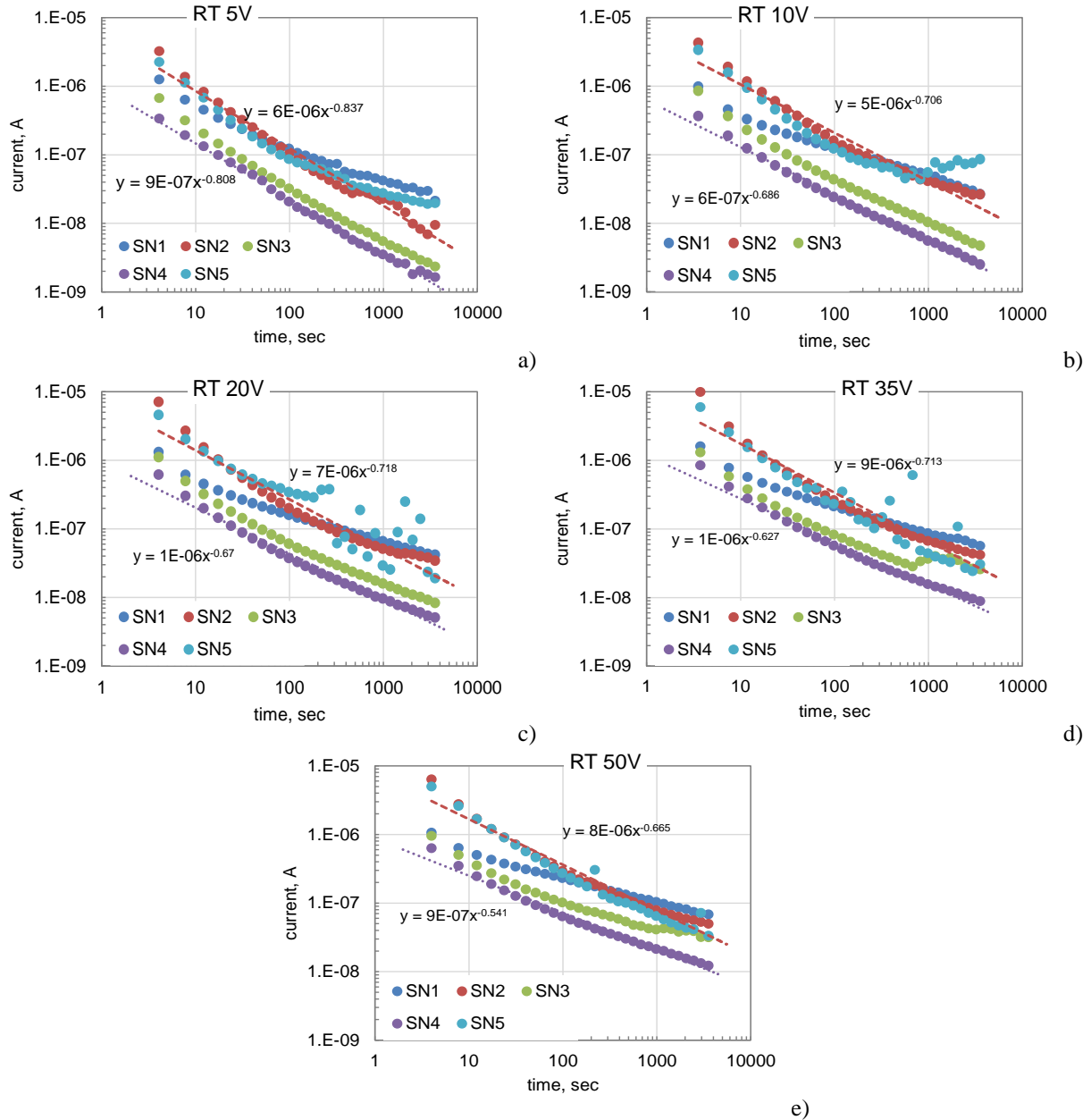s, additional leakage currents after long term bias that results in oxidation of the tubing and anode riser wire are negligible. However, initial leakage currents in the non-oxidized samples can exceed dozens of microamperes and might cause spiking and failures during applications.

For button-style capacitors anodization of the tube and wire will occur during voltage conditioning and might cause anomalies in the currents' behavior. Leakage currents in the system where oxide is formed at the same voltage as the operating one might be unstable thus increasing noise in the system during applications. These currents can also result in electrolysis of the electrolyte and increase pressure in the case. The effects of gas generation will be discussed in the next section.

To evaluate leakage currents in cases with non-oxidized surfaces of tantalum electrodes and assess the effect of the case size, 10 more test structures were manufactured similar to those described above. Five structures were prepared using case sizes T3 and five with case sizes T1. All samples had ~ 0.1 g of electrolyte and minimal length of wires (below the length of the tubes). Leakage currents were monitored for 100 hours consequently at 0.5 V, 10 V, and 50 V. The samples were tested initially at 0.5 V, then SN1 was tested at 10 V, and after that SN1 and SN2 were tested at 50 V. Finally, to compare variations of leakage currents in pre-tested and virgin samples, testing at 50 V for 250 hours was carried out using SN1, SN2, and SN3 (virgin). Results of these tests are shown in Fig. III.3.9 and indicate the following:

1. Initial leakage currents at 0.5 V are below ~ 10 µA, decrease according to a power law with the exponent ~ 0.4 to below 1 µA after ~300 sec, and stabilize at 10 to 20 nA for cases T1 and at a few nanoamperes for cases T3. Because the geometry and sizes of glass seals in T1 and T3 cases are the same and testing was carried out in the upward position of anodes, the difference in leakage currents is difficult to explain.

2. At 10 V the currents are similar for T1 and T3 cases, have a value of a few milliamperes initially, and decrease according to the power law, first with the exponent ~ 0.62, and then, after ~ 300 sec faster, with the exponent 0.94. It is possible, that the oxide is mostly formed within ~ 5 min at 10 V, and then the current decay is due to the absorption processes.

3. During first testing at 50 V (Fig. III.3.9d), leakage currents for samples in T3 cases are ~ 2 times greater than for T1 cases, but both are decreasing with time according to the power law with the exponent ~ 0.71. No substantial difference was observed for virgin samples and samples tested at 10 V (SN1). Also, initial currents are ~ a few miliamperes and are similar to those measured at 10 V. Both facts indicate that a thin oxide formed during 10 V testing did not play any significant role in the process of oxidation at 50 V.

4. Repeat testing at 50 V (Fig. III.3.9e) showed that initial currents in virgin samples might reach dozens of milliamperes but reduce to dozens or hundreds of microamperes after 5 min of electrification. The currents are decreasing to the submicroampere range only after hundreds of hours of testing. Currents in samples pre-oxidized at 50 V for 100 hours (SN1 and SN2) were more than an order of magnitude below currents in virgin samples initially, but had a trend of decreasing with time slower than for the virgin samples, so the difference after 250 hours of testing decreases substantially.
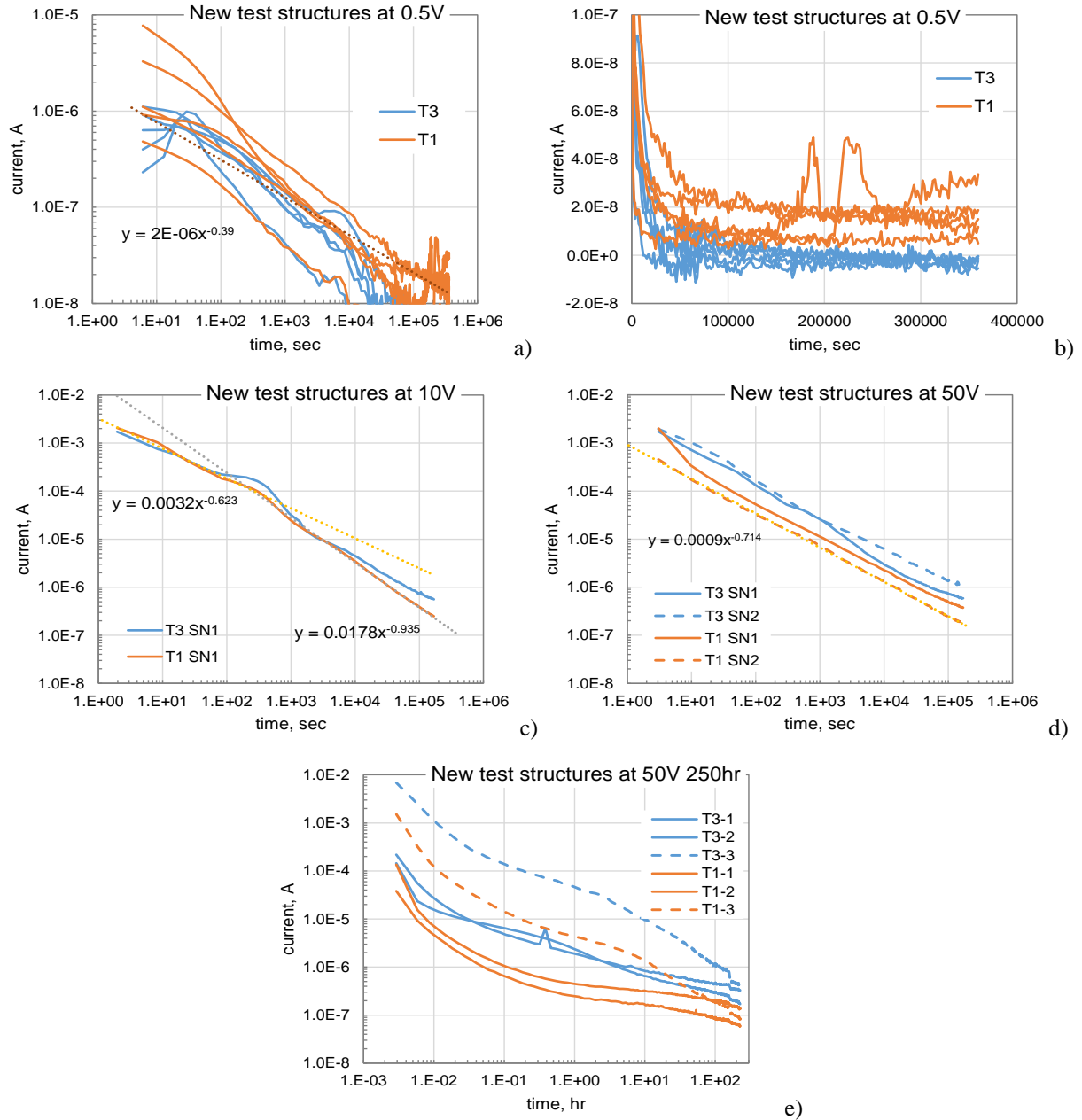
Figure III.3.9.   Leakage currents in new test structures prepared in cases T3 and T1 during 100 hour testing consequently at 0.5 V (a and b), 10 V (c), and 50 V (d). Additional testing at 50 V for 250 hours is shown in figure e). Dashed lines correspond to virgin samples that had been tested at 0.5 V only. Note that figures a) and b) show variations of leakage currents with time in double logarithmic (a) and linear (b) coordinates. All samples were tested in the upward positions of anode terminals.

III.4. SEM examinations.

Sample SN5 that had the longest wire was decapsulated and the surface of the wire and tube were inspected in SEM. EDS analysis was used to determine the composition of observed contaminations.

Fig. III.4.1 and III.4.2 show that the surface of the wire was covered with Ta2O5 oxide layer and had multiple defects that are often associated with field crystals surrounded by the peeled back oxide in a characteristic circular shape. A large area of the crystals might be due to a high incidence of impurity on the surface of wires [51]. It might be also specific for oxides grown in sulfuric acids and is different from pyramidal shape crystals with a much less peeled back oxide that is often observed after anodization in phosphoric acids. For example, testing of Nb2O5 structures revealed large circular areas of crystals with oxide pushed back when anodization of niobium was carried out in the ammonium pentaborate electrolyte [52]. However, no crystals were observed when oxide was formed in phosphoric acid.

Hossick-Scott [53] observed similar areas of crystallization on sheets of tantalum anodized at 260 V and tested with time at 255 V. He also observed humps on I-t characteristics that have been explained by the crystalization process. The crystals grow laterally at the oxide-electrolyte interface thus increasing the current. After the entire surface is crystallized, the current falls again due to the crystalline oxide thickness grows.

The thickness of oxide on the surface of the wire was ~ 150 nm, which is substantially greater than the calculated value of 85 nm (see next section). It is possible that thicker oxides can grow in sulfuric than in phosphoric acids, for which calculations were made. It is also possible that thicker oxides grow at high temperatures (145 °C) compared to 85 °C for a normal oxidation process for tantalum slugs.

Crystals of sulfur (Fig. III.4.1b) and organic S/O/C compositions (Fig. III.4.1c and d) were likely formed after electrolyte drying. In one area, contaminations (not shown) had EDS spectrum indicating presence of Al and Si; however, the source of these elements is not clear.
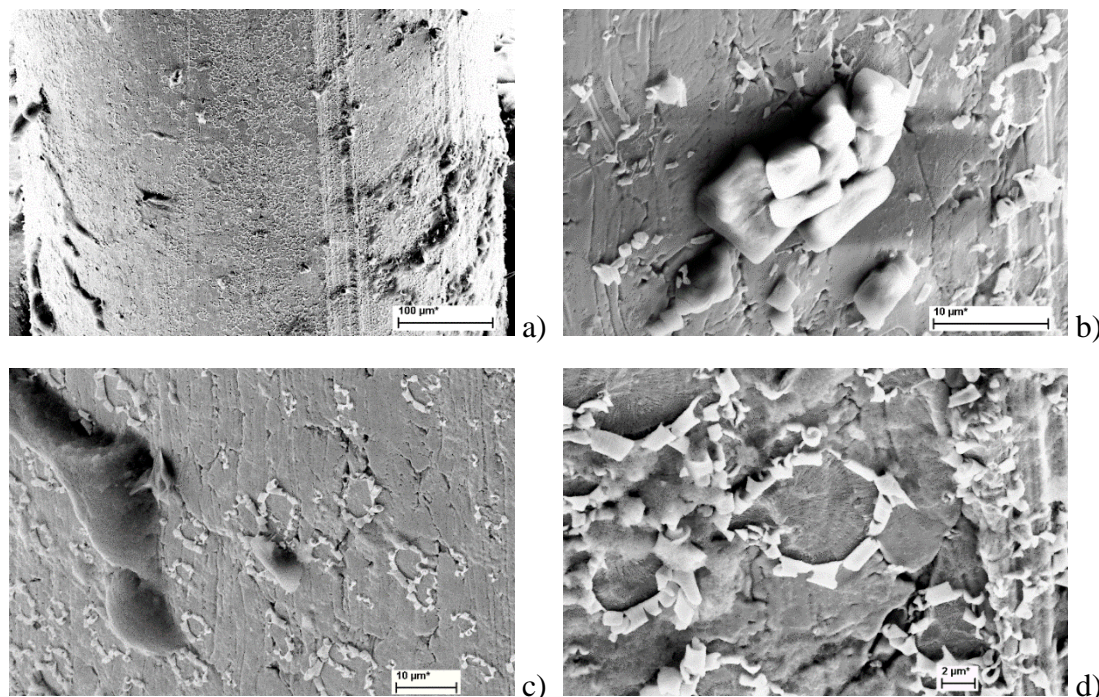
Figure III.4.1. Oxide and contaminations on the surface of wire. a) overall view, b) sulfur crystals (d), compositioon of S/O/C, and c) close-up views of broken oxide on the surface. Estimations showed that the thickness of the oxide is ~ 150 nm.
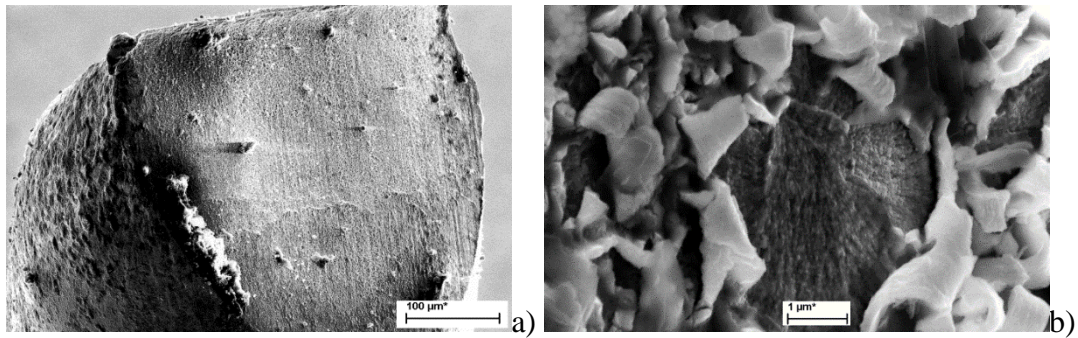
Figure III.4.2. Overall (a) and close-up (b) views of the tip of the wire.

Oxide formed on the surface of the tube (see Fig. III.4.3) was different compared to the oxide on the surface of the wire. The surface appeared to have nodules with cracks that are likely indicate an initiation of peeling. It is possible that exposure to high temperatures during the glass fusion process at ~ 1000 C resulted in a thermal oxide growth and formation of Ta2O5 nodules. Additional anodic oxidation during the testing degraded the oxide and caused formation of crystalls.
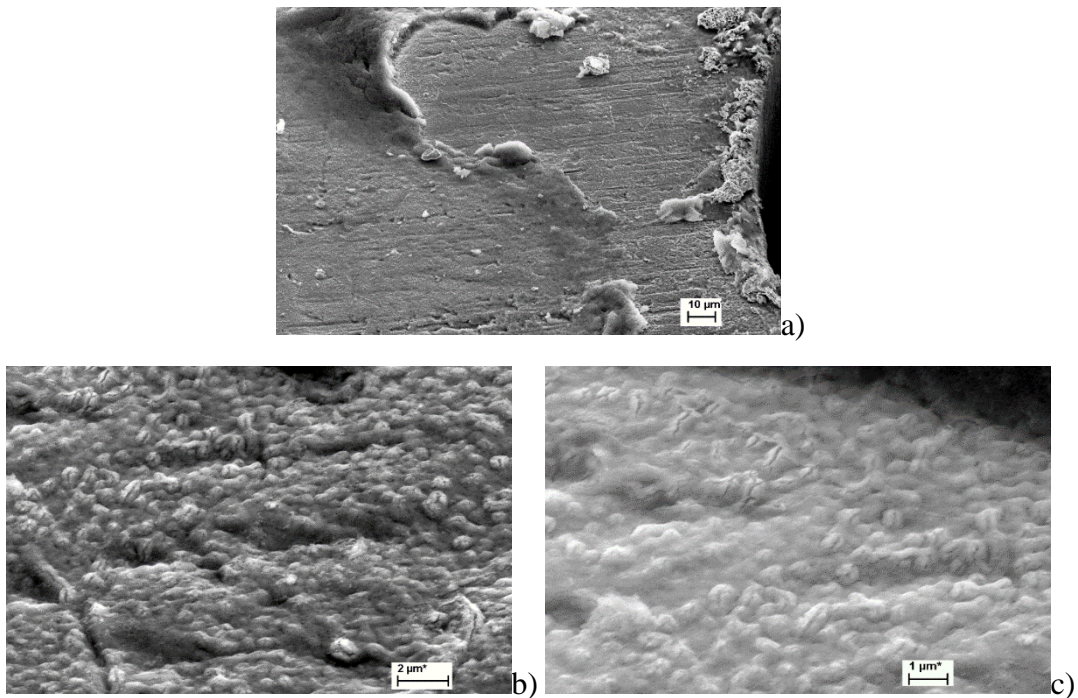
Figure III.4.3. An overall view of the surface of the tube (a) and close-up views of the oxide (b, c)

Interestingly, in spite of severe crystallization on the surface of the wire and multiple cracks on the oxide formed on the tube, the currents decreased substantially after long-term testing at high temperatures. This indicates that field crystallization that is often observed on the surface of anode slugs might be not the major cause of excessive leakage currents in wet tantalum capacitors.

The presence of multiple defects confirms that oxides formed on the surface of the wire and tube are of poor quality, which might be a reason of excessive and unstable leakage currents discussed in previous sections.

III.5. Discussion

Leakage currents along the glass seal depend on the conductivity of the electrolyte layer on the surface of the glass and on the conductivity of a tantalum pentoxide dielectric anodically grown on the surface of the tubular outlet and riser wire. To estimate the resistance of the electrolyte layer, let us assume that the current is flowing from the electrode with a diameter D_t that is equal to the external diameter of the tubular outlet (D_{t_ext}) to the electrode with a diameter equal to a diameter of glass seal, D_s (see Fig. III.5.1). Sizes of these and other case elements used for calculations below are shown in Table 1. Here L_t and L_w are the length of the outlet and the wire.

Table1. Sizes of elements in mm.

	D_{t_ext}	D_{t_int}	D_s	D_w	L_t	L_w
T3	1	0.6	2.5	0.45	4.7	var
T1	1	0.6	2.5	0.45	5.5	1
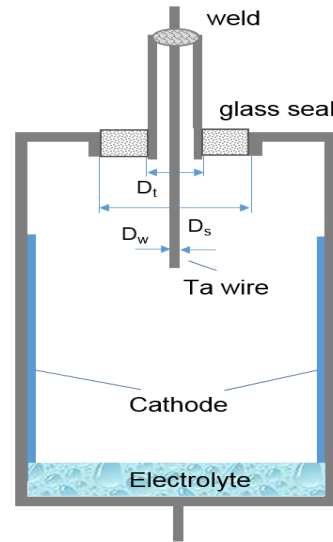
Figure III.5.1. An internal view of the glass seal (a) and schematic of the test structures (b).

Resistance of the electrolyte layer that has a thickness t_{el} can be calculated as:

$$R = \frac{\ln\left(D_s / D_t\right)}{2 \times \pi \times t_{el} \times \sigma_{el}} , \qquad (III.1)$$

where $\sigma_{el} = 0.75$ S/cm is the specific conductivity of the electrolyte.

Based on the case geometry and mass of electrolyte, the thickness of the electrolyte layer, t_{el}, at the downward position of anodes is expected in the range from 0.1 mm to 1 mm. At $D_s = 2.5$ mm and $D_t = 1$ mm, R is in the range from 2 to 20 Ohm. In the upward position, the layer is formed by condensation and is likely much thinner, but even at $t_{el} \sim 0.1$ μm, R still remains in the kiloohm range, ~20 kohm. This means that in the absence of oxide on the surface of electrodes, leakage currents at 0.5 V should be ~25

μA, which is consistent with the initial leakage currents measured within a few seconds (see Fig. III.3.9a). However, after a few hours of electrification the currents decrease two to three orders of magnitude (see Fig. III.3.9b) indicating a substantial increase of the resistance at the electrolyte/tantalum interface. This resistance might be due to either formation of oxide that occurs even at voltages as low as 0.5 V or most likely to the polarization of electrolyte (migration of ions to electrodes) and formation of potential barriers at the interfaces (concentration polarization).

Experimental data at voltages above 5 V show that the observed leakage currents are limited by the growing oxide. The thickness of the dielectric at a formation voltage V_f can be assessed as $t_{diel} \approx 1.7 \times V_f$, where t_{diel} is in nm and V_f is in V. At $V_f = 50$ V, $t_{diel} \approx 85$ nm. The internal surface of the outlet for T3 cases is ~ 9 mm^2, and of wire with 7 mm length is $\sim$10 mm^2. Considering that the dielectric constant of Ta2O5 is 27, the capacitance of samples with short wires (e.g. SN3) should be ~ 25 nF, and for SN5, that had a wire of ~ 7 mm length, the calculated capacitance is ~ 53 nF. Measurements at low frequencies resulted in capacitance values close to the calculated ones (see Fig.III.5.2). However, at high leakage currents of the dielectric, the measured capacitance is greater than the actual value, which is in agreement with results discussed in the previous section, where the estimated thickness of the oxide was $\sim$150 nm.
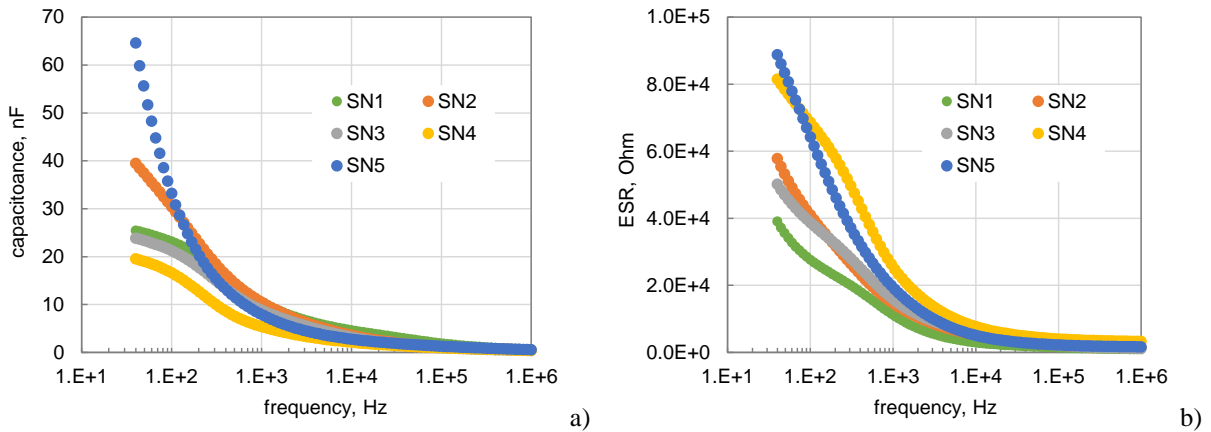
Figure III.5.2. Frequency dependencies of capacitance (a) and ESR (b) in the model structures after the testing.

Leakage currents at room temperature and 50 V in T3 structures that have been tested for ~30 hours at 145 °C and 50 V were below 0.1 μA (1000 sec measurements, Fig. III.3.8e.). However, similar structures after 100 hours of testing at 50 V and room temperature that have not been tested at high temperatures had currents ~50 μA (1000 sec measurements, SN1 and SN2 in Fig. III.3.9e). This indicates that formation of the dielectric continues at high temperatures even after long-term polarization at room temperature. Also, likely a thicker and better quality dielectric is formed at high (145 °C) temperatures.

To assess quality of the dielectric layers formed at different conditions, test structures that were conditioned at 145 °C, 50 V for ~30 hours and structures conditioned for 350 hours (SN1 and SN2) and 250 hours (SN3) at 50 V and room temperature, were tested for breakdown voltages using the constant current stress test [21]. Results of the testing (see Fig.III.5.3) show that structures conditioned at 145 °C had VBR ~105 V, whereas structures conditioned at room temperature had substantially smaller breakdown voltages ~70 V. Note, that SN3 that was conditioned at room temperature for 250 hours had

somewhat lower VBR (~60 V) and more severe scintillation events (amplitudes of current spikes) compared to 350 hour structures. It is interesting to note that the breakdown voltages were much greater compared to the formation voltages. The effect was also observed in [54], where the effect of type and concentration of electrolyte on VBR was studied. High-temperature conditioning resulted in a better quality dielectrics, and might be recommended for button-style capacitors to form oxide on the surface of the outlets and non-oxidized portions of the wire.
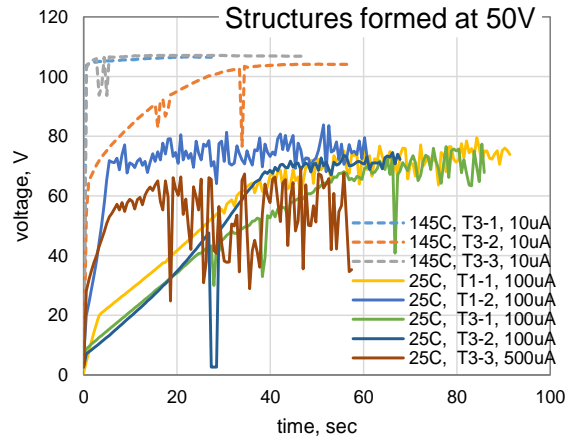

Figure III.5.3. Constant current stress testing for test structures after different conditioning: 145 ℃, 50V for 30 hours (dashed lines) and 350 hours (SN1 and SN2) and 250 hours (SN3) at 50V at room temperature (solid lines).

Formation of Ta2O5 dielectric is caused by the anodic reactions that can be presented in the following form:

$$2Ta + 5H2O = Ta2O5 + 10H^+ + 10e^-$$ (III.2)

This equation indicates that to produce 1 mol of Ta2O5, the charge equal to 10 moles of electrons should be transferred. According to the Faraday's law this charge can be calculated as:

$$Q = \frac{m}{M} \times z \times F \quad ,$$ (III.3)

where, $M = 442$ g/mol is the molar mass of the oxide, m is the mass of the oxide, $z = 10$ is the number of moles of electrons needed to form one mole of oxide, and $F = 96,485$ C/mol is the Faraday constant.

Considering that the surface area of the outlet and the wire, $S \approx 0.2$ cm^2, the volume of the oxide grown after testing at 50 V is 1.7×10^{-6} cm^3. At the density of oxide $\rho = 8.2$ g/cm^3, the mass of the formed oxide is 1.4×10^{-5} g or 3.15×10^{-8} moles. Considering that the efficiency of anodic oxidation of tantalum is above 90% [50], according to Eq.(III.3) the oxide growth corresponds to a charge of 0.003 C. At currents ~1 mA (see Fig. III.3.9e) this charge can be transferred in less than 3 sec. This means that the oxide growth occurs relatively fast and the slow, during hundreds of hours, decay of currents is likely due to a combination of absorption processes, slow increasing of the oxide thickness, or restructuring of the oxide that reduces its conductivity.

Formation of each mole of Ta2O5 goes along with generation of 5 moles of hydrogen gas. Additional pressure created by this gas can be calculated based on the gas law:

$$P = n_m \times \frac{RT}{V} ,$$

(III.4)

where n_m is the amount of gas in moles, $R = 8.314$ J/K_mol is the gas constant, $T \approx 300$ K is the room temperature, and V is the volume of the chamber.

For the oxide growth considered above, the amount of hydrogen generated is $n_m = 1.6 \times 10^{-7}$ mole. Assuming that for case sizes T3 and T4 the volume of the chamber above the crimping area is ~0.1 cm^3, the pressure caused by H2 generation is 3,900 Pa or 0.039 atm. For the case size T1 this volume is much less, ~0.03 cm^3; however, even in this case the pressure remains small (~0.1 atm) and is likely not a reliability concern.

In the presence of electrolyte, the upper chamber of a capacitor can be presented as an electrolytic cell with a tantalum case as one electrode, sulfuric acid absorbed on the surface of the glass seal as the electrolyte, and tantalum outlet tubing/riser wire as the second electrode. Gas generation in this cell might continue as long as the voltage drop across the electrolyte exceeds a certain "electrolyte breakdown" voltage that is necessary for its decomposition. For water, this voltage is ~ 1.2 V, and for the electrolyte it has likely a similar value. Although the conductivity of oxide at formation voltages is relatively large, it is still at least ~ 2 orders of magnitude less than for the electrolyte. This means that even at 50 V applied to a capacitor, the voltage drop across the electrolyte is less than 0.5 V, which is insufficient for its decomposition. However, the purity of materials used for the raiser wires and outlets is typically not as high as for tantalum powder used to form anode slugs. In the presence of defects on the surface, tantalum will not oxidize properly, and a substantial portion of the applied voltage will drop across the electrolyte resulting in gas generation at the defect area (see Fig. II.2.1). The surface area where the contamination is present might be small, so even at relatively large densities of leakage currents, total current in the system might remain low. As the worst case condition, we can assume that all charge transferred in the capacitor is associated with the hydrogen and oxygen generation.

Hydrogen is produced during the reduction of water at the cathode:

$$2e^- + 2H2O(L) => H2(g) + 2OH^- (aq) .$$

(III.5a)

According to this reaction, 2 moles of electrons are required to produce a mole of hydrogen, hence in the Faraday law, Eq.(III.3), $z = 2$. In this case, $Q \approx 2 \times 10^4 \times n_m$, where Q is in Coulombs and n_m in moles.

Anodic reaction results in generation of oxygen:

$$4OH^- => O2(g) + 2H2O + 4e^-.$$

(III.5b)

Note that per each mole of oxygen two mole of hydrogen will be generated. This means that even if due to high diffusivity of H2 in tantalum most of hydrogen would escape from the case, approximately 30% of the total pressure will remain due to the presence of oxygen.

Using approximation of I-t characteristics with a power function and assuming that this law is valid for long-term operations, the charge transferred in the structure during time τ can be calculates using parameters I_o (current at 1 sec) and the exponent n:

$$Q_t = \int_0^\tau I_0 \times t^{-n} \times dt = \frac{I_0}{1-n} \times \tau^{1-n} ,$$

(III.6)

Results of these calculations are shown in Table III.2. The estimated charge after 10 years of operation is in the range from ~0.3 C to ~8 C, and the corresponding amount of hydrogen is from 1.5×10^{-5} to 4×10^{-4} moles. According to the gas law, Eq.(III.4), this amount of H2 in a volume of 0.1 cm^3 would create additional pressure from 3.6 atm to 100 atm. Considering that the critical pressure for the case is in the range from 50 atm to 80 atm, gas generation poses a risk of case rupture. If most hydrogen is released due to the permeability of tantalum, the pressure created by oxygen would be below the critical level, but still remain high.

Table III.2. Transfer charge in Coulombs calculated per Eq.(6) for different times of operation.

time	25C, 20V (Fig. 2.e)	85C, 20V (Fig. 7.a)	85C, 50V (Fig. 7.b)
3 hr	0.01	0.0014	0.017
1 month	0.1	0.023	0.46
1 year	0.25	0.082	2
10 years	0.61	0.26	7.76
100 years	1.5	0.83	30

The transferred charge calculated by direct integration of $I\text{-}t$ characteristics during measurements at 50 V for 250 hours (see Fig. 10e) is displayed in Table III.3. The table shows also the calculated amount of generated hydrogen and additional pressure that is expected in the structures by the end of testing. The pressure was calculated based on Eq. (III.4) assuming that the volume of case T3 is 1.4 cm^3 and 0.21 cm^3 for T1. Note that samples SN3 had values of Q and P more than an order of magnitude greater than other samples and approached the critical levels of pressure. This is related to the prehistory of the samples: SN1 and SN2 were anodized during previous testing, while SN3 were virgin samples. Results indicate that insufficient oxidation of the outlet and wire increases risks of failures associated with excessive currents and gas generation in the seal area.

Table III.3. Transfer charge, calculated amount of hydrogen and pressure in the case after 250 hr testing of different test structures at 50 V.

	T3 SN1	T3 SN2	T3 SN3	T1 SN1	T1 SN2	T1 SN3
Q, C	0.86	1.27	37.8	0.76	0.22	8.17
n_H2, mol	4.3E-05	6.35E-05	1.9E-03	3.8E-05	1.10E-05	4.09E-04
P, atm	0.8	1.1	33.4	4.5	1.3	48.2

The above estimations are based on several assumptions. First, it is assumed that there is unlimited source of hydrogen in the electrolyte, second, that all generated gas remains in the case, and third, that all transferred charge results in gas generation.

To estimate the total amount of hydrogen that can be generated by electrolysis, let us assume that the case has 0.1 g of electrolyte, 0.04 g of which is H2SO4 (98 g/mol) and 0.06 g is H2O (M = 18 g/mol). This corresponds to 4×10^{-4} moles of H2SO4 and 3.3×10^{-3} moles of H2O, so the maximum amount of H2 is 3.7×10^{-3} moles. To generate this amount of gaseous hydrogen, 361 C of charge should be transferred, which is almost two orders of magnitude greater than the charge estimated based on observed leakage currents. Obviously, the first assumption is reasonable and no substantial depletion of electrolyte happens as a result of electrolysis.

Analysis in the part II of this report shows that the assumption that all hydrogen remains in the case during long-term operations is not valid. A substantial amount of H2 will be absorbed in the case and slug, leaked out through the seal or diffused through the case. All these factors might reduce the risk of over-pressurizing the case by hydrogen substantially. However, the total pressure in the can is a sum of pressures created by hydrogen and oxygen, and approximately one third of the pressure caused by electrolysis is due to oxygen. Oxygen has much lower absorption and diffusion coefficients in tantalum compared to hydrogen and will remain in the case unless the seal leak is large enough.

The assumption that the whole leakage current flowing along the glass seal is faradaic and results in gas generation is not valid. Most likely, gas evolution occurs only at defect sites of the oxide where the voltage drop across electrolyte is large enough. The exact proportion of this leakage current is difficult, if possible, to estimate, so calculations made above should be considered as a worst case scenario.

Due to a relatively fast removal of hydrogen from the case, a slow seeping of electrolyte through the internal seal during long-term operations of capacitors most likely is not a serious reliability concern. However, a gradual accumulation of electrolyte in the glass seal area during long-term storage might create problems when the part is first powered up. In this case, large currents will generate substantial amount of gas quickly, so most of the hydrogen will remain in the case thus increasing the pressure substantially.

Analysis shows that proper internal sealing is important for double-seal designs of capacitors. For the button style cases that do not have internal seals, a special procedure that would result in formation of adequate quality oxide at the non-oxidized areas, e.g. constant current conditioning at high temperatures or multi-step polarization at gradually increasing voltages, is recommended.

In many cases, space systems are in the dormant stage or stored for years before launch or initiation of operation. To assure that leakage currents along the glass seals in wet tantalum capacitors will not cause reliability problems, a high temperature storage (HTS) testing should be a part of qualification testing for capacitors intended for space applications.

Recommendations

Room temperature DCL measurements carried out in this work, showed that the DCL limit can be established based on the CV values of the capacitors at $2.5 \times 10^{-4} \times C_0 \times VR$. Compared to the actual leakage currents measured at room temperature after 5 min of electrification, this criterion provides approximately 5-fold margin.

Considering differences in the voltage breakdown margins, voltage derating requirements for high-voltage (100 V and 125 V) capacitors should be increased to 0.5, for capacitors rated to 50 V and 75 V the derating requirement can be left at the existing level (0.6), but it can be relaxed to 0.7 for lower voltage ratings.

Risks associated with DCL failures due to electrolyte penetration to the glass seal area are greater for capacitors in small size cases (T1). These parts have also smaller amount of electrolyte that increases the possibility of drying during long-term operations. Considering that optimization of the crimping process and accurate positioning of Teflon spacers are more difficult for these parts, more strict requirements related to hermeticity and radiography inspection are necessary.

To assure that additional gas pressure that is built up during long-term operations of capacitors as a result of electrolysis of electrolyte is below the critical level that might cause rupture of the case, the level of intrinsic leakage currents should be below values shown in Table II.4.2. Measurements of the intrinsic leakage currents should be made at the end of the voltage conditioning (48 hours at rated voltage and 85 ℃) after cooling samples under bias to 25 ℃.

The presence of defects in dielectric layers might result in unstable leakage currents, e.g. spiking and/or erratic variations with time that increases noise in the systems during applications, raises internal gas pressure, and might cause failures. To reduce these risks, the currents should be monitored during voltage conditioning by scanning every 100 sec (TBD), and no spiking should be allowed.

To improve quality of the dielectric layers formed on the initially non-oxidized surfaces of button style capacitors, voltage conditioning for these parts is recommended to carry out at 105 °C by steps in 3 hours starting with 0.1VR. The applied voltage should be increased incrementally by 0.3VR until the rated voltage is reached, at which level the parts should be conditioned for 96 hours.

To reduce the risks of drying out of electrolyte and avoid contamination of sensitive optical equipment, the fine leak testing of capacitors intended for space applications should be carried out for 100% of capacitors as a part of the screening process.

Possible accumulation of electrolyte on the surface of the glass seal during long-term storage might substantially increase currents during first power turn on in the system and result in a fast pressure increase. For this reason, rescreening that includes DCL measurements and monitored voltage conditioning is recommended for capacitors stored for more than 5 years.

In many cases space systems after integration and testing are stored for several years before launch or operation. To mitigate the risk that possible penetration of electrolyte to the glass seal area will cause failures and to verify integrity of the case during long-term operations, wet tantalum capacitors should be tested for high temperature storage (HTS) as a part of qualification testing. During HTS testing, 12 samples should be stored for 1000 hours at 150 ℃. Criteria for the test acceptance are TBD.

Excessive case bulging in capacitors after life testing indicates a substantial increase of the internal gas pressure. The level of bulging after life testing should be verified, and lots with excessive bulging that exceeds 50% of the critical level (see Table II.4.2) should not be accepted.

Acknowledgments

References.

[1]   A. Holladay, "History of the CLR79 all-tantalum wet slug electrolytic capacitor," in *10th Capacitors and Resistors Technology Symposium*, 1990, pp. 5-8.
[2]   W. M. Rowe and P. H. Eisenberg, "Factors Affecting the Reliability of Wet Tantalum Capacitors," in *Reliability Physics Symposium, 1967. Sixth Annual*, 1967, pp. 243-255.

[3]   D. Hayward, "Failure mechanisms in wet tantalum capacitors," *Electrocomponent Science and Technology,* vol. 2, pp. 249-257, 1976.

[4]   Difott, "Product Evaluation of MIL-C-390006/22 Nonsolid Electrolyte Tantalum Capacitors-Determination of the Performance of These Capacitors When Exposed to Vibration Environments," in *5th Capacitors and Resistors Technology Symposium*, San Diego, CA, 1985, pp. 133-140.

[5]   D. M. Edson and J. S. Bates, "Electrical Properties of a Novel High CV Wet Tantalum Capacitor System," in *CARTS*, 2009.

[6]   M. Mosier, "High performance wet tantalum capacitors for space applications," in *CMSE*, Los Angeles, CA, 2012.

[7]   C. Tzu-Yen, W. Xu, D. A. Evans, S. L. Roberson, and J. P. Zheng, "Characterization of tantalum oxide-ruthenium oxide hybrid capacitors," *Industrial Electronics, IEEE Transactions on,* vol. 51, pp. 1313-1317, 2004.

[8]   D. Evans, "Tantalum Hybrid Button Cell Capacitor," in *CARTS 2004: 24th Capacitor And Resistor Technology Symposium*, San Antonio, Texas, 2004, pp. 182-186.

[9]   A.Teverovsky, "Random Vibration Testing of Advanced Wet Tantalum Capacitors," presented at the Quality and Reliability Technical Symposium (QRTS) Hilton Phoenix/Mesa, 2015.

[10]   A. Berduque, Z. Dou, and R. Xu, "Electrochemical studies for aluminum electrolytic capacitor applications: Corrosion analysis of aluminum in ethylene glycol-based electrolytes," in *CARTS Europe*, Virtual Conference, 2009, pp. 1-10.

[11]   M. Sampson, J. Brusse, and A. Teverovsky, "Humidity Steady State Low Voltage Testing of MLCCs (Based on NESC Technical Assessment Report)," in *CARTS USA*, Jacksonville, Fl, 2011.

[12]   A. Riz, D. Fodor, O. Klug, and Z. Karaffy, "Inner gas pressure measurement based life-span estimation of electrolytic capacitors," in *Power Electronics and Motion Control Conference, 2008. EPE-PEMC 2008. 13th*, 2008, pp. 2096-2101.

[13]   M. Hahn, R. Kötz, R. Gallay, and A. Siggel, "Pressure evolution in propylene carbonate based electrochemical double layer capacitors," *Electrochimica Acta,* vol. 52, pp. 1709-1712, 12/1/ 2006.

[14]   D. Evans, "Determination of Capacitor Life as a Function of Operating Voltage and Temperature," in *21st International Seminar on Double Layer Capacitors & Hybrid Energy Storage Devices*, Deerfield Beach, FL, 2011.

[15]   A. Teverovsky, "Effect of Reverse Bias Stress on Leakage Currents and Breakdown Voltages of Solid Tantalum Capacitors," in *CARTS USA*, Jacksonville, Fl, 2011.

[16]   A. Teverovsky, "Reliability issues with new technology wet tantalum capacitors," in *17th annual International conference "Commecialization of Military and Space Electronics"*, Los Angeles, CA, 2013.

[17]   A. Teverovsky, "Ripple Current Testing and Derating for Wet Tantalum Capacitors," NASA/GSFC, Greenbelt, MD2013.

[18]   A. Teverovsky, "Guidelines for Selection, Screening and Qualification of Low-Voltage Commercial Multilayer Ceramic Capacitors for Space Programs," NASA/GSFC, Greenbelt, MD2012.

[19]   "Sectional Specification: Aluminium Electrolytic Capacitors With Solid And Non-solid Electrolyte," in *European Committee for Standards - Electrical, EN 60384-4:2007* ed, 1998.

[20]   J. Both, "Leakage current properties of modern electrolytic capacitors," ed: Tadiran Batteries GmbH, 2007.

[21]   A. Teverovsky, "Scintillation Breakdowns and Reliability of Solid Tantalum Capacitors," *IEEE Transactions on device and materials reliability,* vol. 9, pp. 318-324, 2009.

[22]   A. Teverovsky, "Scintillation and Surge Current Breakdown Voltages in Solid Tantalum Capacitors," *IEEE Transactions on Dielectrics and Electrical Insulation,* vol. 16, pp. 1134-1142, 2009.

[23]   A. Teverovsky, "Absorption Voltages and Insulation Resistance in Ceramic Capacitors with Cracks," *IEEE Transactions on Dielectrics and Electrical Insulation,* vol. 21, pp. 2020-2027, 2014.

[24]   A. Teverovsky, "Insulation Resistance and Leakage Currents in Low-Voltage Ceramic Capacitors With Cracks," *Components, Packaging and Manufacturing Technology, IEEE Transactions on,* vol. 4, pp. 1169-1176, 2014.

[25]   P. C. Dow, "An Analysis of Certain Errors in Electronic Differential Analyzers II-Capacitor Dielectric Absorption," *Electronic Computers, IRE Transactions on,* vol. EC-7, pp. 17-22, 1958.

[26]   F. C. Aris and T. J. Lewis, "Steady and Transient Conduction Processes in Anodic Tantalum Oxide," *Journal of Physics D-Applied Physics,* vol. 6, pp. 1067-1083, 1973.

[27]   E. M. Seregina, L. A. Rozenberg, V. I. Bocharova, and P. P. Zegzhda, "A study on electronic currents in the Ta-Ta2O5 electrolyte system," *Physica Status Solidi a-Applied Research,* vol. 124, pp. 499-504, Apr 1991.

[28]   C. Chaneliere, S. Four, J. L. Autran, R. A. B. Devine, and N. P. Sandler, "Properties of amorphous and crystalline Ta2O5 thin films deposited on Si from a Ta(OC2H5)(5) precursor," *Journal of Applied Physics,* vol. 83, pp. 4823-4829, May 1998.

[29]   J.-P. Manceau, S. Bruyerel, S. Jeannot, A. Sylvestre, and P. Gonon, "Leakage current variation with time in Ta2O5 MIM and MIS capacitors," presented at the IEEE International Integrated Reliability Workshop, 2006.

[30]   E. Loh, "DC conduction mechanism in tantalum chip capacitors," *Journal of Physics D-Applied Physics,* vol. 13, pp. 1101-1111, 1980.

[31]   D. Spassov, E. Atanassova, and D. Virovska, "Electrical characteristics of Ta2O5 based capacitors with different gate electrodes," *Applied Physics a-Materials Science & Processing,* vol. 82, pp. 55-62, Jan 2006.

[32]   F. Chiu, J. Wang, J. Lee, and S. Wu, "Leakage currents in amorphous Ta2O5 thin films," *Journal of Applied Physics,* vol. 81, pp. 6911-6915, 15 May 1997 1997.

[33]   S. Ezhilvalavan and T. Tseng, "Conduction mechanisms in amorphous and crystalline Ta2O5 thin films," *Journal of applied physics,* vol. 83, pp. 4797-4801, 1998.

[34]   R. Ramprasad, "Phenomenological theory to model leakage currents in metal-insulator-metal capacitor systems," *Physica Status Solidi B-Basic Research,* vol. 239, pp. 59-70, Sep 2003.

[35]   J. G. Simmons, "Richardson-Schottky effect in solids," *Physical Review Letters,* vol. 15, pp. 967-968, 1965.

[36]   A. Teverovsky, "Reverse bias behavior of surface mount tantalum capacitors," in *Capacitor and Resistor Technology Symposium, CARTS*, New Orleans, LA, 2002, pp. 105-123.

[37]   A. Teverovsky, "Degradation of leakage currents in solid tantalum capacitors under steady-state bias conditions," in *Electronic Components and Technology Conference (ECTC), 2010 Proceedings 60th*, 2010, pp. 752-757.

[38]   C. H. Greenewalt, "Partial Pressure of Water Out of Aqueous Solutions of Sulfuric Acid," *Industrial & Engineering Chemistry,* vol. 17, pp. 522-523, 1925/05/01 1925.

[39]   A. Teverovsky, "Guidelines for Selection, Screening and Qualification of Advanced Wet Tantalum Capacitors Used for Space Programs," NASA/GSFC, Greenbelt, MD2012.

[40]   R. T. Ferrell and Himmelbl.Dm, "Diffusion coefficients of hydrogen and helium in water," *Aiche Journal,* vol. 13, pp. 702-&, 1967.

[41]   E. Hinshaw and K. Moser, "Understanding hydrogen, tantalum and niobium materials of construction," presented at the Canadian Chemistry Conference, Sunriver, Oregon, 2001.

[42]   G. Schauman, J. Volkl, and G. Alefeld, "Diffusion coefficients of hydrogen and deuterium in vanadium, niobium, and tantalum by Gorsky-effect measurements," *Physica Status Solidi,* vol. 42, pp. 401-&, 1970.

[43]   A. M. Stoneham, "Theory of the diffusion of hydrogen in metals," *Berichte der Bunsengesellschaft für physikalische Chemie,* vol. 76, pp. 816-823, 1972.

[44]   R. Hempelmann, "Diffusion of hydrogen in metals," *Journal of the Less Common Metals,* vol. 101, pp. 69-96, 8// 1984.

[45]   M. Becke, *Tantal*: Verlag Chemie. Gmbh. Weinheim/Bergstr, 1970.

[46]   J. P. Zheng and T. R. Jow, "A new charge storage mechanism for electrochemical capacitors," *Journal of the Electrochemical Society,* vol. 142, pp. L6-L8, Jan 1995.

[47]   S. Sopčić, Z. Mandić, G. Inzelt, M. K. Roković, and E. Meštrović, "Ion dynamics in the pseudocapacitive reaction of hydrous ruthenium oxide. Effect of the temperature pre-treatment," *Journal of Power Sources,* vol. 196, pp. 4849-4858, 5/15/ 2011.

[48]   M. Taxak, S. Kumar, B. B. Kalekar, and N. Krishnamurthy, "Effect of nickel addition on the solubility of hydrogen in tantalum," *International Journal of Hydrogen Energy,* vol. 38, pp. 7561-7568, Jun 2013.

[49]   C. Y. Ang, "Activation energies and diffusion coefficients of oxygen and nitrogen in niobium and tantalum," *Acta Metallurgica,* vol. 1, pp. 123-125, 1953 1953.

[50]   D. A. Vermilyea, "The formation of anodic oxide films on tantalum in non-aqueous solutions," *Acta Metallurgica,* vol. 2, pp. 482-486, 5// 1954.

[51]   L. F. Harris, "Trends in the Design and Performance of Tantalum Capacitors," *ElectroComponent Science and Technology,* vol. 1, pp. 11-16, 1974.

[52]   H. O. Habazaki, T; Konno, H; Shimizu, K; Nagata, S; Skeldon, P ... "Field crystallization of anodic niobia," *Corrosion Science,* vol. 49, pp. 580-593, 2007.

[53]   J. Hossick-Schott, "Charge-based Model for the Time Progression of Field Crystallization in Tantalum Pentoxide," presented at the 29th symposium for passive components, CARTS'09, Jacksonville, FL, 2009.

[54]   K. C. Kalra and P. Katyal, "Electrical breakdown and electronic current of tantalum-tantalum oxide-aqueous electrolyte systems," *Thin Solid Films,* vol. 201, pp. 203-216, 6/30/ 1991.